INVESTIGATIONS OF C-H AND N-H ACTIVATION WITH ELECTRON DEFICIENT IRIDIUM PINCER COMPLEXES

Alison Cartwright Sykes

A dissertation submitted to the faculty of the University of North Carolina at Chapel Hill in partial fulfillment of the requirements for the degree of Doctor of Philosophy in the Department of Chemistry

Chapel Hill
2006

Approved by:

Advisor: Professor M. S. Brookhart

Reader: Professor J. L. Templeton

Reader: Professor H. Thorp

ABSTRACT

ALISON CARTWRIGHT SYKES: Investigations of C-H and N-H Activation with Electron Deficient Iridium Pincer Complexes
(Under the direction of Professor Maurice Brookhart)

Transition metal reactions that involve C-H and N-H bond activation provide a potential method for functionalizing hydrocarbons and amines. For the past three decades there have been numerous advances in this field; however, developing new approaches to activation of these bonds continues to be a significant endeavor. Recently pincer ligands have been successfully used to stabilize metal complexes at elevated temperatures. When chelated to iridium, these pincer complexes have been shown to be very active as transfer dehydrogenation catalysts. This has been exemplified by Kaska, Goldman, and Jensen using Ir complexes containing the 2,6-$(CH_2P\textit{t}Bu_2)_2C_6H_3$ (PCP) ligand and by Brookhart using the Ir complexes of the more electron-deficient bis(phosphinite) pincer ligand (POCOP). This dissertation explores alternative reactivity of these bis(phosphinite)iridium complexes.

Chapter 2 focuses on the reactions of [(POCOP)Ir] with N-H bonds, in particular those of both anilines and benzamides. The electronic character of the anilines plays an important role in the reactivity; more electron-withdrawing anilines favor oxidative addition while the more electron-donating anilines favor σ-bond formation. An explanation for this behavior is

provided along with a kinetic analysis of the oxidative addition and reductive elimination of anilines. A comparison of the reactivity of anilines to that of benzamides is also discussed.

In Chapter 3, cationic [(POCOP)Ir(H)(L)][BAr_F] complexes are examined that contain tetrakis(trifluoromethylphenyl)borate (BAr_F) as a non-coordinating counterion. Since these complexes are cationic, the metal center is even more electron deficient than those mentioned above. The structure of [(POCOP)Ir(H)(H_2)][BAr_F] was determined based on an H-D coupling constant of 33 Hz. In addition to the structural analysis, the rate of exchange between the hydride and the dihydrogen has also been determined.

Cationic olefin complexes, [(POCOP)Ir(H)(L)][BAr_F] (L = C_2H_4, C_3H_6, norbornene, methyl acrylate) have also been synthesized. Their dynamic behavior has been assessed using both line-broadening and spin-saturation transfer NMR techniques. The rates of olefin rotation and insertion into the Ir-H bond were analyzed and energy barriers to these processes were calculated. A brief examination of the reactivity of the cationic norbornene complex with nucleophiles has also been explored; however the results showed no C-Nuc bond formation.

To My Family:

Craig and Rusty

Mom, Dad, and Mark

ACKNOWLEDGMENTS

I would like to take a moment to thank the people who have been very influential and supportive of me throughout the past five years. First and foremost, I would like to thank Prof. Brookhart. From the beginning you have made me feel at home in your group. You had a knack of throwing me a compliment when the chemistry was not working right which keep me motivated and proud of the work I have done. You genuinely care about all your students which is a trait that is admirable. I think the best decision I made in graduate school was joining your lab.

My parents have also been there for me not only for the past five years but for the past twenty-seven. Mom and Dad, it is the values that you instilled upon me that have led me down this path and I am very grateful to you for that.

With in the lab, there have been numerous people that have been a source of entertainment and of course knowledge. And just to name a few. Mark, Jason, Jon, Scotty and Olafs taught me most of my skills in the lab and helped me get on my feet when I first joined. I will always think of you guys when Bon Jovi plays. Tomislav, you were an asset to the lab and we appreciated how much you enjoyed helping and teaching everyone. The Top of Lenoir has not been the same without you. Amy, I couldn't have asked for a better person to sit behind me for the three years. I appreciate all the talks and discussions, you kept me sane

when sanity seemed to be lost. And of course the members of the lab that are still there, Abby, Stephanie and Emily, I will miss you guys, keep everyone one in check over there ☺.

Last, and by far least, I would like to thank Craig. If I was to ever question my choice in coming to North Carolina, meeting you shows that it was meant to be. You have been there through all five years, through the good and the bad. For those frustrating days, it is so nice to know that I have you to come home to. Craig, I love you and want to thank you for being there and supporting me in all my decisions.

TABLE OF CONTENTS

LIST OF TABLES

Page

LIST OF SCHEMES

Page

LIST OF FIGURES

Page

LIST OF ABBREVIATIONS AND SYMBOLS

‡	denotes transition state
°C	degrees Celsius
δ	chemical shift
ΔG	change in Gibbs' free energy
ν	frequency, in Hertz
Ar	aryl
atm	atmosphere
BAr_F	$[B(3,5\text{-bis}(CF_3)C_6H_3)_4]^-$
d	doublet
eq	equation
equiv	equivalents
Et	ethyl, $-C_2H_5$
g	grams
h	hours
Hz	Hertz
*i*Pr	isopropyl, $-CH(CH_3)_2$
J	scalar coupling constant, in Hz
k	rate constant
K	equilibrium constant
K	degrees Kelvin
kcal	kilocalorie
M	molar (moles solute/liter solution)

m	multiplet
m	meta
Me	methyl, -CH_3
mL	milliliter
mol	moles
*n*Bu	normal butyl, -$CH_2CH_2CH_2CH_3$
NMR	nuclear magnetic resonance
o	ortho
p	para
PCP	2,6-$(CH_2P$*t*$Bu_2)_2C_6H_3$
Ph	phenyl
POCOP	2,6-$(OP$*t*$Bu_2)_2C_6H_3$
ppm	parts per million
q	quartet
RT	room temperature
s	seconds
s	singlet (used in NMR data)
soln	solution
t	triplet
*t*Bu	tertiary butyl, -$C(CH_3)_3$

CHAPTER ONE

Funtionalization of Carbon-Hydrogen Bonds through the Activation of C-H and N-H Bonds by Transition Metal Complexes: Introduction and Background

Since the first example of C-H oxidative addition of benzene to a soluble transition metal complex was observed by Chatt and Davidson in 1965[1], the understanding and potential of C-H activation reactions has been extensively studied. Activation of saturated alkanes was believed to be more difficult than that of arenes despite the lower bond strength (~95 kcal/mol), but this was finally achieved nearly simultaneously by Bergman[2] and Graham[3] using Ir(I) complexes. Throughout the 1980's and into the 1990's, a significant amount of research was focused on better understanding C-H bond activation through investigations of intermediates, thermodynamics and kinetics, and selectivity of various stoichiometric reactions.[4-19]

There had been reactions in which the oxidative addition of a saturated alkane had been postulated[20-22], but it was not until Bergman's findings in 1982[2] that a stable intermediate M(H)(alkyl) species was observed. Irradiation of $Cp^*Ir(PMe_3)H_2$ in an alkane solvent was shown to induce loss of H_2 followed by formation of the $Cp^*Ir(PMe_3)(H)(alkyl)$ complex which was observed by ^1H NMR spectroscopy (Scheme 1.1). In this early stage it was

shown that activation of a primary C-H bond is favored over a secondary C-H bond. Graham observed the same results with after irradiation of $Cp^*Ir(CO)_2$ in neopentane and cyclohexane solvent.[3] Shortly thereafter, Jones reported similar behavior of an analogous rhodium system.[6] The $L_nRh(H)(alkyl)$ species, however, are significantly less stable and undergo reductive elimination of the alkane at -15°C.

Scheme 1.1. First observation of an alkyl hydride complex by Bergman in 1982[2]

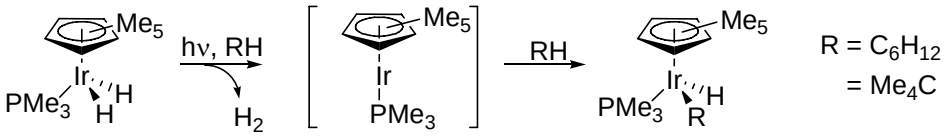

One striking outcome of this research was a deeper understanding of the selectivity of alkane activation. The $[Cp^*Ir(PMe_3)]$ species prefers activation of the stronger rather than the weaker C-H bond of alkanes (i.e. 1° > 2° >> 3°). This preference was ascribed to steric effects. This finding was especially interesting because the regioselectivity shown by this reaction was the reverse of that seen in radical-induced alkane functionalization (3° > 2° > 1°).

Following detailed studies of stoichiometric C-H oxidative addition reactions, the next goal was to develop transition metal-catalyzed processes to functionalize C-H bonds of alkanes. Such catalytic reactions have been particularly challenging. While numerous routes to functionalized products have been discovered, problems including over oxidation forming either a mixture of products or the undesired product, poor region- or chemoselectivity, competing side reactions, and slow rates are encountered in developing such processes.

One still elusive goal is the practical oxidation of methane to methanol catalyzed by a transition metal.[23-26] This reaction is of significance as it would provide a safe, convenient, and economical method for converting methane to a liquid fuel. Observed in 1972 by Shilov, oxidation of methane to methanol under reasonably mild conditions was achieved using a platinum(II) catalyst. This reaction had one major fault that prevented its use commercially: although it was catalytic in platinum(II), a stoichiometric amount of platinum(IV) was need to reoxidize the platinum(II) (Scheme 1.2).

Scheme 1.2. Shilov's oxidation of methane to methanol by Pt(II)/Pt(IV)[23-26]

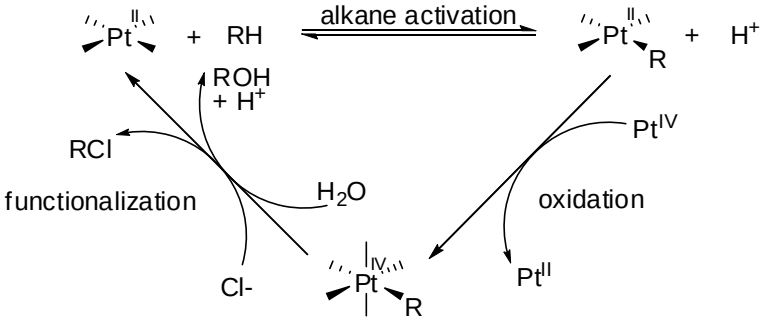

More recently, Periana and coworkers, then at Catalytica, improved upon Shilov's system. They developed a platinum catalyzed system that catalytically functionalizes methane to methyl bisulfate, a methanol derivative, and at moderate temperatures with yields of 72% (Scheme 1.3).[27] This reaction is performed in concentrated sulfuric acid in which SO_3 serves as the oxidant.

Scheme 1.3. Catalytic conversion of methane to methyl bisulfate by a platinum catalyst developed by Periana and coworkers

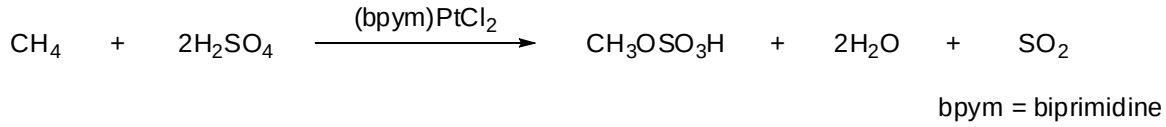

Often thermodynamics and kinetics work against the functionalization of alkanes, so strategies to overcome these barriers must be developed. Two methods of circumventing this problem are the use of a secondary reaction to offset the energy requirements or driving the reaction photochemically.

Insertion of carbon monoxide into a C-H bond, or carbonylation, for example, is an endothermic process. There exist only a few examples of this reaction that involve alkanes. One such reaction was discovered by Tanaka using the rhodium complex, $Rh(PMe_3)_2(CO)(Cl)$ (Scheme 1.4). In this case, light is used to drive the reaction. Remarkably, this reaction showed significant regioselectivity, and the linear product was favored by about 45:1 as shown in Scheme 1.3[28]

Scheme 1.4. Carbonylation of pentane by $Rh(PMe_3)_2(CO)(Cl)$ reported by Tanaka[28]

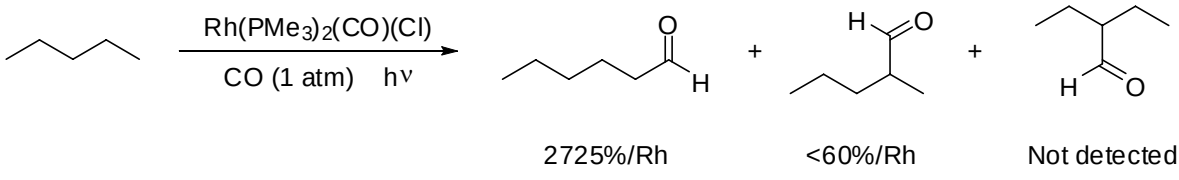

Another important reaction based on C-H oxidative addition is alkane dehydrogenation. This reaction provides a method of converting alkanes to alkenes,e one of the most important feedstocks used in industry. As in the carbonylation reactions mentioned above,

dehydrogenation is an thermodynamically uphill process (ca. +33 kcal/mol).[29] Since the entropy of this process is positive, in some systems under elevated temperatures the equilibrium might lie on the side of the dehydrogenated products. However, for these reactions to proceed under moderate reaction conditions, the use of a sacrificial hydrogen acceptor is often used to offset the energy requirement. The sacrificial hydrogen acceptor, often *tert*-butylethylene (TBE), is hydrogenated to *tert*-butylethane, a thermodynamically downhill reaction. Through the removal of hydrogen from the catalyst precursor, TBE allows the formation of the active species. Scheme 1.5 shows the dehydrogenation of cyclopentane by a cationic iridium catalyst with the addition of the hydrogen acceptor, TBE, reported by Crabtree and coworkers.[29] Cyclopentane can be dehydrogenated twice followed by oxidative addition to the iridium to form the cyclopentadienyl complex.

Scheme 1.5. Dehydrogenation of cyclopentane to cyclopentadiene with the use of a hydrogen acceptor[29]

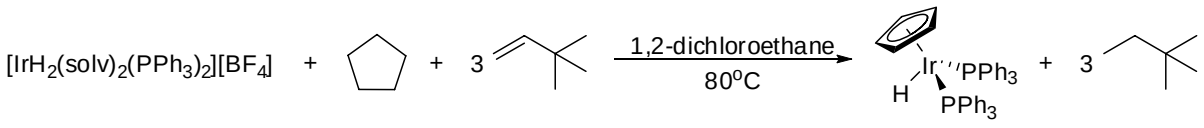

Around the same time as Crabtree's report, Felkin showed that heptahydridobis(triarylphosphine)rhenium catalyzed the dehydrogenation of not only cycloalkanes but also of linear alkanes. In this reaction, the dehydrogenated product, η^4-trans-1,3-pentadiene remains coordinated to rhenium. However, addition of trimethylphosphite allows for the selective formation of 1-pentene. This was a promising result in that it showed selective conversion of linear alkanes to the α-olefin product.[30] (Scheme 1.6)

Scheme 1.6. Selective dehydrogenation of *n*-pentane by $(Ar_3P)_2ReH_7$ to form 1-pentene[30]

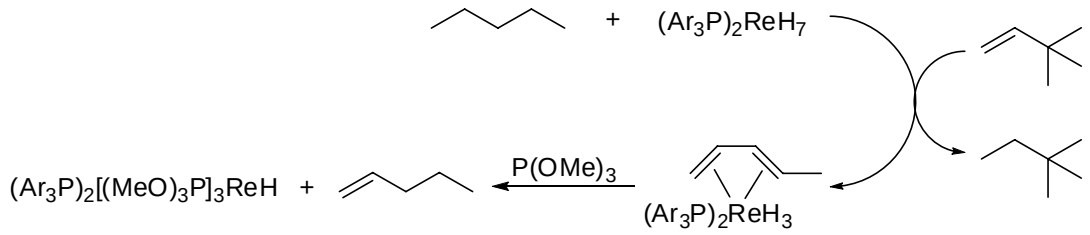

In the past decade, iridium pincer complexes such as those shown in Figure 1.1 have been used as catalysts for dehydrogenation of alkanes. The pioneering studies on complex **1** began in the late 1990's by Kaska, Jensen and Goldman.[31-34] The pincer ligand stabilized the iridium dihydride complexes so that little or no decomposition occurred during dehydrogenation even at extremely high temperatures (150-200°C). As in the dehydrogenation reactions described above, TBE was added to the reaction mixture as a hydrogen acceptor. However, when the reactions are run at 200°C, the use of TBE was not necessary ("acceptorless" conditions) because at this temperature hydrogen reductively eliminates from **1** and is driven off through vigorously refluxing the solvent. This complex showed versatility as it not only dehydrogenates cycloalkanes, but also reacts with tetrahydrofuran[31], ethylbenzene[31], and ethylcyclohexane,[31] and more recently tertiary amines to form enamines.[35] Catalyst **2** selectively dehydrogenates *n*-alkanes to α-olefins at 150°C with moderate conversions.[36]

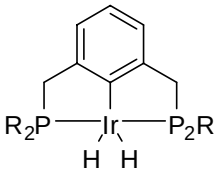

R	#
*t*Bu	**1**
*i*Pr	**2**

Figure 1.1. Pincer complexes shown to be active transfer dehydrogenation catalysts

In 2004, our group developed the bis(phosphinite) pincer complexes **3-8** (Figure 1.2), with the idea that removing more electron density from the iridium center might achieve higher rates and turnover numbers for transfer dehydrogenation than the parent system and still retain stability at high temperatures.[37-39] In fact this was the case. The bis(phosphinite) complex, **8**, with the most electron-withdrawing substituent on the ligand backbone was the most active derivative for this reaction with a turnover number of 2210 at 200°C when cycooctane (3030:1, COA:Ir) was used as a substrate. Active catalysts are generated by the addition of 1.1 equivalents of NaO*t*Bu to the hydridochloride to form the active 14-electron intermediate. Under the same reaction conditions, the parent system, (PCP)Ir(H)(Cl), the catalyst precursor to **1**, showed an activity of only 230 TO's.[38]

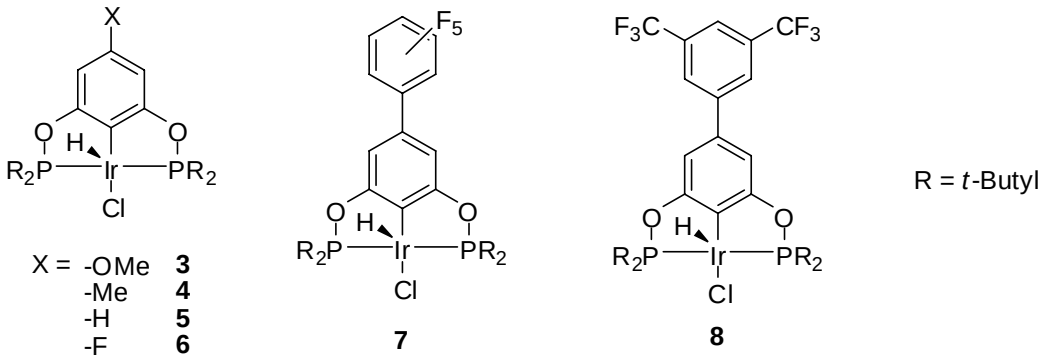

Figure 1.2. Bis(phosphinite)Ir(H)(Cl) complexes **3-8** developed in the Brookhart lab[38]

Late transition metals have shown potential in hydroamination, a reaction of intense current interest.[40-46] Hydroamination provides a synthetically convenient method for the formation of C-N bonds. Molecules that contain nitrogen atoms, such as amines, are of interest industrially, especially for pharmaceutical products. However, currently amines are

typically formed by multistep syntheses. Application of hydroamination to synthesize these types of products could lead to fewer or even one step processes.

There are two mechanisms that are widely accepted for hydroamination by late-transition metals (Scheme 1.7). In the first mechanism,[40,47] often seen in palladium and platinum systems, the alkene coordinates to the metal center, activating it toward nucleophilic attack. The amine nucleophile can then attack the olefin with loss of a proton. Two possible products can then be formed. Through protonolysis of the M-C bond, the hydroamination product can result. Alternatively, β-hydride elimination can occur and the oxidative amination product is formed.[40]

Scheme 1.7. Mechanism for late-transition metal hydroamination

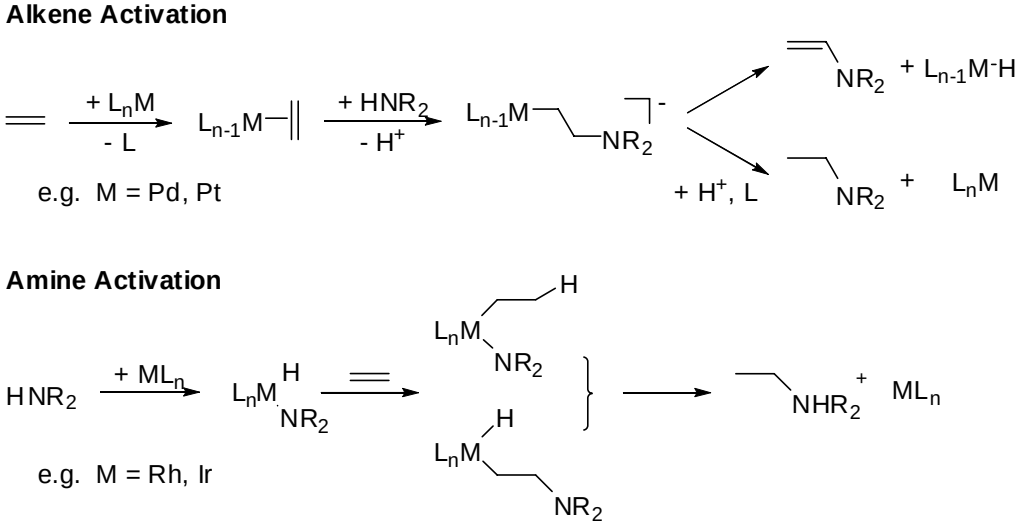

For rhodium and iridium, hydroamination typically occurs via activation of the amine by oxidative addition, followed by olefin insertion into either the M-H bind or M-N bond. Reductive elimination of the product yields the desired amine.[40,48] (Scheme 1.7) Reactions

involving the oxidative addition of nitrogen-hydrogen bonds to a transition metal center are surprisingly much less studied than C-H bond activation despite the similarities in homolytic bond strength. In fact, there exist only a few examples of catalytic reactions involving the oxidative addition of an N-H bond to a metal center. Casalnuovo and Milstein have shown that hydroamination of norbornene by a coordinatively unsaturated iridium complex occurs by the initial activation of amine.[49] In this case the active Ir(I) catalyst, "$Ir(PEt_3)_2Cl$," is formed by dissociation of two ethylene molecules from $Ir(PEt_3)_2(C_2H_4)_2Cl$. Aniline then undergoes oxidative addition to the iridium center followed by coordination of norbornene. Iridium has a two fold role in this reaction; it not only activates the norbornene to nucleophilic attack but also activates the lone pair on the aniline. This lone pair attacks the olefin forming a metallacyclic intermediate. The catalyst is regenerated and the product is formed by C-H reductive elimination and dissociation of the product amine. (Scheme 1.8)

Scheme 1.8. Hydroamination of norbornene by Casalnuovo and Milstein with an iridium catalyst[49]

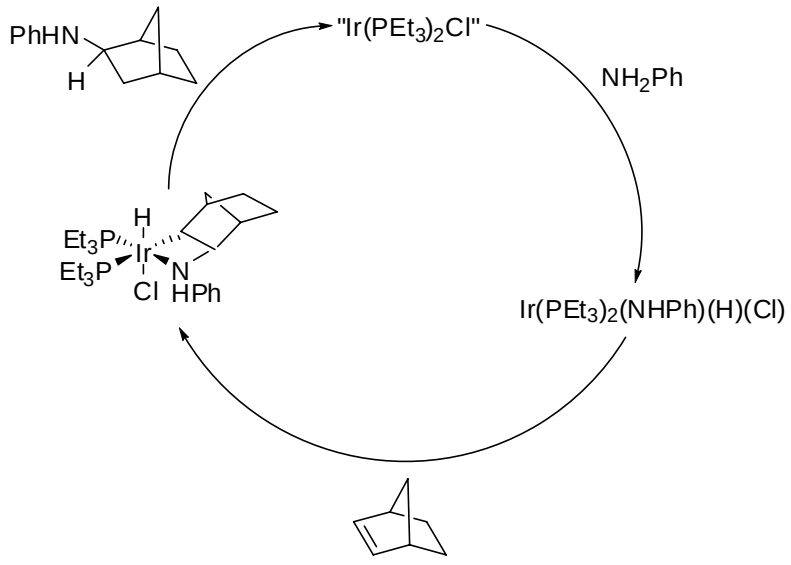

The Ir(I) pincer complex **1,** described above as a good transfer dehydrogenation catalyst, also shows reactivity with N-H bonds,[50] although to date no hydroamination reactions have been reported. As illustrated in Scheme 1.9, the aniline N-H bond can be activated through oxidative addition to the iridium center of **9** to form **10**. The dihydride complex **1** is converted to the 14-electron active species **9** by reaction with the hydrogen acceptor *t*butylethylene (TBE).

Scheme 1.9. The oxidative addition of aniline to (PCP)IrH_2, **1**[50]

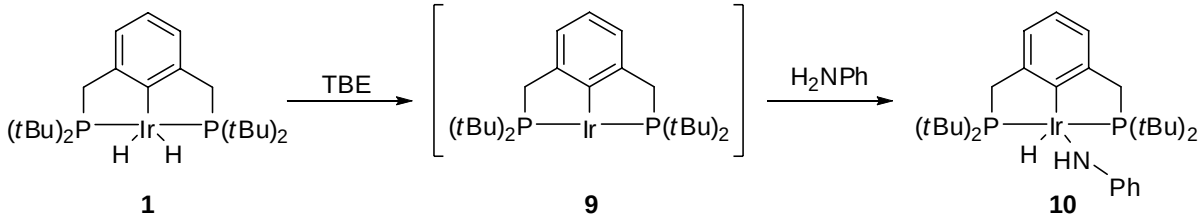

1 **9** **10**

Even more significant is that reaction of (PCP)Ir(H)(Cl)(NH_3) and $KN(SiMe_3)_2$ generated the amido hydride complex **12** at -78°C (Scheme 1.10). (PCP)Ir(H)(Cl)(NH_3) **11** was formed from the reaction of (PCP)Ir(H)(Cl) ammonia. [50] This is one of only a few examples in the literature were the amido hydride of ammonia has been observed.[51,52] If **12** is warmed to room temperature the σ-bound ammonia complex **13** is formed. Complex **13** can also be formed directly from the addition of ammonia and TBE at room temperature to **1**.[50]

Scheme 1.10. Reaction of PCP iridium complexes with ammonia[50]

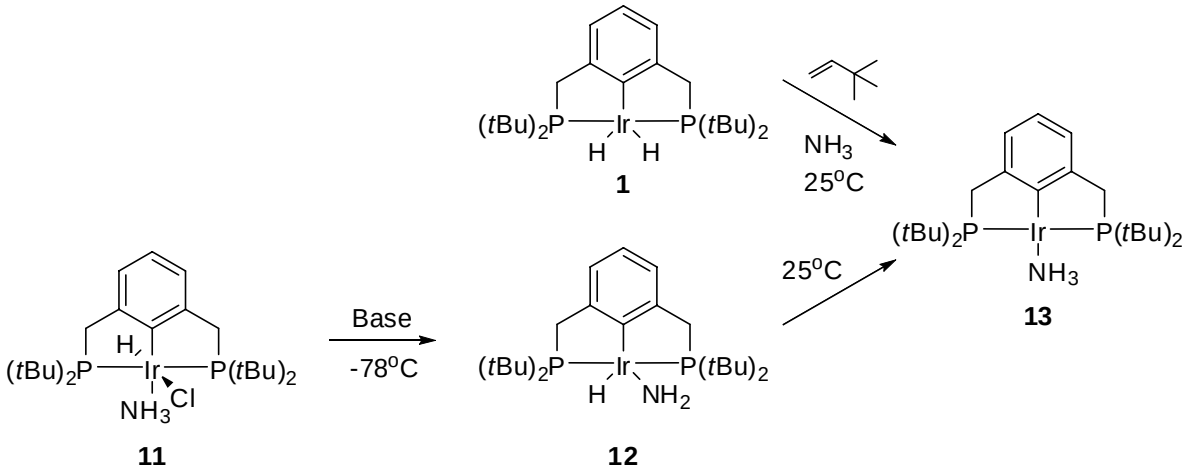

Typically, by adding more electron density to a metal center oxidative addition to the metal becomes more favorable. Based on this trend, Goldman and Hartwig et. al. developed a new iridium(I) pincer complex that has a more electron-donating aliphatic ligand backbone, **14**. This ligand significantly altered the reactivity of the Ir pincer complex to favor oxidative addition. Indeed, when complex **14** was treated with ammonia at room temperature the amido hydride complex **15** was formed (Scheme 1.11).[53]

Scheme 1.11. Oxidative addition of ammonia at room temperature by a pincer complex with an electron-donating ligand.

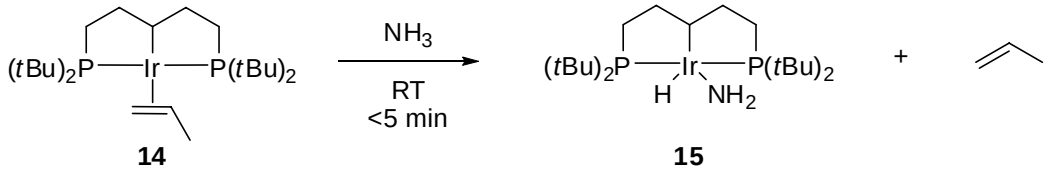

Research Goals and Achievements

As mentioned above the functionalization of C-H bonds is a desirable process. Recent studies of Ir(I) pincer complexes have shown that they are reactive with C-H and N-H bonds of numerous substrates. The most useful reaction based on C-H activation by these complexes has been dehydrogenation of alkanes to alkenes. However, there is still a significant amount of research needed to fully explore the potential of these iridium pincer complexes. The goal of the research presented in the following chapters is to obtain a better understanding of the reactivity of Ir(I) pincer complexes containing the more electron-withdrawing bis(phosphinite) pincer ligand.

Chapter one describes the reactivity of the [(POCOP)Ir] moiety with various anilines, NH_2Ar. The active [(POCOP)Ir] fragment is generated in situ in these reactions by treating (POCOP)Ir(H)(Cl) with NaO*t*Bu in an aromatic solvent (benzene or toluene). The aromatic solvent is necessary to stabilize the reactive intermediate. When anilines are present an equilibrium is established between (POCOP)Ir(H)(Ar), (POCOP)Ir(NH_2Ar) and (POCOP)Ir(H)(NHAr). Electronic effects were probed by examining the change in the equilibrium ratios of these three species as a function of the substituents on the aniline.

Details of the oxidative addition and reductive elimination of the anilines were further studied to gain mechanistic information on these reactions. A comparison of the rates reductive elimination of the more electron-withdrawing anilines from the d^6 five-coordinate (POCOP)Ir(H)(NHAr) and the d^6 six-coordinate (POCOP)Ir(H)(CO)(NHAr) is also presented. The mechanisms of these two processes are compared to known mechanisms for reductive elimination from d^6 systems. A brief comparison of the oxidative addition of the anilines to similar reactions of benzamide is presented as well.

Chapter Two describes the synthesis of more electron-deficient cationic iridium(III) pincer complexes, [(POCOP)Ir(H)(L)][BAr_F] (BAr_F = tetrakis(3,5-bis(trifluoromethyphenyl))-borane). Theses complexes (L = olefin) were prepared with the goal of using them for catalytic hydroamination as shown below for the simple case L = C_2H_4 (Scheme 1.12).

Scheme 1.12. Potential catalytic cycle for hydroamination with [(POCOP)Ir(H)(L)][BAr_F] L = C_2H_4

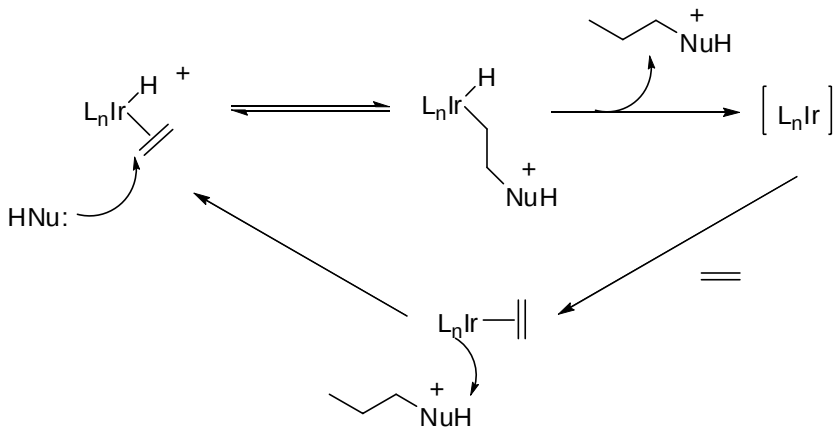

Although implementations of this catalytic cycle were not successful, a number of new complexes of the type [(POCOP)Ir(H)(L)][BAr_F] were prepared and found to have interesting structural and dynamic features.

An in depth analysis of [(POCOP)Ir(H)(H2)][BAr_F] is described. NMR data provides evidence supporting a dihydrogen/hydride complex rather than a trihydride complex. Exchange rates among the hydrogens are measured and presented as well.

The dynamics of the complexes where L equals ethylene, propylene, norbornene, and methyl acrylate are studied as well, in particular the rotation of the olefin, as well as the rate

of insertion of the olefin into the M-H bond. Attempts at C-H functionalization of the olefins were attempted with the addition of aniline and thiol to the cationic olefin complexes.

References

(1) Chatt, J.; Davidson, J. M. *J. Chem. Soc.* **1965**, 843.

(2) Janowicz, A. H.; Bergman, R. G. *J. Am. Chem. Soc.* **1982**, *104*, 352.

(3) Hoyano, J. K.; Graham, W. A. G. *J. Am. Chem. Soc.* **1982**, *104*, 3723.

(4) Jones, W. D.; Feher, F. J. *J. Am. Chem. Soc.* **1982**, *104*, 4240.

(5) Janowicz, A. H.; Bergman, R. G. *J. Am. Chem. Soc.* **1983**, *105*, 3929.

(6) Jones, W. D.; Feher, F. J. *J. Am. Chem. Soc.* **1984**, *106*, 1650.

(7) Periana, R. A.; Bergman, R. G. *Organometallics* **1984**, *3*, 508.

(8) Wax, M. J.; Stryker, J. M.; Buchanan, J. M.; Kovac, C. A.; Bergman, R. G. *J. Am. Chem. Soc.* **1984**, *106*, 1121.

(9) Halpern, J. *Inorg. Chim. Acta.* **1985**, *100*, 41.

(10) Jones, W. D.; Feher, F. J. *J. Am. Chem. Soc.* **1985**, *107*, 620.

(11) Stoutland, P. O.; Bergman, R. G. *J. Am. Chem. Soc.* **1985**, *107*, 4581.

(12) Baker, M. V.; Field, L. D. *J. Am. Chem. Soc.* **1986**, *108*, 7436.

(13) Baker, M. V.; Field, L. D. *J. Am. Chem. Soc.* **1986**, *108*, 7433.

(14) Baker, M. V.; Field, L. D. *Organometallics* **1986**, *5*, 821.

(15) Desrosiers, P. J.; Shinomoto, R. S.; Flood, T. C. *J. Am. Chem. Soc.* **1986**, *108*, 1346.

(16) Desrosiers, P. J.; Shinomoto, R. S.; Flood, T. C. *J. Am. Chem. Soc.* **1986**, *108*, 7964.

(17) Periana, R. A.; Bergman, R. G. *J. Am. Chem. Soc.* **1986**, *108*, 7332.

(18) Jones, W. D.; Feher, F. J. *Acc. Chem. Res.* **1989**, *22*, 91.

(19) Shinomoto, R. S.; Desrosiers, P. J.; Harper, T. G. P.; Flood, T. C. *J. Am. Chem. Soc.* **1990**, *112*, 704.

(20) Baudry, D.; Ephritikhine, M.; Felkin, H. *J. C. S. Chem. Comm.* **1980**, 1243.

(21) Crabtree, R. H.; Mihelcic, J. M.; Quirk, J. M. *J. Am. Chem. Soc.* **1979**, *101*, 7738.

(22) Baudry, D.; Ephritikhine, M.; Felkin, H. *J. Chem. Soc., Chem. Comm.* **1980**, 1243.

(23) Gol'dshleger, N. F.; Es'kova, V. V.; Shilov, A. E.; Shteinman, A. A. *Zhurnal Fizicheskoi Khimii* **1972**, *46*, 1353.

(24) Shilov, A. E.; Shul'pin, G. B. *Chem. Rev.* **1997**, *97*, 2879.

(25) Shilov, A. E.; Shteinman, A. A. *Coord. Chem. Rev.* **1977**, *24*, 97.

(26) Kushch, L. A.; Lavrushko, V. V.; Misharin, Y. S.; Moravskii, A. P.; Shilov, A. E. *Nouveau Journal de Chimie* **1983**, *7*.

(27) Periana, R. A.; Taube, D. J.; Gamble, S.; Taube, H.; Satoh, T.; Fujii, H. *Science* **1998**, *280*, 560.

(28) Sakakura, T.; Tanaka, M. *J. Chem. Soc., Chem. Comm.* **1987**, 758.

(29) Crabtree, R. H.; Mellea, M. F.; Mihelcic, J. M.; Quirk, J. M. *J. Am. Chem. Soc.* **1982**, *104*, 107.

(30) Baudry, D.; Ephritikhine, M.; Felkin, H.; Zakrzewski, J. *J. Chem. Soc., Chem. Comm.* **1982**, 1235.

(31) Gupta, M.; Kaska, W. C.; Jensen, C. M. *Chem. Comm.* **1997**, 461.

(32) Xu, W.-w.; Rosini, G. P.; Krogh-Jespersen, K.; Goldman, A. S.; Gupta, M.; Jensen, C. M.; Kaska, W. C. *Chem. Comm.* **1997**, 2273.

(33) Gupta, M.; Hagen, C.; Flesher, R. J.; Kaska, W. C.; Jensen, C. M. *Chem. Comm.* **1996**, 2083.

(34) Gupta, M.; Hagen, C.; Kaska, W. C.; Cramer, R. E.; Jensen, C. M. *J. Am. Chem. Soc.* **1997**, *119*, 840.

(35) Zhang, X.; Fried, A.; Knapp, S.; Goldman, A. S. *Chem. Comm.* **2003**, 2060.

(36) Liu, F.; Pak, E. B.; Singh, B.; Jensen, C. M.; Goldman, A. S. *J. Am. Chem. Soc.* **1999**, *121*, 4086.

(37) Goettker-Schnetmann, I.; Brookhart, M. *J. Am. Chem. Soc.* **2004**, *126*, 9330.

(38) Goettker-Schnetmann, I.; White, P.; Brookhart, M. *J. Am. Chem. Soc.* **2004**, *126*, 1804.

(39) Goettker-Schnetmann, I.; White, P. S.; Brookhart, M. *Organometallics* **2004**, *23*, 1766.

(40) Muller, T. E.; Beller, M. *Chem. Rev.* **1998**, *98*, 675.

(41) Roesky, P. W.; Muller, T. E. *Angew. Chem. Int. Ed.* **2003**, *42*, 2708.

(42) Takemiya, A.; Hartwig, J. F. *J. Am. Chem. Soc.* **2006**, *128*, 6042.

(43) Johns, A. M.; Utsunomiya, M.; Incarvito, C. D.; Hartwig, J. F. *J. Am. Chem. Soc.* **2006**, *128*, 1828.

(44) Li, X.; Chianese, A. R.; Vogel, T.; Crabtree, R. H. *Org. Lett.* **2005**, *7*, 5437.

(45) Field, L. D.; Messerle, B. A.; Vuong, K. Q.; Turner, P. *Organometallics* **2005**, *24*, 4241.

(46) Qian, H.; Widenhoefer, R. A. *Org. Lett.* **2005**, *7*, 2635.

(47) Michael, F. E.; Cochran, B. M. *J. Am. Chem. Soc.* **2006**, *128*, 4246.

(48) Beller, M.; Trauthwein, H.; Eichberger, M.; Breindl, C.; Herwig, J.; Muller, T. E.; Thiel, O. R. *Chem.--Eur. J.* **1999**, *5*, 1306.

(49) Casalnuovo, A. L.; Calabrese, J. C.; Milstein, D. *J. Am. Chem. Soc.* **1988**, *110*, 6738.

(50) Kanzelberger, M.; Zhang, X.; Emge, T. J.; Goldman Alan, S.; Zhao, J.; Incarvito, C.; Hartwig John, F. *J. Am. Chem. Soc.* **2002**, *125*, 13644.

(51) Jayaprakash, K. N.; Conner, D.; Gunnoe, T. B. *Organometallics* **2001**, *20*, 5254.

(52) Holland, A. W.; Bergman, R. G. *J. Am. Chem. Soc.* **2002**, *124*, 14684.

(53) Zhao, J.; Goldman Alan, S.; Hartwig John, F. *Science* **2005**, *307*, 1080.

CHAPTER TWO

Reactions of Anilines and Benzamides with a Fourteen-Electron Iridium(I) Bis(Phosphinite) Complex: N-H Oxidative Addition versus Lewis Base Coordination

(This chapter has been adapted with permission from: Sykes, A. C., White, P., Brookhart, M. *Organometallics* **2006**, *25*, 1664-1675. Copyright 2006 American Chemical Society.)

Introduction

Carbon-hydrogen bond activation by late transition metal complexes has received intense scrutiny over the past two decades since the classic work of Bergman[1], Jones[2], and Graham[3]. Fundamental studies including kinetics, thermodynamics, and selectivities of the oxidative addition reactions of C-H bonds to a variety of transition metal centers together with theoretical investigations have appeared.[4,5] More recently, these reactions have been incorporated into catalytic cycles, and there are now numerous useful catalytic organic transformations based on C-H bond activation reactions.[6-12]

Although N-H and C-H bonds exhibit similar homolytic bond strengths, many fewer investigations of late metal activation of N-H bonds have been carried out.[13-16] Such studies

could impact the rapidly growing number of metal-catalyzed transformations of amine and related compounds including hydroaminations of alkenes, styrenes, dienes, and alkynes.[17-20] Some of these transformations appear to involve oxidative addition of N-H bonds,[21,22] while the mechanisms of many other transformations are unknown, but some could involve an N-H oxidative addition step.

An early instructive example of oxidative addition of N-H bonds to late transition metal centers was reported by Merola who showed that the N-H bonds of pyrroles and indoles oxidatively add to the Ir(I) moiety, $(COD)(PMe_3)_3Ir^+$, to yield the eighteen-electron, octahedral Ir(III) species as illustrated in Scheme 2.1.[23]

Scheme 2.1. Example of oxidative addition of N-H bonds to a Ir(I) moiety by Merola

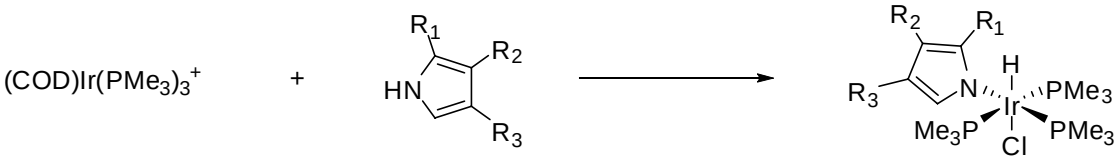

The Goldman, Jensen, and Kaska groups have shown that the 14-electron complex (PCP)Ir (PCP = 2,6-$(CH_2P\textit{t}Bu_2)_2C_6H_3$), **1**, generated from treatment of the dihydride $(PCP)Ir(H)_2$ with acceptors such as *tert*-butylethylene, readily oxidatively adds C-H bonds of alkanes and arenes.[24,25] Such species are highly active for catalytic transfer dehydrogenation of alkanes and can also be used for synthesis of enamines through transfer dehydrogenation of tertiary amines.[26] Goldman and Hartwig have recently observed that the (PCP)Ir complex **1** oxidatively adds the N-H bond of aniline to produce the Ir(III) anilino hydride **2** as shown in Scheme 2.2.[27] In benzene, adduct **2** equilibrates with the phenyl hydride complex **3**. The equilibrium favors the anilino hydride complex with a $K_{eq} = 105$ at 22°C (Scheme 2.3).

Scheme 2.2. Oxidative addition of aniline to [(PCP)Ir] to form (PCP)Ir(H)(NHC_6H_5) by Goldman and Hartwig

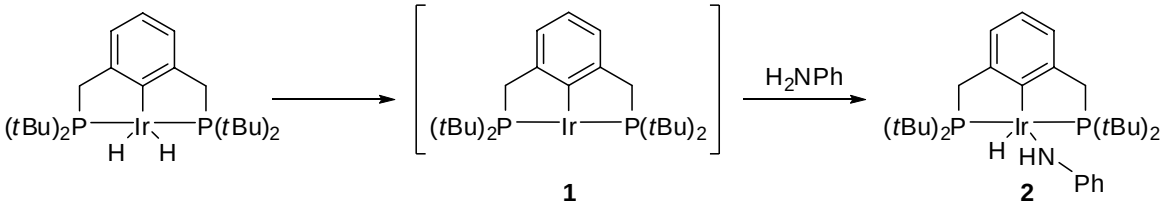

Scheme 2.3. Equilibrium between (PCP)Ir(H)(Ph) + $NH_2C_6H_5$ and (PCP)Ir(H)(NHC_6H_5) + C_6H_6 at room temperature

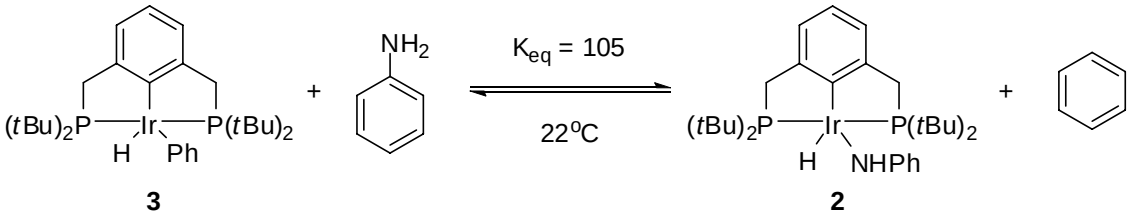

Attempted oxidative addition of the better σ-donor ammonia results in the Ir(I) ammonia complex **4**. The amido hydride **5** could be independently generated by dehydrochlorination of **6** at -78°C. Warming to 25°C resulted in conversion to ammonia complex **4**, indicating that thermodynamically the ammonia complex is favored over the amido hydride (Scheme 2.4). When a more electron-donating saturated backbone is incorporated in the pincer ligand, oxidative addition of ammonia occurs rather than simple coordination.[28] Treatment of **7** with ammonia forms the Ir(III) amido hydride in high yields at 25°C (Scheme 2.5).

Scheme 2.4. Generation of (PCP)Ir(H)(NH_2) at low temperature followed by formation of (PCP)Ir(NH_3) by warming to room temperature

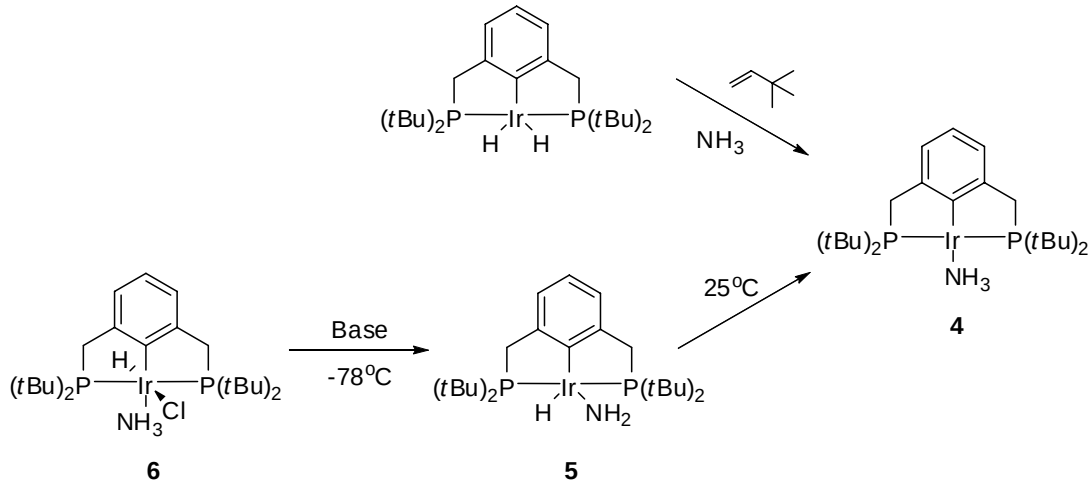

Scheme 2.5. Activation of ammonia at room temperature by an iridium(I) complex with an electron-donating pincer backbone

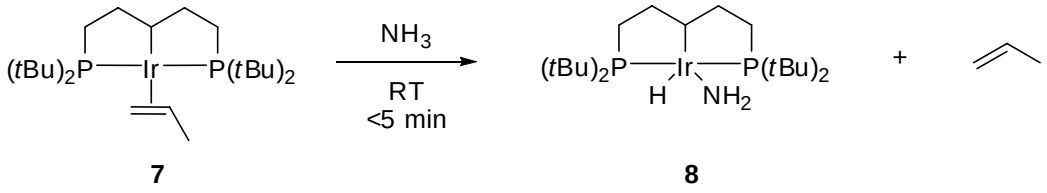

Our laboratory[29-31] has investigated the chemistry of more electron-deficient Ir pincer complexes based on the bis(phosphinite) ligand, POCOP = 2,6-(OP*t*Bu$_2$)$_2$C$_6$H$_3$. The highly active 14-electron complex **10** can be conveniently generated *in situ* by treatment of the hydrido chloride **9** with sodium *tert*-butoxide (Scheme 2.6). Generation of **10** in a cyclooctane/*tert*-butylethylene mixture produces a highly active catalyst system for transfer dehydrogenation and production of cyclooctene and cyclooctadiene (Scheme 2.7). Detailed mechanistic studies of this system have complemented the studies of Goldman on **1** and

provided interesting contrasts suggesting the phosphinite POCOP system prefers the Ir(I) oxidation state relative to the PCP systems.[29-31]

Scheme 2.6. In situ formation of the active 14-electron iridium species, [(POCOP)Ir]

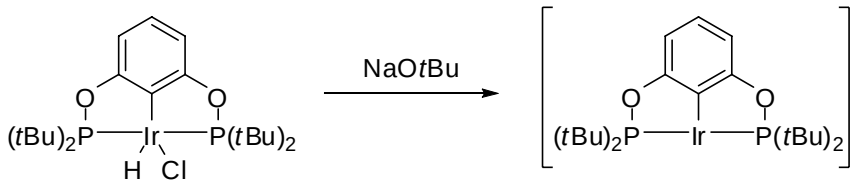

9 **10**

Scheme 2.7. Transfer dehydrogenation of cyclooctane with (POCOP)Ir(H)(Cl) as the catalyst precursor

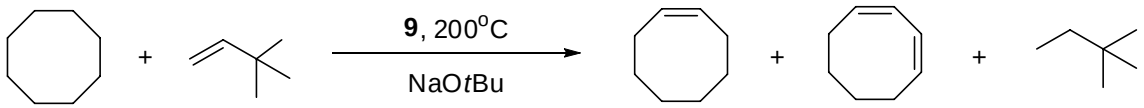

This chapter describes the reaction of a series of substituted anilines and benzamides with the phosphinite pincer complex **10**. In the case of the anilines, either the Ir(III) oxidative addition adduct, the Ir(I) σ-complex, or a mix of these products is formed depending on the nature of the *para*-substituent. Rates of reductive elimination of the Ir(III) species have been measured, as well as the equilibria in benzene between the aniline adducts and the phenyl hydride. Information on the mechanism of reductive elimination was attained through the study of low temperature reactions of both the *p*-chloroaniline and the *p*-methoxyaniline complexes.

Results and Discussion

I) Reaction of (POCOP)Ir pincer complexes with various anilines (11a-g)

a) Equilibration of (POCOP)Ir(H)(C_6H_5) (12) with various (POCOP)Ir(NH_2Ar) (13) and (POCOP)Ir(H)(NHAr) (14)

The reactions of anilines shown in Figure 2.1 with the fourteen-electron (POCOP)Ir pincer complex **10** were carried out by treatment of the hydrochloride complex **9** with NaO*t*Bu and anilines **11a-g** in benzene at room temperature for 1.5 hours. The phenyl hydride complex **12** is in rapid equilibrium with **10**,[31] and thus reacts with the aniline to form either the σ-complex **13** or the oxidative addition adduct **14**. The three species, **12**, **13**, and **14** depicted in Scheme 2.8 are all in equilibrium at 25 °C. ^{31}P NMR spectroscopy was used to determine the ratios of the three species. Complex **12** exhibits a ^{31}P shift at 182 ppm[31] while the Ir(I) sigma complexes show resonances in the 173.4-173.6 ppm range and ^{31}P signals of the Ir(III) oxidative addition adducts occur in the 171.7-173.3 ppm range. The ^{1}H NMR data, as well as a crystal structure of **14f** (see below), confirm the structural assignments of these species. The σ-complexes exhibit a broad 2H resonance around 5.2 ppm, distinct from the $ArNH_2$ resonance for free anilines, indicating these species are exchanging slowly on the NMR time scale. The ArNHIr ^{1}H signals for the oxidative addition adducts appear in the 3.0-5.6 ppm range and are paired with a Ir-H triplet (J_{PH} = 12.6-13.5 Hz) at high fields (-34.1 to -42.2 ppm range). The Ir hydride signal for **12** cannot be detected at room temperature due to rapid exchange with benzene via complex **10**.[31]

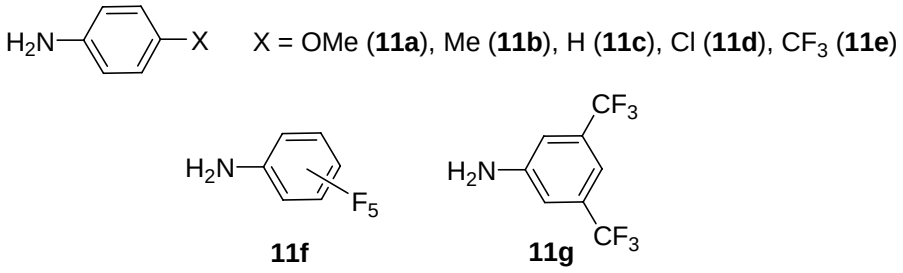

Figure 2.1. Anilines of varying electron withdrawing/donating ability (**11a-g**)

Scheme 2.8. Equillibria between (POCOP)Ir(H)(Ph) (**12**), (POCOP)Ir(NH_2Ar) (**13**), and (POCOP)Ir(H)(NHAr) (**14**)

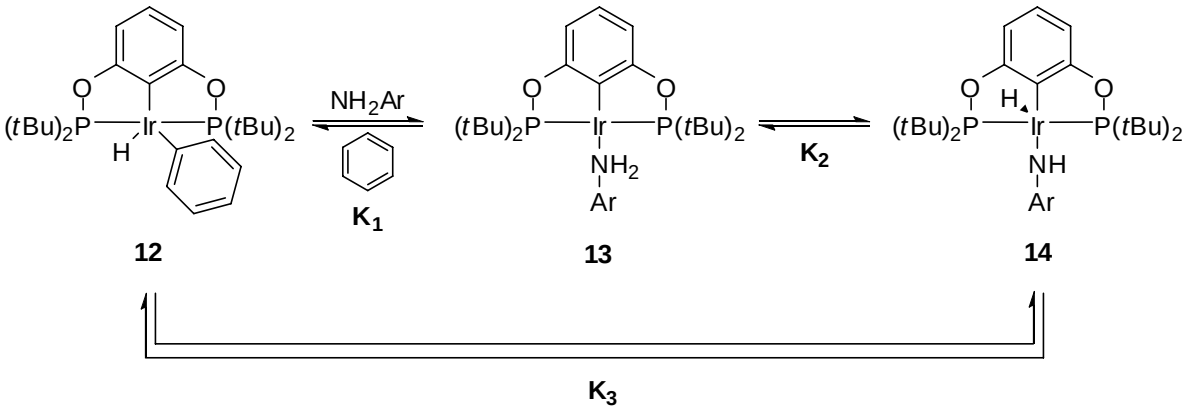

The equilibrium constants, K_1, K_2 and K_3 measured by ^{31}P NMR spectroscopy at 25°C are summarized in Table 2.1. For the electron-rich *p*-methoxyaniline **11a**, only the Ir(I) σ-adduct **13a** can be observed. As the substituents become more electron-withdrawing, the Ir(III) oxidative addition adduct becomes increasingly favored. For example, a 1:1 ratio of Ir(III):Ir(I) is now observed for *p*-chloroaniline **11d**. For even less electron-rich anilines **11e-g**, the Ir(I) species can no longer be spectroscopically detected and K_2 cannot be measured. The equilibrium constants K_3 between the aryl hydride and Ir(III) complexes can still be determined since benzene is in large excess relative to aniline and **12** can be detected. The reasons for the trends in these substituent effects will be discussed below.

Table 2.1. Equilibrium constants[a] for **12** + NH_2Ar ⇌ **13** + Benzene ⇌ **14** + Benzene at 25°C.

Aniline (**11**)	K_1	K_2	$K_3 = (K_1K_2)$
a	1130	—[b]	—[b]
b	456	0.04	18
c	188	0.1	19
d	55	1	55
e	—[c]	—[c]	260
f	—[c]	—[c]	2190
g	—[c]	—[c]	2770

a) Equilibrium values are based on an average of 2-3 runs.
b) Concentration of **14a** too low to detect
c) Concentrations of **13e-g** too low to detect

To confirm the structures of the anilino hydrides, a single crystal X-ray diffraction analysis of a crystal of **14f** grown from pentane at -35°C was carried out. An ORTEP diagram of the structure, including key bond distances and angles, is shown in Figure 2.2. The complex is square pyramidal with the hydride in an apical position. There is an empty coordination site *trans* to the hydride. The dihedral angle Ir(1)–N(1)–C(2)–C(7) is 32.5° indicating the arene ring sits approximately perpendicular to the square plane and the filled *p*-orbital on nitrogen lies parallel to the square plane. The N-H bond lies *anti* to the Ir-H bond (H-Ir(1)-N(1)-H dihedral angle = 177.3°), and thus there can be no N-H--H-Ir interaction as seen in related systems such the iridium complex shown in Figure 2.3.[32,33]

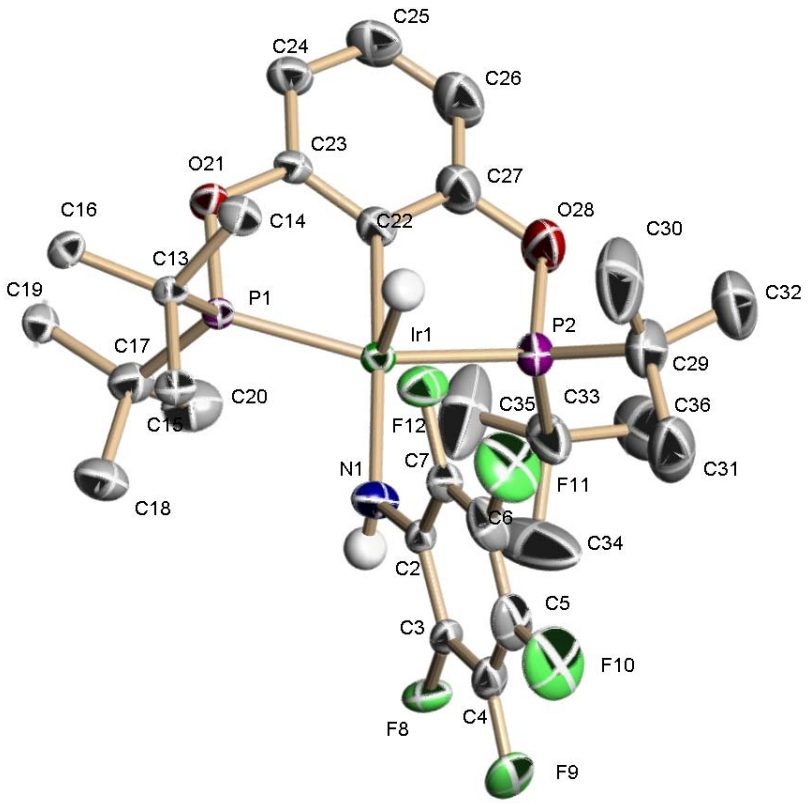

Figure 2.2. ORTEP diagram of **14f**. Only the hydrogens on iridium and nitrogen are shown for clarity. Key bond distances (Å) and bond angles (degrees): Ir(1)–N(1) 2.145 Å, N(1)–C(2) 1.348 Å, Ir(1)–C(22) 2.013 Å, Ir(1)–P(1) 2.294 Å, Ir(1)–P(2) 2.309 Å, C(22)–Ir(1)–N(1) 177.32°, P(1)–Ir(1)–N(1) 99.20°, P(2)–Ir(1)–N(1) 101.42°, Ir(1)–N(1)–C(2)–C(7) 32.5°, H-Ir(1)–N(1)–H 177.31°

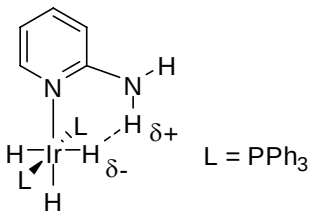

Figure 2.3. An example of an unconventional hydrogen bond by Crabtree et. al.

It is worth noting that the crystal structure of **14f** is representative of the (POCOP)Ir(III) complexes of the electron-withdrawing anilines **14e-g**. The ^{1}H resonance of the hydride in these complexes falls between -41 and -43 ppm, which is characteristic of hydride shifts in these (POCOP)Ir pincer complexes when there is an empty coordination site *trans* to the hydride. However, for the (POCOP)Ir(III) complexes of the less electron-withdrawing anilines **14b-d** the chemical shift for the hydride falls between -33.3 and -35.9 ppm. This surprisingly downfield chemical shift might be indicative of a change in orientation of the aniline substituent, where the hydride and the *N*-hydrogen are *cis* to each other with a possible hydrogen bonding interaction.[33] A corresponding shift in the ArN*H* signal occurs moving from ca. 3.0-4.4 ppm in the adducts involving electron-withdrawing anilines (**14e-g**) to 5.6 ppm for *p*-chloroaniline adduct **14d**.

By comparing the equilibrium data for reaction with aniline with those of Goldman and Hartwig,[27] it is clear that the more electron-withdrawing (POCOP) phosphinite Ir system more strongly prefers the Ir(I) oxidation state relative to the (PCP)Ir system. At room temperature, the reaction of **1** with $H_2NC_6H_5$ favors the oxidative addition product and forms only the Ir(III) anilino hydride complex. In benzene solution, an equilibrium is established between (PCP)Ir(H)(NHC_6H_5) and (PCP)Ir(H)(C_6H_5) with a K_{eq} of 105 favoring the formation of the iridium anilino complex.[27] In the POCOP system, reaction of **10** with $NH_2C_6H_5$ favors the Ir(I) σ-complex with an equilibrium ratio of Ir(I):Ir(III) complexes of ca. 10:1 (See Scheme 2.9). These results are also supported by IR data. Comparison of the IR stretching frequency of coordinated carbon monoxide in (POCOP)Ir(CO) (**15**) (υ_{co} = 1949 cm^{-1})[31] and (PCP)Ir(CO) (**16**) (υ_{co} = 1927.7 cm^{-1})[34] shows a higher frequency C≡O stretch for

15 than for **16**, indicating that the more electron-withdrawing ligand leads to a more electron-deficient metal center.

Scheme 2.9. Comparison of the reactions of (PCP)Ir(H)(Ph) (**3**) and (POCOP)Ir(H)(Ph) (**10**) with $NH_2C_6H_5$.

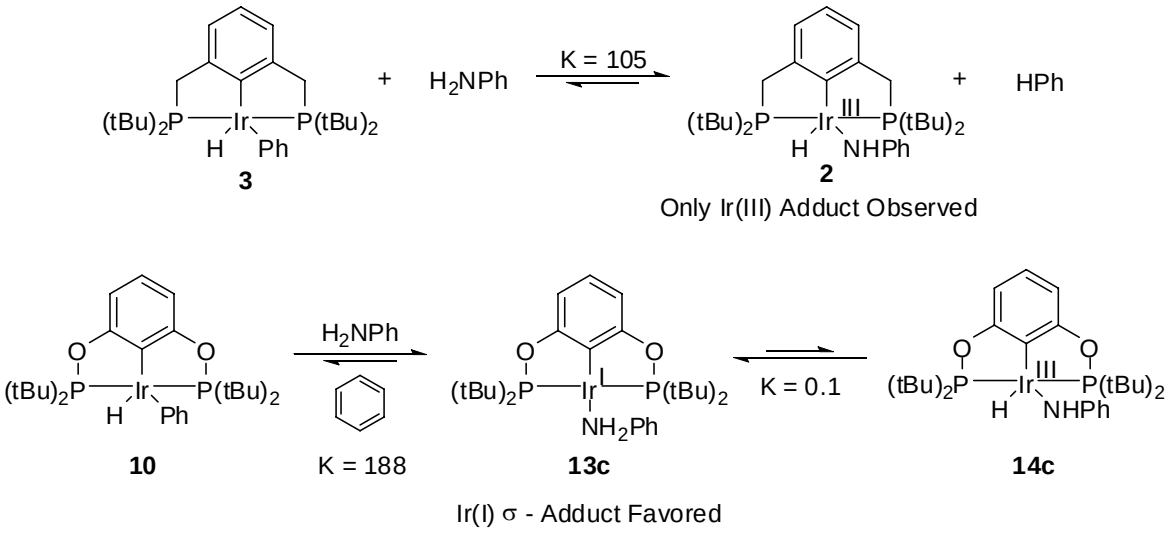

The increasing donor ability of the lone pair of electrons on the aniline is reflected, as expected, by the increasing stability of the Ir(I) σ-aniline complexes relative to the Ir(III) phenyl hydride complex (compare K_1 values, Table 1). The stability of the Ir(III) anilino hydride complexes relative to the Ir(III) phenyl hydride increases as the arene ring of the aniline becomes more electron-withdrawing (K_3 values). This behavior can be rationalized in two ways. In the d^6-Ir(III) complexes, **14**, all the $d\pi$ orbitals are filled and thus there are unfavorable p_π-d_π interactions[35,36] in **14e-g**. The crystal structure of **14f** shows that the Ir-N-C plane lies perpendicular to the Ir(III) square plane. As illustrated in Figure 2.4, there is repulsive interaction between the filled Ir d_{xy} orbital and the filled N p_y orbital. As the

arene becomes more electron-withdrawing, the energy of the p_y orbital is lowered and the destabilizing interaction is reduced. This can account for the substituent effect on relative stabilities. An alternative view is that the eletronwithdrawing-substituents stabilize the negative charge on the anilino ligand, enhancing the electrostatic interaction between the metal and the anilino group, thus strengthening the Ir-N bond.[37,38]

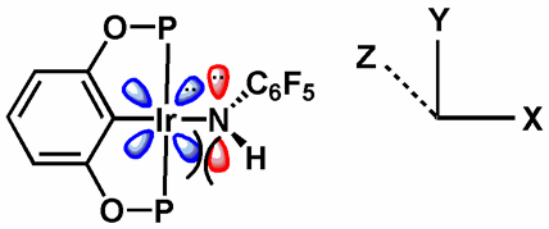

Figure 2.4. The destabilizing interaction between the filled N-π orbital (p_y) and the filled Ir d_{xy} orbital. (Apical hydride not shown)

b) Rates of oxidative addition of anilines to (POCOP) iridium pincer complexes.

Low temperature ^{1}H and ^{31}P studies showed that in the case of *p*-chloroaniline (which yields a 1:1 equilibrium mixture of **13d** and **14d**) the kinetic product of reaction with **10** is the σ-complex **13d**. Generation of the tolyl hydride complexes **17** (a mixture of the *meta* and *para* isomers[31]) in toluene was achieved in the usual way by reaction of the hydrochloride complex in toluene with NaO*t*Bu. Treatment of this solution with excess *p*-chloroaniline (10 equivs.) at -50°C initially yields only the σ-complex, **13d** (Scheme 2.10). Slow formation of the oxidative addition product **14d** is observed at this temperature. While it seems likely that the oxidative addition occurs directly from the σ-complex, we have no direct proof of this. After formation of the σ-complex **13d**, the rate of oxidative addition of the *p*-chloroaniline to form **14d** was measured at -12°C via ^{1}H low temperature NMR spectroscopy. The first-order

rate constant was found to be 4.8 x $10^{-4}s^{-1}$ with $\Delta G^{\ddagger}$ = 19.7 kcal/mol. (A sample of a first-order plot for the conversion of **13d** to **14d** can be found in Appendix I, Figure I.1)

Scheme 2.10. Formation of the (POCOP)Ir(NH_2(*p*-ClC_6H_4)) at low temperature followed by oxidative addition upon warming to form (POCOP)Ir(H)(NH(*p*-ClC_6H_4))

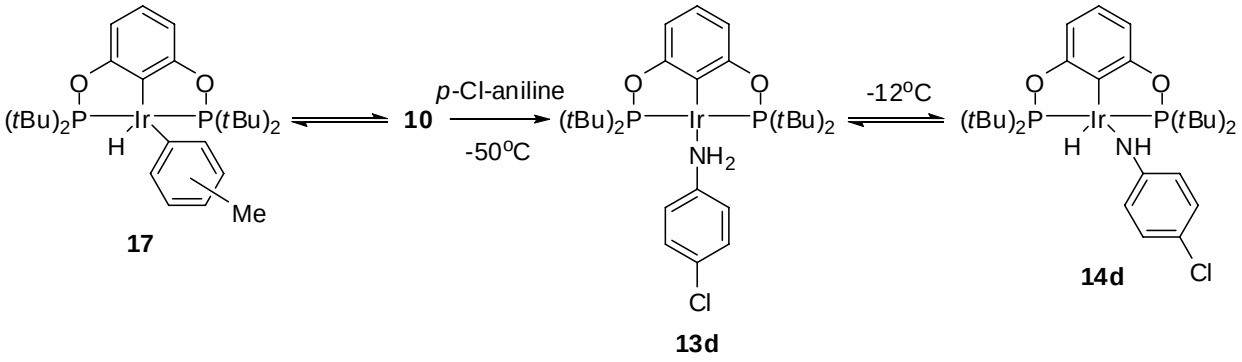

Similar low temperature experiments were conducted with 3,5-bis(CF_3)aniline **11g**. At the highest achievable concentrations of aniline, a trace of a species tentatively assigned to the σ-complex (^{31}P = 173.2, max concentration ca 3.0%) could be detected as a transient during reactions carried out at -37°C. (Scheme 2.11). These results are consistent with formation of the σ-complex as the kinetic product which never builds up to significant concentrations due to rapid oxidative addition to form **14g** (Path A). Again, we can not rule out direct formation of **14g** from reaction of **10** with **11g** (Path B).

Scheme 2.11. Possible mechanism for oxidative addition of **11g**.

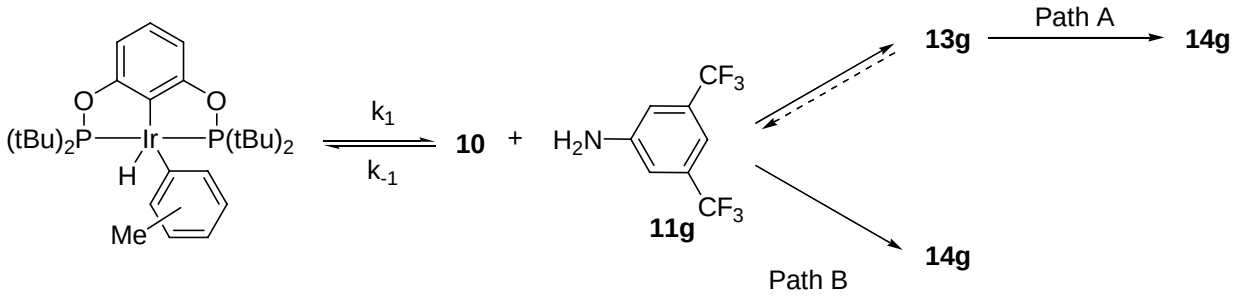

c) Rates of reductive elimination of electron-withdrawing anilines from five-coordinate (POCOP) iridium pincer complexes using ethylene as a trapping ligand.

The rates of reductive elimination of **14e**, **14f**, and **14g** were measured by heating the Ir(III) adducts in the presence of ethylene as a trapping ligand, L, to form the iridium(I) ethylene adduct **18**, as shown below in Scheme 2.12. Complexes **14e-g** were chosen for study since K_2 and K_3 are sufficiently large that the Ir(III) complexes can be prepared cleanly with no contamination by aryl hydride **12** or Ir(I) complexes. The trapping ligand must be chosen so that the 18-electron Ir(III) six-coordinate complex is not formed. A survey of several trapping ligands revealed that ethylene was ideal for this purpose (PMe_3 and carbon monoxide form the octahedral complexes **19**[39] and **20** prior to reductive elimination, see below).

Scheme 2.12. Reaction of **14** with ethylene, trimethylphosphine, and carbon monoxide

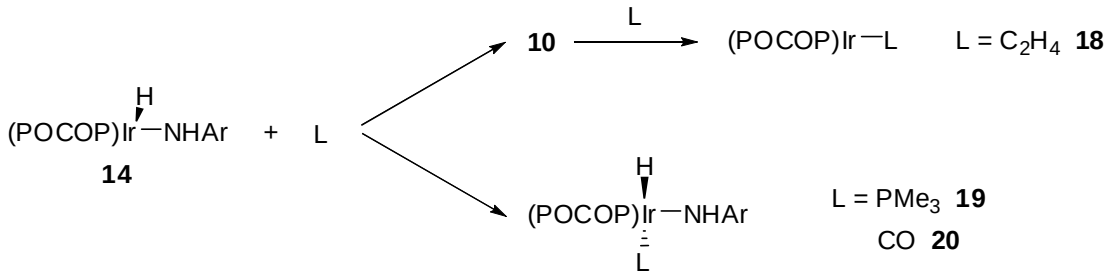

The disappearance rates of adducts **14e-g** were measured at 9 °C in the presence of excess ethylene and found to be independent of ethylene concentration (Scheme 2.13). Measured rate constants and free energies of activation are summarized in Table 2.2. A sample rate plot for the reductive elimination of pentafluoroaniline from **14f** can be found in Appendix I, Figure I.2.

Scheme 2.13. Reaction of **14e,f,g** with ethylene at 9°C to form **18**

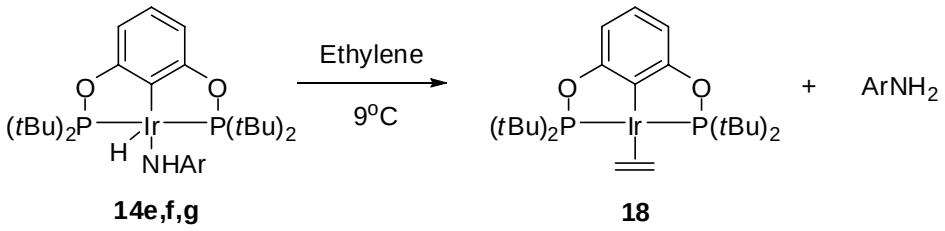

The reductive eliminations follow the same trend as the equilibrium reactions above; the more electron-withdrawing aniline reductively eliminates more slowly (Table 2.2). This is also evident by comparing the free energies of activation, $\Delta G^{\ddagger}$ values, for the reductive eliminations. As the electron-withdrawing ability of the aniline increases, the $\Delta G^{\ddagger}$ also increases from 20.8 kcal/mol for aniline **11e** to 22.1 kcal for **11g**.

Table 2.2. Rates of reductive elimination of anilines (**11e-g**) from (POCOP)Ir(H)(NHAr) at 9°C in toluene.

Ir(III) Complex	Concentration of C_2H_4, M	k, s^{-1} x 10^4	average k, s^{-1} x 10^4	$\Delta G^{\ddagger}$ kcal/mol
14e (0.022 M)	0.087	4.0	4.2	20.8
	0.28	4.4		
14f (0.022 M)	0.022	3.0	2.8	21.1
	0.19	2.6		
	1.1	2.8		
14g (0.036 M)	0.18	0.42	0.45	22.1
	0.34	0.47		

In order to determine if these barriers are the true barriers for reductive elimination of anilines from **14e-g**, several mechanistic scenarios, consistent with the observation that the rates of formation of ethylene complex **18** are independent of ethylene concentration, were considered. These are summarized in cases A-C in Scheme 2.14. In case A, slow reductive elimination leads *directly* to **10** followed by fast trapping by ethylene leading to formation of ethylene complex, **18**. In view of the above experiments with *p*-chloroaniline which suggest the σ-complex is the precursor to oxidative addition adducts, case A seems less likely than cases in which reductive elimination initially leads to the σ-complex. In case B, the σ-complex **13** is the precursor to **10** which is then rapidly trapped by ethylene. It is possible that the rate of formation of **13** is rate-determining (i.e., $k_2 > k_1, k_{-1}$) or that **13** and **14** are in equilibrium followed by slow formation of **10** ($k_2 < k_{-1}$). (In this latter case, the measured $\Delta G^{\ddagger}$'s do not correspond to the true barriers for reductive elimination of **14e-g**) In case C,

formation of **13** is rate-determining, followed by rapid associative displacement of the aniline by ethylene.

Scheme 2.14. Three possible mechanisms for the reductive elimination of NH_2Ar from **14**

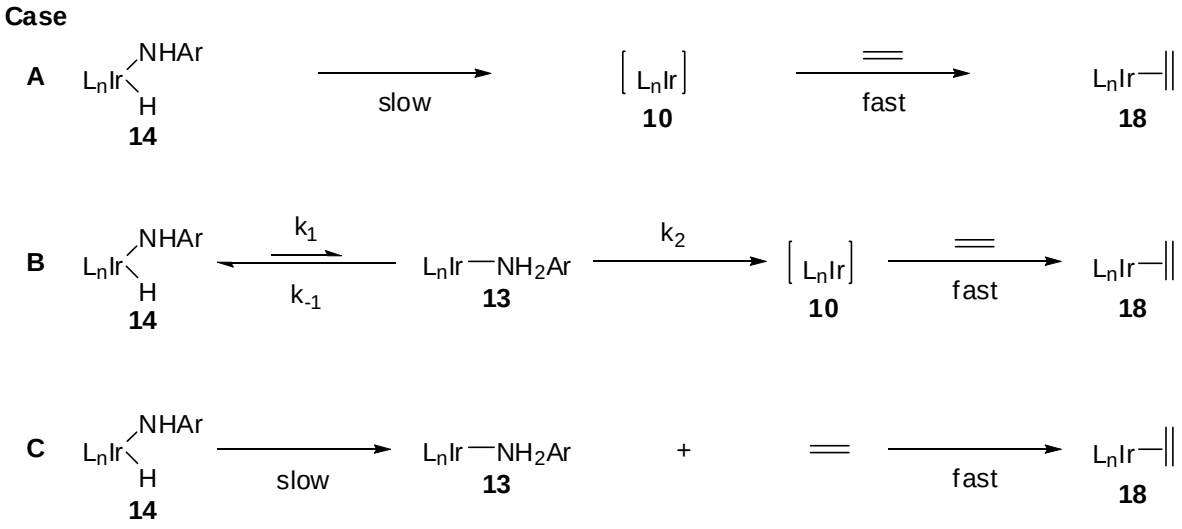

To probe whether displacement of anilines from **13** by ethylene is associative or dissociative we examined the reaction of **13a**, a system for which the σ-complex **13a** can be generated free of the Ir(III) oxidative addition adduct, **14a**. Generation of **13a** in toluene at room temperature followed by exposure to ethylene at -8°C results in quantitative formation of ethylene complex **18** (Scheme 2.15). A sample plot of this reaction can be found in Appendix I, Figure I.3.

Scheme 2.15. Displacement of $NH_2C_6H_4$-*p*OMe from **13a** with ethylene through a dissociative mechanism

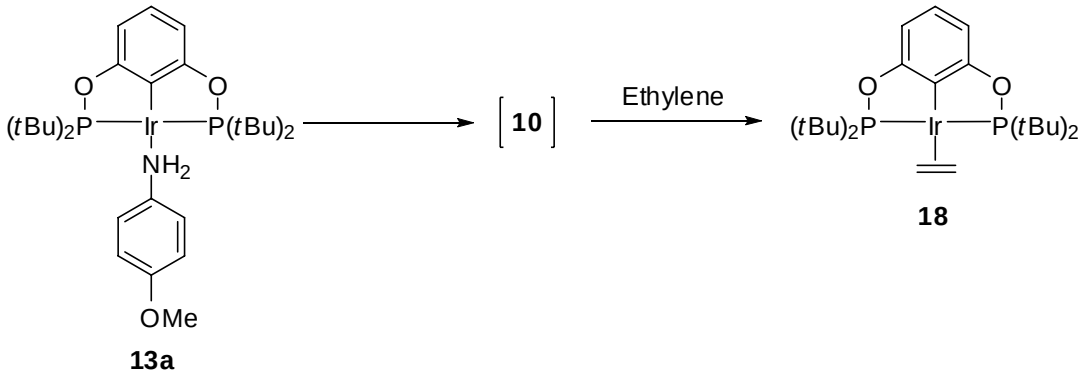

Using 0.015-0.019 M **13a** and excess ethylene concentrations of 0.25 M and 0.48 M, clean first-order kinetics are observed at -8°C with measured rate constants of 3.3 x 10^{-4} s^{-1} and 2.7 x 10^{-4} s^{-1}, respectively. No dependence of the rate on ethylene is observed which implies that dissociation of *p*-methoxyaniline from **13a** is rate-determining with a free energy of activation, $\Delta G^{\ddagger}$, of 19.8 kcal/mol. This result rules out case C above and indicates case B as the most likely choice.

In examining case B more closely, it is instructive to consider free energy diagrams for both the *p*-chloroaniline system **13d**/**14d** and **14e-g** (for simplicity consider **14f** as representative of **14e-g**). (Figure 2.5 and 2.6) In the case of **13d**⇌**14d**, K_{eq} = 1; therefore, barriers for reductive elimination and oxidative addition are the same, 19.7 kcal/mol. Now consider **14f**. Since **14f** is somewhat more stable than **13f** one would expect the $\Delta G^{\ddagger}_{1}$ to be slightly greater than 19.7 kcal/mol, say 19.7 + δ, and $\Delta G^{\ddagger}_{-1}$ to be slightly less, 19.7 - δ', as shown in Figure 2.6. Since $(CF_3)_2C_6H_3NH_2$ is a poorer donor than *p*-methoxyaniline, the barrier for dissociation from (POCOP)Ir should be somewhat less than the 19.8 kcal/mol measured for **13a**, designated in Figure 2.6 as 19.8 – δ". It is difficult to predict whether δ' or

δ" is larger and thus which transition state, TS_1 or TS_2, is higher in energy, but it is likely that the difference is quite small. The $\Delta G^{\ddagger}_1$ for **14f** cannot exceed 21.1 kcal/mol (see Table 2.1) but is certainly greater than 19.7 kcal/mol and thus is narrowly bracketed. In view of this analysis the $\Delta G^{\ddagger}$ values in Table 1 likely reflect fairly accurately the barriers for reductive elimination of **14e-g**.

Figure 2.5. Reaction coordinate diagram for the interconversion of **13d** and **14d**

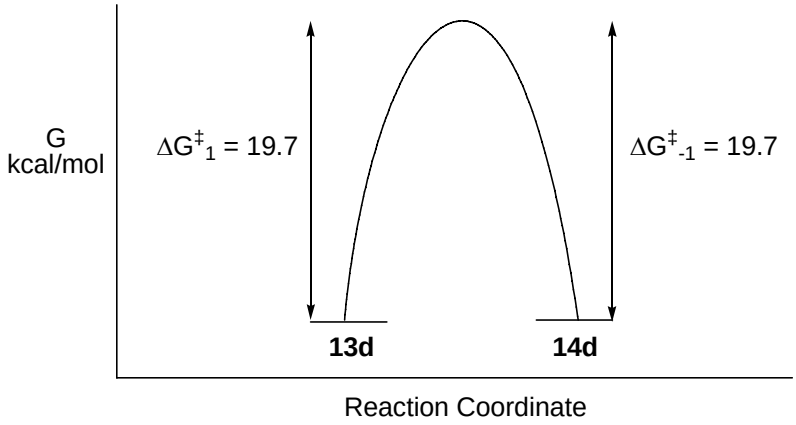

Figure 2.6. Reaction coordinate diagram for the conversion of **14f** to **18**

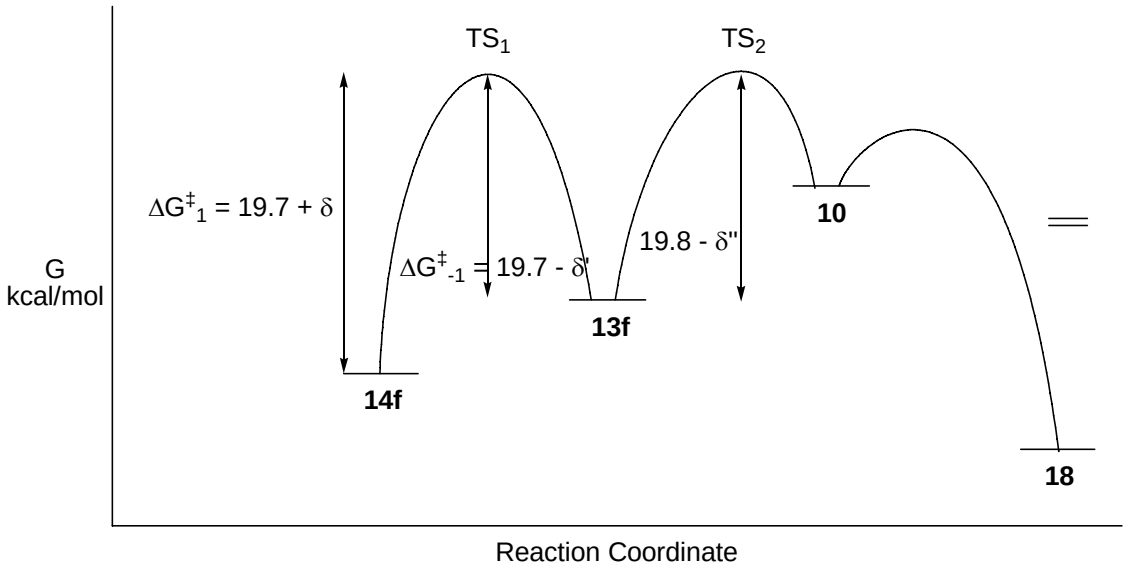

It is informative to compare the barriers of reductive elimination observed here which are in the 21-22 kcal/mol range to the barrier of reductive elimination of (POCOP)Ir(H)(Ar') (Ar'- = 3,5-$Me_2C_6H_3$-) of 14.1 kcal/mol.[40] This likely reflects a stronger Ir-N bond relative to the Ir-C bond.[37]

d) Reaction of (POCOP)Ir(H)(NHAr) complexes (14e,f) with carbon monoxide

Generation of the tolyl hydrides **17** at -78°C as described above followed by treatment with $C_6F_5NH_2$ (ca. 1.1 equiv.) and CO resulted in formation of (POCOP)Ir(CO)(H)(NHC_6F_5), **20f**, as the major product via CO trapping of **14f**. (Minor amounts of (POCOP)IrCO, **15**, are formed presumably by CO displacement of aniline from (POCOP)Ir($NH_2C_6F_5$) since reductive elimination of aniline from either **14f** or **20f** is very slow at -78°C.) Removal of toluene and addition of a minimal amount of pentane at -78°C resulted in the precipitation of **20f** in low yield. Key NMR parameters of **20f** include a ^{31}P signal at 157 ppm and a ^{1}H resonance for the iridium hydride at -8.6 ppm. The downfield hydride shift is indicative of ligand coordination *trans* to the apical hydride. A solution of **20f** in toluene at 25°C undergoes slow reductive elimination; (POCOP)Ir(CO) and free pentafluoroaniline are visible by ^{1}H NMR spectroscopy after 18 hours.

X-ray quality crystals of **20f** were obtained through slow crystallization from pentane at -35°C. The ORTEP diagram of **20f** (Figure 2.7) indicates an Ir(III) octahedral complex with the CO bound in an apical site *trans* to the hydride and the aniline ligand *trans* to C_{ipso}. Since the crystal structure of **14f** showed an empty coordination site in the position *trans* to the hydride, CO coordination to this site is consistent with rapid addition of CO to generate **20f** as the kinetic product. Interestingly, there is a change in the orientation of the aniline

ligand upon binding of CO. As mentioned earlier, in **14f** the dihedral angle H-Ir(1)-N(1)-H was 177° with the hydride and *N*-H *trans* to each other. The dihedral angle H(1)-Ir(1)-N(11)-H(11) in **20f** after CO coordination is now 42°, indicating that the aniline ligand has rotated ca. 125° and the hydride and *N*-H are now nearly *cis* to each other.

Reaction of (POCOP)Ir(H)(NHAr-*p*CF_3) (**14e**) with CO was also investigated. Complex **14e** was generated *in situ* at 25°C by treatment of tolyl hydrides **17** with $CF_3C_6H_4NH_2$ (ca. 1.5 equiv) at 25°C. Cooling the toluene solution to -78°C and purging with CO resulted in formation of four complexes. The major product was the expected CO addition product, (POCOP)Ir(H)(CO)(NHC_6H_5-*p*CF_3), **20e**. The ^{1}H and ^{31}P NMR data support a structure analogous to **20f**. Two minor complexes corresponded to *para* and *meta* tolyl hydride carbonyl complexes (POCOP)Ir(tolyl)(H)(CO). These structures were fully characterized by 2D ^{1}H NMR spectroscopy and independently generated by treatment of **17** with CO. Distinct ^{1}H NMR signals for these complexes are the downfield shifts (8.05-8.16ppm) of the aryl protons *ortho* to Ir, and the two Ir hydride triplets at -8.69 and -8.70ppm. The fourth complex, also verified by independent synthesis, is (POCOP)Ir(H)(Cl)(CO) from CO trapping of unreacted starting material. By increasing the concentration of aniline used, formation of the tolyl complexes was inhibited. We were unable to crystallize **20e** and column chromatography resulted in its decomposition.

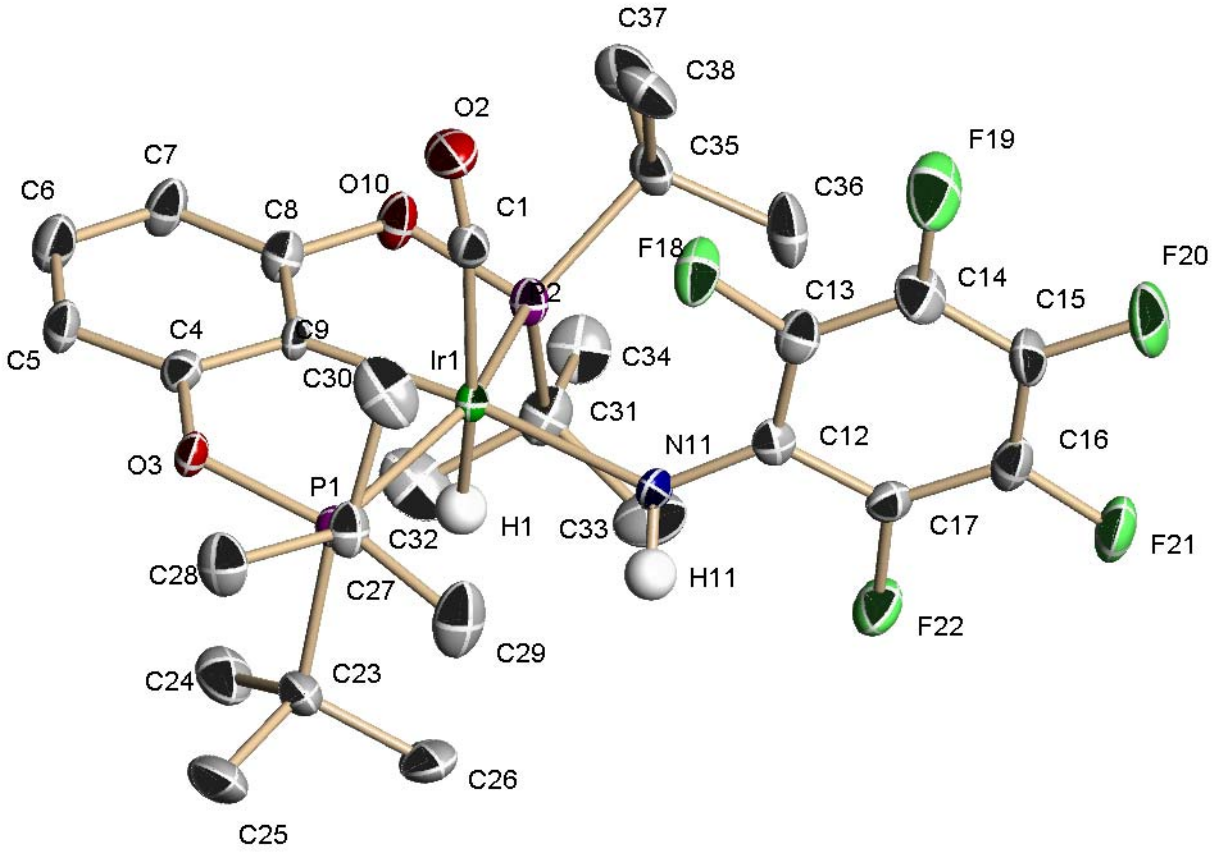

Figure 2.7. ORTEP diagram of (POCOP)Ir(H)(CO)(NHC_6F_5) (**20f**). Only the hydrogens on iridium and nitrogen are shown for clarity. Key bond distances (Å) and bond angles (degrees): Ir(1)–N(11) 2.168 Å, N(11)–C(12) 1.361 Å, Ir(1)–C(9) 2.046 Å, Ir(1)–P(1) 2.337 Å, Ir(1)–P(2) 2.329 Å, H(1)-Ir(1)–N(11)–H(11) 42.22°, C(9)–Ir(1)–N(11) 173.3°, P(1)–Ir(1)–N(11) 98.82°, P(2)–Ir(1)–N(11) 100.97°, Ir(1)–N(11)–C(12)–C(13) 139.79°.

Complex **20e** undergoes reductive elimination at a much slower rate than the five-coordinate analogue **14e**. Heating an *in situ* generated toluene-d_8 solution of (POCOP)Ir(H)(CO)(NHAr-*p*CF_3), **20e**, at 63°C results in the formation of (POCOP)Ir(CO) and free 4-trifluoromethylaniline. In contrast, reductive elimination of five-coordinate **14e** occurs at 9°C. A detailed kinetic analysis of the reductive elimination was not carried out due to the difficulties in preparing **20e** cleanly and complications due to the presence of excess product aniline. However, qualitatively the rate of reductive elimination is retarded

when carried out under 1-3 atmospheres of carbon monoxide. This is consistent with loss of CO to form five-coordinate **14e** prior to reductive elimination as might be expected based on previous work concerning reductive elimination of six-coordinate Pt(IV) complexes.[41]

e) Reductive elimination of $NH_2C_6H_4$-*p*CF_3 from 6-coordinate (POCOP)Ir(H)(NHAr)(CO)

Although there are some examples of reductive elimination occurring directly from a d^6 six-coordinate species, the majority of reductive eliminations occur after ligand dissociation to generate a five-coordinated complex prior to reductive elimination. This phenomenon has been extensively documented and reviewed by Goldberg.[41] For example, it has been shown that the six-coordinate (dppe)$PtMe_4$ (dppe = $Ph_2PCH_2CH_2PPh_2$) complex reductively eliminates ethane after the dissociation of a chelating arm of the dppe ligand at high temperatures (165°C-205°C). When a more rigid chelating ligand dppbz (dppbz = *o*-$PPh_2(C_6H_4)PPh_2$) is used a depression of the rate is observed.[41,42] This supports the proposed mechanism since a more rigid ligand would be harder to dissociate. Whether dissociation prior to reductive elimination occurs depends on the coordination strength and/or chelating strength of the ligand, as well as, how facile the reductive elimination is (i.e. C-H reductive elimination typically has a lower energy barrier than C-C reductive elimination).[41] For example, the rates of reductive elimination of methane from *fac*-(dppe)$PtMe_3H$ and *fac*-(dppbz)$PtMe_3H$ at room temperature were of similar rates. Therefore, the rigidity of the chelating ligand is not a factor in the rate, indicating that the C-H reductively elimination via a direct elimination mechanism.[41] On the other hand, C-H reductive elimination by $Tp^{Me2}Pt(CH_3)H$ (Tp^{Me2} = hydridotris(3,5-dimethylpyrazolyl)borate) occurs through a five-coordinate Pt complex after dissociation of an arm of the Tp^{Me2} ligand.[43]

For Ir(III), Rh(III), Os(II), and Ru(II) systems, mechanisms for both direct elimination and dissociation prior to reductive elimination have both been described in the literature.[41] Therefore, it was of interest to investigate the mechanism of N-H reductive elimination from the d^6 six-coordinate iridium complex, (POCOP)Ir(H)(CO)(NHC_6H_4-*p*CF_3) **20e**. Schemes 2.16 and 2.17 illustrate the two possible mechanisms for reductive elimination of NHC_6H_4-*p*CF_3 from **20e**.

Scheme 2.16. Direct reductive elimination of NHC_6H_4-*p*CF_3 **11e** from (POCOP) Ir(H)(CO)(NHC_6H_4-*p*CF_3) **20e**

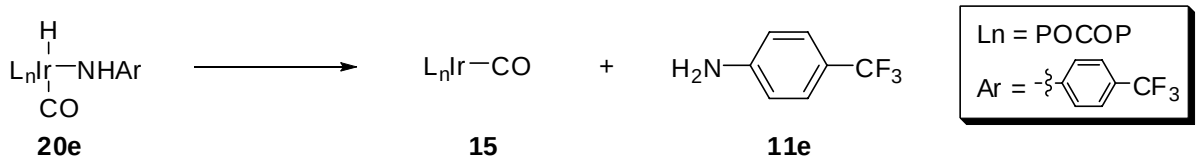

Scheme 2.17. Mechanism for the reductive elimination of **11e** from **20e** via dissociation of CO prior to reductive elimination

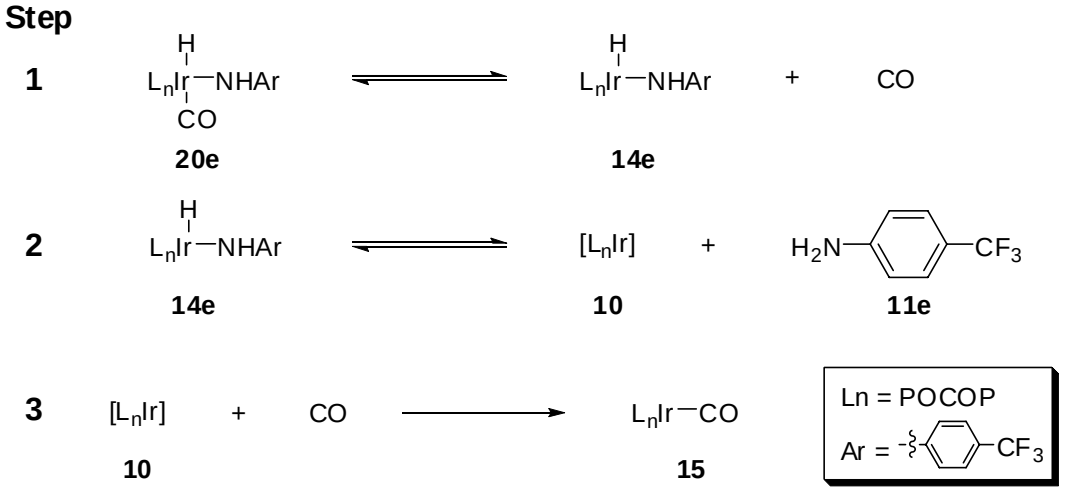

The course of reductive elimination of **11e** was monitored using variable temperature NMR spectroscopy under varying carbon monoxide pressures and varying concentrations of aniline **11e**. In order to accurately compare the reactions, J. Young tubes were used to maintain constant CO pressure throughout the reactions. Each NMR tube was charged with 0.03 mol/L of **20e** in toluene-d^8, after which **11e** and/or CO was added to the reaction mixture. The reductive elimination was monitored by measuring the decrease in integration of either an aniline aryl resonance or the NH resonance of **20e** in the ^{1}H NMR spectrum at 345K

While keeping the concentration of aniline constant, the half-life ($t_{1/2}$) for the reductive elimination increases as more carbon monoxide is introduced into the system (Table 2.3). This shows an inverse dependence of the reaction rate on CO concentration, indicating that CO must reversibly dissociate from the metal center. This effect is graphically represented in Figure 2.8. As mentioned above the dissociation of CO is not unexpected based on previous studies by Goldberg et. al.[41] If this was a simple inverse first-order dependence on CO concetration, the half-life should increase by the same factor that the carbon monoxide pressure increased. By comparing entries 1-4 and 6-7 in Table 2.3, it is clear that this is not the case. The half life increases as the concentration of carbon monoxide increases, but by less than expected for an inverse first-order dependence.

Table 2.3. Qualitative comparison of the half-lives for the reductive elimination of NH_2Ar from a 6-coordinate iridium complex at 345K

Entry	P_{CO} (atm)	11e (M)[a]	1^{st} $t_{1/2}$ (s)
1	0	0.060	2193
2	1	0.067	2669
3	2	0.064	3170
4	3	0.064	3533
5	0	0.20	4943
6	0	0.63	7547
7	3	0.63	14729

a) Concentration of **11e** at the start of the reaction.
b) $[Ir]_0 = 0.03$ mol/L

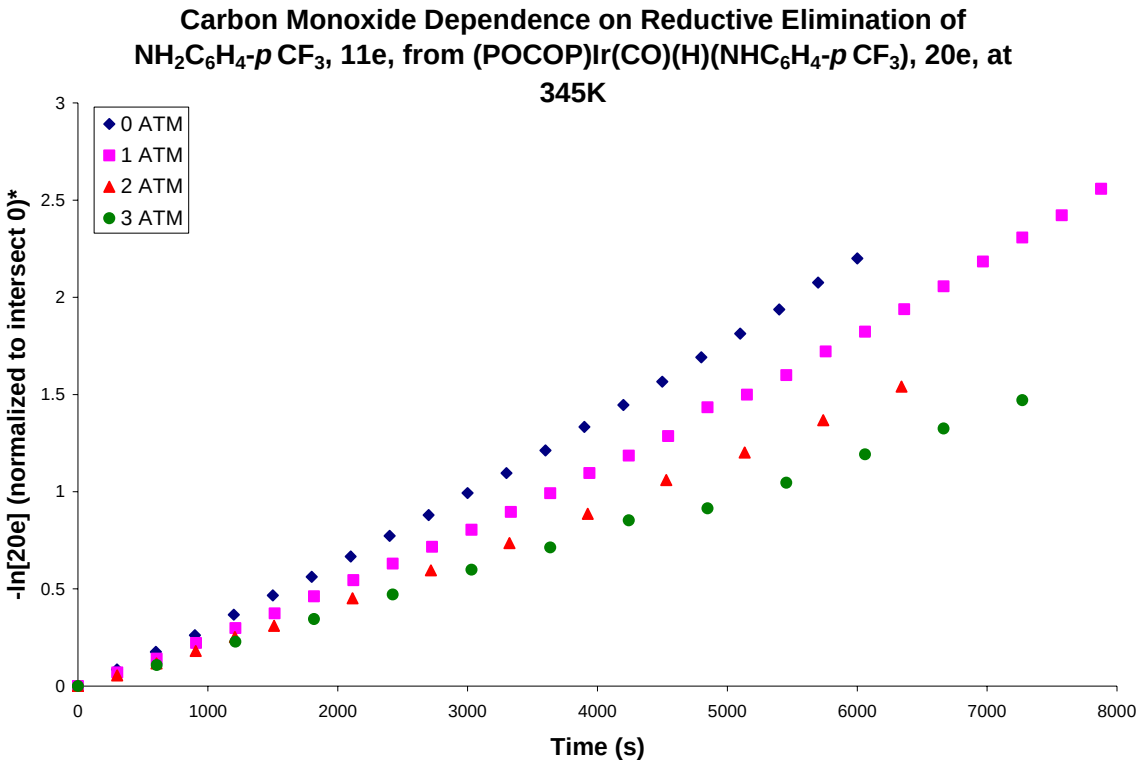

* To account for slight difference in concentrations, the value at t_0 was subtracted out to force the curve through the 0,0 point. This allows for an easier comparison.

Figure 2.8. Graphical depiction of the depression of rate as the concentration of carbon monoxide increases for the reductive elimination of $NH_2C_6H_4$-*p*CF_3 from **20e**

When the CO pressure remains constant while the concentration of **11e** is varied, an increase in $t_{1/2}$ is also observed, indicating that the aniline concentration is also part of the rate expression. These results are shown in Table 2.3 as a simple half-life value, as well as graphically in Figure 2.9. A comparison of entries 4-6 in Table 2.3 shows an increase in half-life as the concentration of **11e** increases, but as in the case for carbon monoxide, this rate is not a simple inverse first-order dependence on **11e**

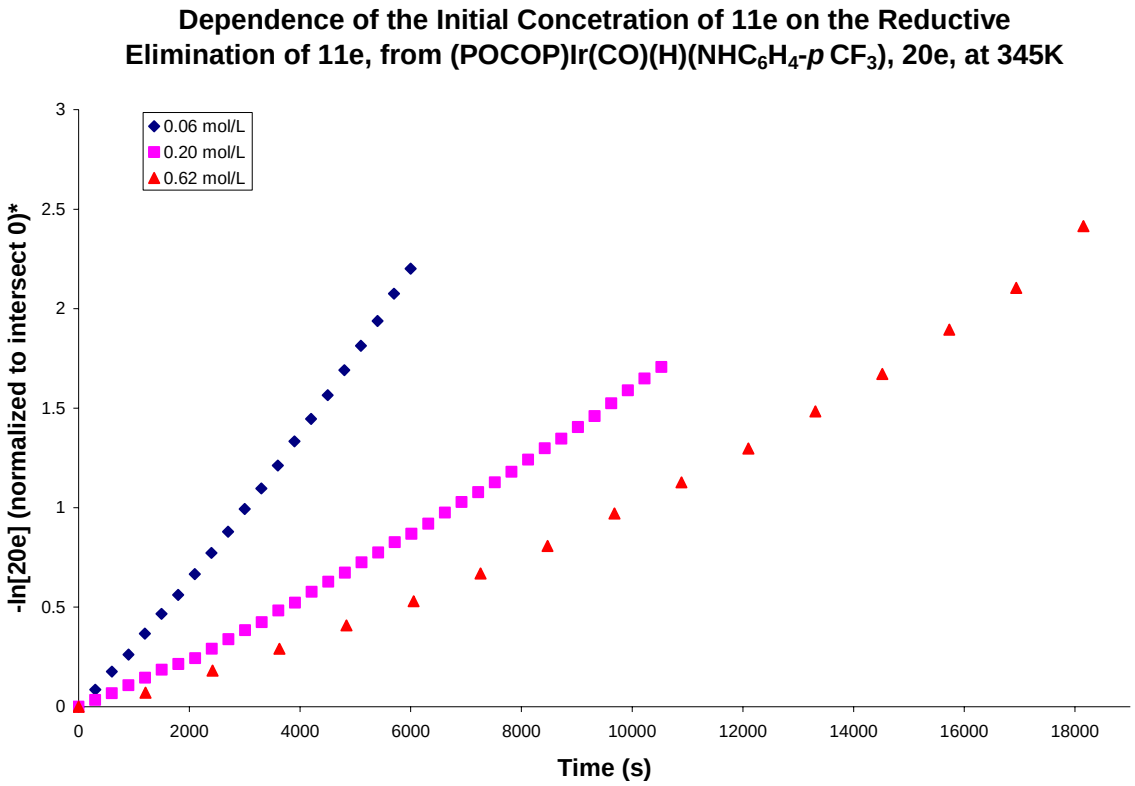

* To account for slight difference in concentrations, the value at t_0 was subtracted out to force the curve through the 0,0 point. This allows for an easier comparison.

Figure 2.9. Graphical depiction of the depression of rate as the concentration of $NH_2C_6H_4$-*p*CF_3 increases for the reductive elimination of $NH_2C_6H_4$-*p*CF_3 from **20e**

The dependence on carbon monoxide concentration rules out the direct reductive elimination mechanism, suggesting that reversible CO dissociation must occur prior to reductive elimination. However, it is not immediately evident, given a rate suppression by both CO and aniline **11e**, how the results fit with the mechanism shown in Scheme 2.17 and what step is the rate-determining step. To gain a qualitative insight into the mechanism, energy diagrams describing the possible mechanistic scenarios are analyzed (Figures 2.10-2.12)

Figure 2.10 describes a situation where the first step is reversible and reductive elimination of **11e** is rate-determining. If this were the case, the rate would be inversely proportional to

the CO concentration (Rate ≈ 1/[CO]) and there would be no dependence on the concentration of aniline. This scheme does not fit the experimental observations.

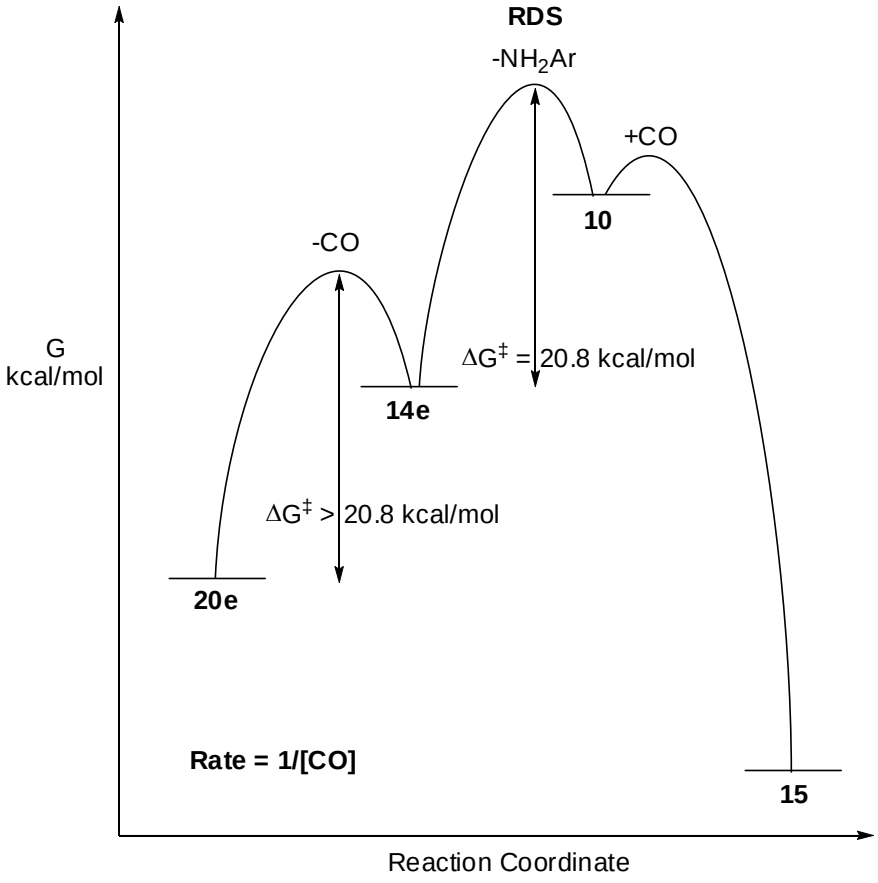

Figure 2.10. Free energy diagram of the reductive elimination of **11e** from **20e** where the first step is reversible and reductive elimination of **11e** is rate-determining

A second possibility is shown in Figure 2.11, where both steps 1 and 2 are reversible and the re-coordination of carbon monoxide (step 3) is the rate-determining step. In this case the rate is only inversely proportional to the concentration of aniline (Rate ≈ 1/[**11e**]). The concentration of carbon monoxide does not affect the rate since both its dissociation and association to iridium are included in the rate expression and therefore cancel each other out.

Since a inverse dependence on carbon monoxide is observed, however, step 3 as the rate-determining step can be ruled out as well.

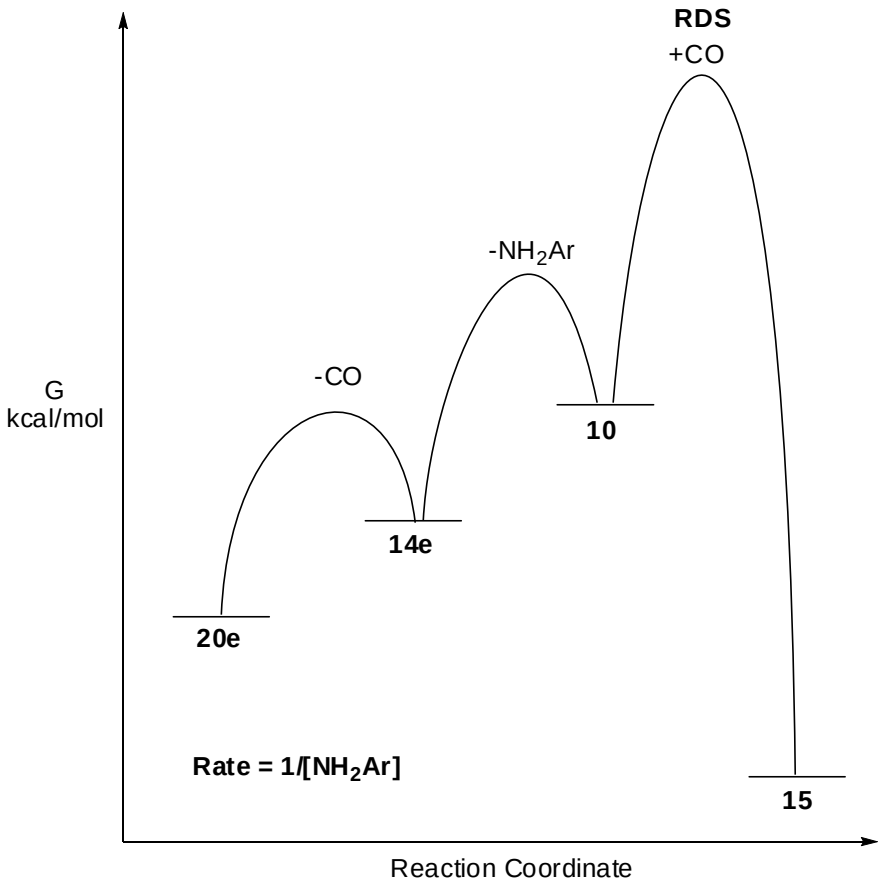

Figure 2.11. Free energy diagram of the reductive elimination of **11e** from **20e** if re-coordination of CO is the rate-determining step

A qualitative explanation which fits the observed rate data is a reaction in which the $\Delta G^{\ddagger}$ for both the reductive elimination of aniline **11e** and the re-coordination of CO are similar. (Figure 2.12) In this case, there is no clear rate-determining step and a rate suppression by both CO and **11e** would be expected but in each case the rate dependence would be less than full inverse first-order.

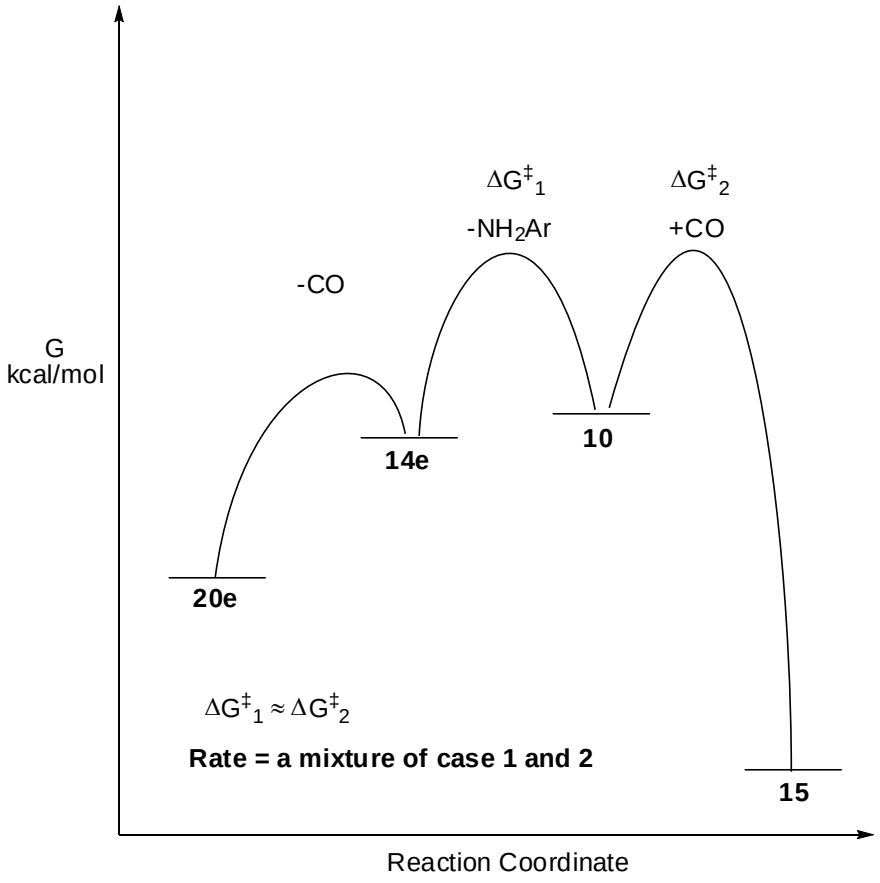

Figure 2.12. Free energy diagram of the reductive elimination of **11e** from **20e** if the reductive elimination of aniline and re-coordination of CO had similar $\Delta G^{\ddagger}$.

II) Reaction of the (POCOP)Ir pincer complex with benzamides $C_6H_5(CO)NH_2$ (21a) and $C_6F_5(CO)NH_2$ (21b)

Reaction of (POCOP)Ir, **10**, (generated by reaction of (POCOP)Ir(H)(Cl), **9**, with NaO*t*Bu) with $NH_2(CO)C_6H_5$, **21a**, and $NH_2(CO)C_6F_5$, **21b**, yields Ir(III) oxidative addition adducts **22a,b** (Scheme 2.18). These adducts are substantially more stable than the anilino hydrides and can be readily isolated as stable solids at room temperature.

Scheme 2.18. Formation of benzamide complexes **21a,b** from (POCOP)Ir(H)(Cl) and NaO*t*Bu

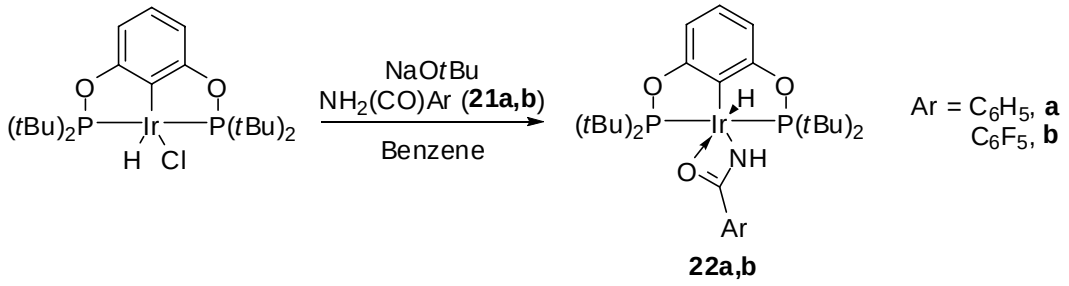

22a,b

An X-Ray diffraction study was carried out on a crystal of **22b** obtained from pentane at -35°C. The ORTEP diagram is shown in Figure 2.13 along with key bond distances and angles. Like the anilino complexes, the amide nitrogen lies in the square plane *trans* to C_{ipso} of the aryl ring of the POCOP ligand. The N-C-O amide plane is perpendicular to the iridium square plane with the carbonyl oxygen *anti* to the axial Ir-H. The Ir-O bond distance of 2.55 Å suggests weak coordination of the amide oxygen to the open axial site *trans* to hydride. It is of interest to compare the iridium-oxygen bond distance in **22b** with Ir-O distances in other iridium amide complexes **23**[44], **24**[45], **25**[46] shown in Figure 2.14. In the eighteen-electron Ir(III) complexes **23** and **24** the Ir-O distances of 3.401A and 3.412A clearly show no Ir-O interaction. The Ir(III) complex **25** is formally a sixteen-electron

complex in the absence of a Ir-O interaction. The Ir-O distance of 2.290 Å is considerably shorter than the Ir-O distances in **23** and **24** and clearly suggests a significant bonding interaction. The fact that the amide in **25** is an alkyl amide with a much more basic oxygen then that in the benzamide of **22b** with a strongly electron-withdrawing C_6F_5 group may in part account for the shorter Ir-O distance in **25**.

The ^1H chemical shifts of the hydride ligands in **22a** and **22b** also support an axial Ir-O interaction. (POCOP)Ir hydride complexes with an empty coordination site *trans* to hydride exhibit hydride shifts in the -41 ppm range. In six-coordinate complexes the hydride shifts to much lower values. For example, in carbonyl adduct **20f**, the ^1H shift is -8.56. The intermediate shifts of the hydrides in **22a** and **22b** of -30.25 and -35.72 support a significant Ir-O interaction. The higher field shift of -35.7 ppm in **22b** suggests a decreased Ir-O interaction compared to **22a**, consistent with a decreased oxygen basicity due to the strongly electron-withdrawing C_6F_5 group.

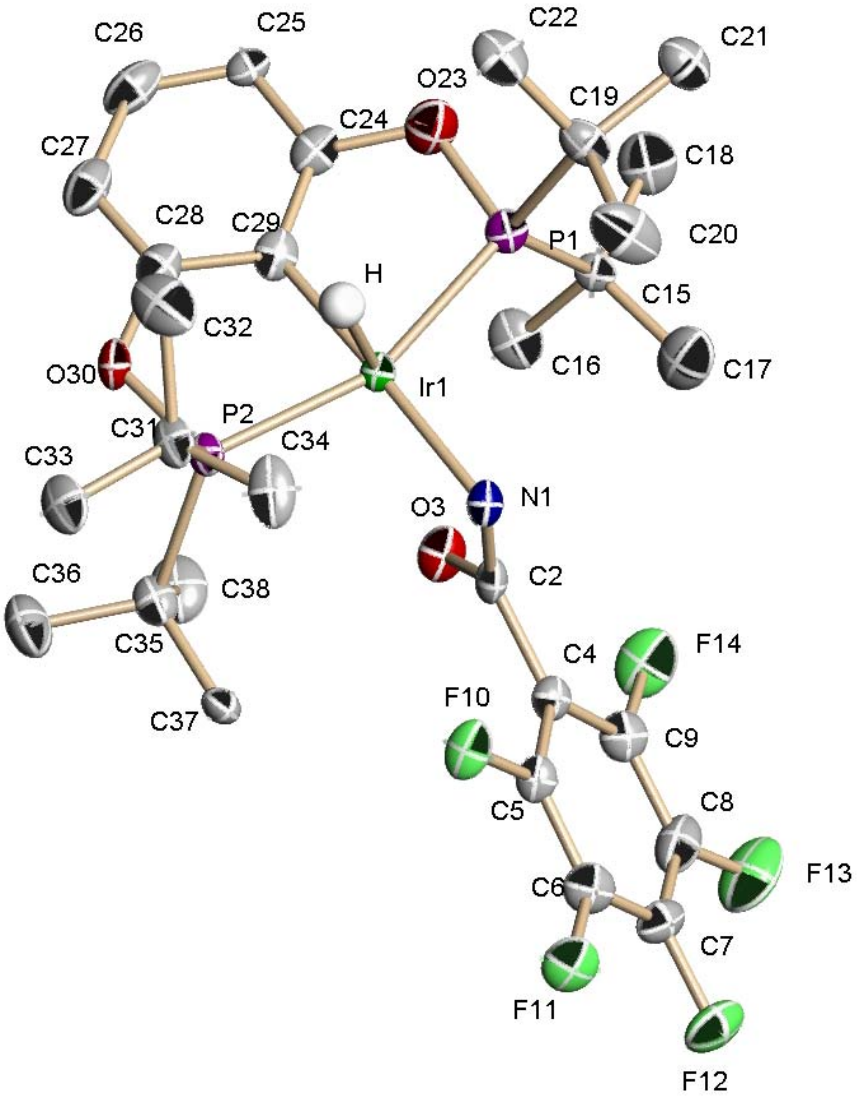

Figure 2.13. ORTEP diagram of (POCOP)Ir(H)(NH(CO)C_6F_5) (**22b**). Only the hydrogens on iridium are shown for clarity. Key bond distances (Å) and bond angles (degrees): Ir(1)–N(1) 2.171 Å, N(1)–C(2) 1.279 Å, Ir(1)–C(29) 2.034 Å, Ir(1)–P(1) 2.412 Å, Ir(1)–P(2) 2.359 Å, H(1)-Ir(1)–N(1)–H(2) -18.67°, C(29)–Ir(1)–N(1) 176.66°, P(1)–Ir(1)–N(1) 104.30°, P(2)–Ir(1)–N(1) 96.77°, Ir(1)–N(1)–C(2)–C(4) -175.64°

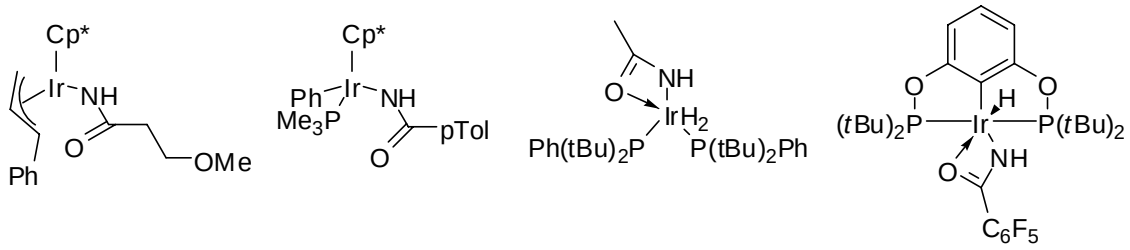

	23 (ref. 37)	24 (ref. 38)	25 (ref. 39)	22b
Ir-O distance Å	3.401Å	3.412Å	2.290Å	2.550Å

Figure 2.14. Comparison of Ir-O bond distances with complexes found in the literature

a) Rates of reductive elimination of $H_2N(CO)C_6H_5$ from (POCOP)Ir(H)(NH(CO)C_6H_5) complexes

Since benzamides form significantly more stable Ir(III) species than their analogous anilino complexes, the rates of reductive elimination were measured at 100°C. Ethylene proved to be a poor choice for a trapping ligand since ethylene concentrations were difficult to control at elevated temperatures. Therefore, triphenyl phosphine which competes reversibly with benzamide for coordination to irdium was used. The equilibrium between (POCOP)Ir(H)(NH(CO)Ph), **22a**, + PPh_3 and (POCOP)Ir(PPh_3) + $H_2N(CO)C_6H_5$ as shown in Scheme 2.19 was measured at three different concentrations of PPh_3 (0.29, 0.59, and 1.18 M) at 100°C. From these data a K_{eq} of 0.18 favoring **22a** was calculated. For the more electron-withdrawing pentafluorbenzamide complex **22b**, the equilibrium constant decreases to 0.07 consistent with the substituent effects observed in the aniline equilibrium studies. At room temperature a one to one ratio of benzamide **21a** (0.0094 M) and triphenylphoshine (0.0094 M) was added to **10** (0.0046 M), generated in the usual manner. ^{31}P NMR analysis showed the formation of **22a** and **26** in a ratio of 2:1. Since interconversion of these species is slow

at 25°C, this ratio represents kinetic trapping and differs from the thermodynamic ratio of ca. 6:1.

Scheme 2.19 Equilibrium between **22a,b** + PPh_3 and **26** + $NH_2(CO)Ar$

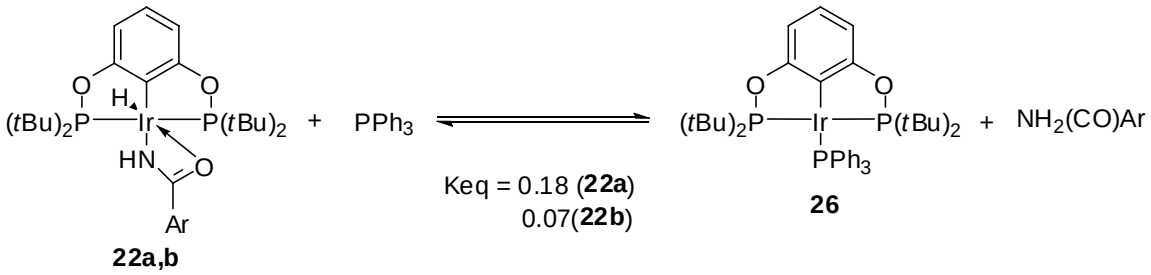

22a,b **26**

Generating **22a** and analyzing the reversible reaction (Scheme 2.19) in the presence of 10 equiv. of **21a** and 10 equiv. of PPh_3, the half-life for reductive elimination of benzamide was found to be ca. 1.7 hours, corresponding to a $\Delta G^{\ddagger}$ of ca. 29 kcal/mol. (A sample first-order rate plot of this reaction is shown in Appendix I, Figure I.4.) This increased barrier to reductive elimination of benzamide relative to that for anilines is due to stronger binding of the benzamido fragment to (POCOP)Ir. The Ir-O interaction as well as a decrease in the repulsive *dπ-p* interaction as a result of the electron-withdrawing ability of the acyl moiety can account for the increased binding energy.

Summary

Reaction of a series of anilines **11a-g** with (POCOP)Ir(C_6H_5)(H), **12**, leads to equilibrium mixtures of **12**, the Ir(I) σ-complexes (POCOP)Ir(NH_2Ar), **13**, and the Ir(III) oxidative addition adducts (POCOP)Ir(H)(NHAr), **14**. Previous studies have shown that **12** undergoes rapid reductive elimination of benzene to form the 14-electron species (POCOP)Ir, **10**, so

complexes **13** and **14** arise from reaction of anilines with **10**. Equilibrium constants connecting these three species have been measured and several features are apparent. As expected, as the basicity of the aniline increases, the equilibrium ratio of **13** + benzene : **12** + aniline increases. Surprisingly, however, as the basicity of the aniline decreases, the ratio of the Ir(III) species **14**, to Ir(I) species **13** increases, as does the ratio of **14** + benzene : **12** + aniline. The increased stability of the oxidative addition adducts bearing electron-withdrawing aryl groups (-*p*$CF_3C_6H_4$ **14e** , -C_6F_5 **14f**, 3,5-$(CF_3)_2C_6F_3$- **14g**) was attributed to decreased repulsion between the filled *dπ* and *N*-p orbitals.

Low temperature NMR experiments employing *p*-chloroaniline show that reaction with **12** forms the Ir(I) σ-complex (POCOP)Ir($NH_2C_6H_4Cl$), **13d**, as the kinetic product which equilibrates with the oxidative addition adduct **14d** at temperatures above -50°C. Complexes **14e-g** undergo reductive elimination at 9°C in the presence of ethylene to yield quantitatively (POCOP)Ir(C_2H_4), **18**, and the respective aniline. Rate measurements demonstrate that these reactions are cleanly first-order and independent of ethylene concentration. Mechanistic analysis suggests that the rate-determining step is formation of the σ-complex followed by loss of the aniline to form **10** which is rapidly trapped by ethylene. The reductive elimination barriers of **14e-g** fall in the range of 21-22 kcal/mol and increase with electron-withdrawing ability of the aryl groups.

Complex **14f** is square pyramidal with the hydride occupying the apical site. Trapping **14f** with CO forms the 18-electron complex (POCOP)Ir(H)(CO)(NHC_6F_5), **20f**. X-Ray analysis of a single crystal of **20f** indicates CO has added at the vacant site *trans* to hydride. The six-coordinate CO adducts are much more stable with respect to reductive elimination. Complex **20e** undergoes reductive elimination at 72°C at rates similar to **14e** reductive elimination at

9°C. Qualitative rate measurements suggest CO must dissociate prior to reductive elimination.

Reaction of **12** with benzamides yields quantatively the Ir(III) oxidative addition adducts, (POCOP)Ir(H)(NHC(O)Ar), **22**. X-Ray analysis of **22b** (Ar = C_6F_5) shows significant interaction of the carbonyl oxygen with Ir in the site *trans* to hydride. The barrier to reductive elimination of **22a**, 29 kcal/mol, is substantially higher than for complexes **14e,f,g**. The increased binding energy of the –NH(CO)Ar group to Ir is ascribed to Ir-O interaction as well as a decrease in the repulsive $d\pi$-p interaction as a result of the strong electron-withdrawing ability of the acyl moiety.

Experimental Section

General Considerations: All manipulations were carried out using standard Schlenk, high-vacuum, and glove box techniques. Argon and nitrogen were purified by passage through columns of BASF R3-11 (chemalog) and 4Å molecular sieves. THF was distilled from sodium benzophenone ketyl under nitrogen. Pentane and toluene were passed through columns of activated alumina and deoxygenated by purging with N_2. Benzene was dried with 4Å molecular sieves and degassed by either freeze-pump-thaw methods or by purging with argon. Toluene was further treated by purging with argon to remove nitrogen. Toluene-d_8 and benzene-d_6 were dried over 4Å molecular sieves and stored under argon in the glove box. Hydrogen and carbon monoxide were used as received from National Specialty Gases of Durham, NC. NMR spectra were recorded on Bruker DRX 400, AMX 300 and 500 MHz instruments and are referenced to residual protio solvent peaks. ^{31}P chemical shifts are

referenced to an external H_3PO_4 standard. Since there is a strong ^{31}P-^{31}P coupling in the pincer complexes, many of the ^{1}H and ^{13}C signals exhibit virtual coupling and appear as triplets. These are specified as vt with the *apparent* coupling simply noted as *J*. IR spectra were recorded on an ASI ReactIR 1000 spectrometer. Elemental analyses were carried out by Atlantic Microlab, Inc. of Norcross, GA. All reagents were purchased from Sigma-Aldrich and used without further purification. The POCOP bis(phosphinite) ligand and (POCOP)Ir(H)(Cl), **9**, were prepared by literature procedures[30]. The $[IrCODCl]_2$ can be purchased from Strem or synthesized using literature procedures.[47]

(POCOP)Ir(H)(Ph) (**12**): Complex **12** was generated *in situ* by treatment of (POCOP)Ir(H)(Cl), **9**, with 1.1 equiv. of NaOtBu in benzene at 75°C for 30 minutes.[29]

General Procedure for the *in situ* generation of complexes 13 and 14: (POCOP)Ir(H)(Cl) **2** was placed in a medium-walled screw-cap NMR tube with 1.1 equiv. of NaO*t*Bu in 0.5 mL of benzene or toluene and heated to 75°C for 45 minutes to generate the aryl hydride complex. The aniline was added to this mixture and allowed to react for 45 minutes at room temperature.

(POCOP)Ir(NH_2(*p*-$OCH_3C_6H_4$)) (**13a**): The general procedure was employed using **9** (0.033 mmol, 21 mg), NaO*t*Bu (0.037 mmol, 3.5 mg) and **11a** (0.099 mmol, 13.5 mg).

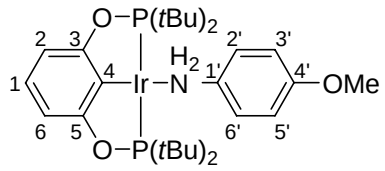

13a

^{1}H NMR (300 MHz, C_6D_6): δ 6.99 (d, $^{3}J_{H\text{-}H}$ = 8.7 Hz, 2H, 2'- and 6'-H), 6.95 (t, $^{3}J_{H\text{-}H}$ = 7.8 Hz, 1H, 1-H), 6.83 (d, $^{3}J_{H\text{-}H}$ = 7.8 Hz, 2H, 2- and 6-H), 6.59 (d, $^{3}J_{H\text{-}H}$ = 8.7 Hz, 2H, 3'- and 5'-H), 5.15 (s, 2H, -NH_2), 3.29 (s, 3H, OC*H*$_3$), 1.28 (vt, *J* = 6.5 Hz, 36H, 2 x P(*t*Bu)$_2$). ^{31}P{^{1}H} NMR (121.5 MHz, C_6D_6): δ 173.6. ^{13}C{^{1}H} NMR (75.5 MHz, C_6D_6): δ 167.9 (C_q, vt, *J* = 8.6 Hz, C3 and C5), 158.2 (C_q, s, C4'), 138.5 (C_q, s, C1'), 124.6 (CH, s, C3' and C5'), 121.3 (CH, s, C1), 114.1 (CH, s, C2' and C6'), 103.3 (CH, vt, *J* = 5.7 Hz, C2 and C6), 55.2 (CH_3, s, OC*H*$_3$), 41.1 (C_q, vt, *J* = 11.0 Hz, *C*(CH_3)$_3$), 28.6 (CH_3, vt, $^{2}J_{P\text{-}H}$ = 3.8 Hz, C(*C*H_3)$_3$). C4 not observed due to low intensity.

(POCOP)Ir(NH$_2$Ar-Me) (**13b**): The general procedure, **13b** was employed using **9** (0.035 mmol, 22 mg) , NaO*t*Bu (0.038 mmol, 3.9 mg) and **11b** (0.1 mmol, 11 mg).

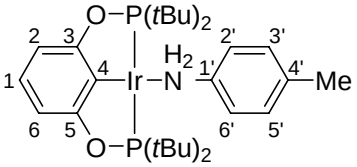

13b

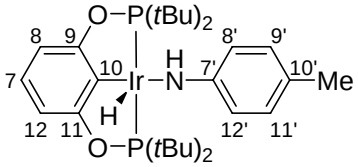

14b

^{1}H NMR (400 MHz, C_6D_6): **13b:** δ 6.77 – 6.96 (7H, aromatic protons), 5.17 (s, 2H, -NH_2), 2.04 (s, 3H, C*H*$_3$), 1.27 (vt, *J* = 6.4 Hz, 36H, 2 x P(*t*Bu)$_2$). **14b:** Concentration of **14b** is very low, resulting in the only distinguishing ^{1}H resonance as the hydride, -33.25 (t, $J_{P\text{-}H}$ = 12.7 Hz, 1H, Ir-*H*). ^{31}P{^{1}H} NMR (121.5 MHz, C_6D_6): δ 173.6 (**13b**), 171.3 (**14b**). ^{13}C{^{1}H} NMR (100.6 MHz, C_6D_6): **13b:** δ 167.8 (C_q, vt, *J* = 8.7 Hz, C3 and C5), 144.7 (C_q, s, C1'), 135.3 (C_q, s, C4'), 129.4 (CH, s, C2' and C6'), 127 (C_q, C4), 123.1 (CH, s, C3' and C5'), 121.2 (CH, s, C1), 103.2 (CH, vt, *J* = 5.9 Hz, C2 and C6), 41.1 (C_q, vt, *J* = 11.0 Hz, *C*(CH_3)$_3$), 28.5 (CH_3, vt, *J* = 3.4 Hz, C(*C*H_3)$_3$), 20.6 (CH_3, s, CH_3).

(POCOP)Ir($NH_2C_6H_5$) (**13c**)/**(POCOP)Ir(H)(NHC_6H_5)** (**14c**): The general procedure was employed using **9** (0.024 mmol, 15 mg), NaO*t*Bu (0.026 mmol, 2.5 mg)and **11c** (0.048 mmol, 4.4 μL). The equilibrating set of complexes **12**, **13c** and **14c** as well as 10% unreacted **9** were all present in the sample thus the ^{13}C NMR spectrum was not useful for structural assignments.

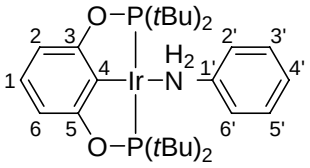

13c

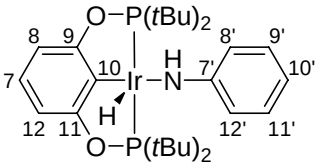

14c

^1H NMR (400 MHz, C_6D_6): **13c:** δ 6.69 – 6.96 (aromatic protons), 5.19 (s, 2H, NH_2), 1.26 (vt, J = 6.4 Hz, 36H, P(*t*Bu)$_2$), **14c:** The concentration of **14c** is very low, resulting in the only distinguishing ^1H resonance as the hydride, -34.05 (t, J = 12.6 Hz). $^{31}P\{^1H\}$ NMR (162 MHz, C_6D_6): δ 173.8 (**13c**), 172.0 (**14c**).

(POCOP)Ir(NH_2(*p*-ClC_6H_4)) (**13d**)/**(POCOP)Ir(H)(NH(*p*-ClC_6H_4))** (**14d**): The general procedure was employed using **9** (0.024 mmol, 15 mg), NaO*t*Bu (0.026 mmol, 2.5 mg) and **11d** (0.048 mmol, 6.1 μL). The equilibrating set **12**, **13d** and **14d**, as well as 3% unreacted **9** were present in the NMR sample.

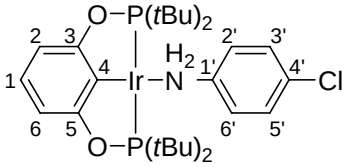

13d

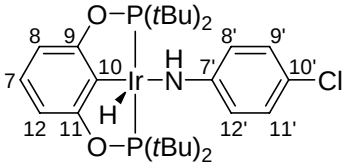

14d

^1H NMR (400 MHz, C_6D_6): δ 6.61-6.97 (m, 14H, aromatic protons for **13d** and **14d**), 5.60 (s, 1H, N*H*), 5.06 (s, 2H, NH_2), 1.08, 1.24 (m, 72H, P(*t*Bu)$_2$), -35.94 (t, $J_{P\text{-}H}$ = 13.2 Hz, 1H, Ir*H*). $^{31}P\{^1H\}$ NMR (162 MHz, C_6D_6): δ 173.9 (**13d**), 172.6 (**14d**).

(POCOP)Ir(H)(NH(*p*-$CF_3C_6H_4$)) (**14e**): The general procedure was employed using **9** (0.032 mmol, 20 mg), NaO*t*Bu (0.032 mmol, 3.1 mg) and **11e** (0.08 mmol, 10 μL).

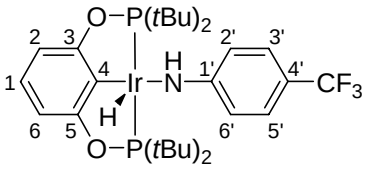

14e

^{1}H NMR (500 MHz, C_6D_6): δ 7.43 (d, $^3J_{H\text{-}H}$ = 8.5 Hz, 2H, 3'- and 5'-H), 6.82 (t, $^3J_{H\text{-}H}$ = 7.8 Hz, 1H, 1-H), 6.73 (d, $^3J_{H\text{-}H}$ = 8.0 Hz, 2H, 2- and 6-H), 6.46 (d, $^3J_{H\text{-}H}$ = 8.5 Hz, 2H, 2'- and 6'-H), 4.37 (s, 1H, N*H*), 1.108 (vt, *J* = 7.5 Hz, 18H, P(*t*Bu)$_2$), 1.046 (vt, *J* = 7.0 Hz, 18H, P(*t*Bu)$_2$), -40.265 (t, $J_{P\text{-}H}$ = 13.3 Hz, 1H, Ir*H*). ^{31}P{^{1}H} NMR (162 MHz, C_6D_6): δ 173.3. ^{19}F NMR (376.5 MHz, C_6D_6): δ -59.1. ^{13}C{^{1}H} NMR (125.8 MHz, C_6D_6): δ 168.0 (C_q, vt, J_C = 5.5 Hz, C3 and C5), 164.0 (C_q, s, C1'), 127.0 (C_q, q, $^1J_{F\text{-}C}$ = 238.9 Hz, CF_3), 126.4 (CH, q, $^3J_{F\text{-}C}$ = 3.6 Hz, C3' and C5'), 126.3 (CH, s, C1), 123.7 (C_q, br, C4), 117.1 (CH, s, C2' and C6'), 112.7 (C_q, q, $^2J_{F\text{-}C}$ = 32.2 Hz, C4'), 104.8 (CH, t, $J_{P\text{-}H}$ = 5.2, C2 and C6), 42.7 (Cq, vt, *J* = 10.8 Hz, *C*(CH_3)$_3$), 38.9 (Cq, vt, *J* = 12.8 Hz, *C*(CH_3)$_3$), 28.0 (CH_3, vt, *J* = 3.2 Hz, C(*C*H_3)$_3$), 27.6 (CH_3, vt, $J_{P\text{-}H}$ = 3.2 Hz, C(*C*H_3)$_3$).

(POCOP)Ir(H)(NHC_6F_5) (**14f**): Simultaneously, **9** (0.034 mmol, 21 mg), NaO*t*Bu (0.037 mmol, 3.6 mg), **11f** (0.068 mmol, 12.4 mg), and benzene-d_6 (0.5 mL) were added to a medium-walled screw-cap NMR tube and heated to 75°C for 1 hour.

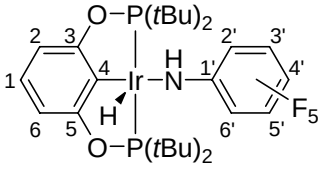

14f

^{1}H NMR (500 MHz, C_6D_6): δ 6.82-6.72 (m, 3H, 1-, 2-, 6-H), 3.01 (s, 1H, N*H*), 1.09-1.03 (m, 36H, P(*t*Bu)$_2$) -42.15 (t, $J_{P\text{-}H}$ = 13.5 Hz, 1H, Ir*H*). ^{31}P{^{1}H} NMR (162 MHz, C_6D_6): δ 172.8. ^{19}F NMR (376.5 MHz, C_6D_6): δ -167.3 (m), -168.9 (m), -187.3 (m). ^{13}C{^{1}H} NMR (125.8 MHz, C_6D_6): δ 168.5 (C_q, vt, J = 5.5 Hz, C3 and C5), 140.4-135.8 (m, C_q, Ar-F_5: C2', C6', C3', C5', and C4'), 126.7 (CH, s, C1), 122.6 (C_q, t, C4), 104.9 (CH, t, $J_{P\text{-}H}$ = 5.3 Hz, C2 and C6), 42.6 (Cq, vt, J = 11.1 Hz, *C*(CH$_3$)$_3$), 39.1 (Cq, vt, J = 12.6 Hz, *C*(CH$_3$)$_3$), 27.7 (CH$_3$, vt, J = 3.2 Hz, C(*C*H$_3$)$_3$), 27.2 (CH$_3$, vt, J = 3.0 Hz, C(*C*H$_3$)$_3$). C1' not observed due to low intensity.

(POCOP)Ir(H)(NH(3,5-(CF$_3$)$_2$C$_6$H$_3$)) (**14g**): The general procedure was employed using **9** (0.035 mmol, 22 mg), NaO*t*Bu (0.039 mmol, 3.7 mg) and **11g** (0.07 mmol, 10.9 μL) .

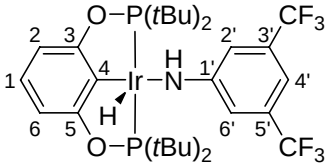

14g

^{1}H NMR (500 MHz, C_6D_6): δ 6.98 (s, 1H, 4'-H), 6.87 (s, 2H, 2'- and 6'-H), 6.81 (t, $^{3}J_{H\text{-}H}$ = 7.9 Hz, 1H, 1-H), 6.73 (d, $^{3}J_{H\text{-}H}$ = 7.9 Hz, 2H, 2- and 6-H), 3.74 (s, 1H, N*H*), 1.06 (vt, J = 7.4 Hz, 18H, P(*t*Bu)$_2$), 0.99 (vt, J = 6.8 Hz, 18H, P(*t*Bu)$_2$), -41.77 (t, $J_{P\text{-}H}$ = 13.5 Hz, 1H, Ir*H*). ^{31}P{^{1}H} NMR (162 MHz, C_6D_6): δ 174.0 (d). ^{19}F NMR (376.5 MHz, C_6D_6): δ -63.2 ^{13}C{^{1}H} NMR (125.8 MHz, C_6D_6): δ 168.5 (C_q, vt, J = 5.6 Hz, C3 and C5), 161.4 (C_q, s, C1'), 132.0 (C_q, q, $^{2}J_{F\text{-}C}$ = 31.4 Hz, C3' and C5'), 127.0 (CH, s, C1), 125.5 (C_q, q, $^{1}J_{F\text{-}C}$ = 273.3 Hz, *C*F3), 124.5 (C_q, m, C4), 115.7 (CH, m, C2' and C6'), 105.0 (CH, t, vt, J = 5.2 Hz, C2 and C6), 102.4 (CH, septet, $^{3}J_{F\text{-}C}$ = 4.0 Hz), 42.8 (Cq, vt, J = 10.9 Hz, *C*(CH$_3$)$_3$), 38.7 (Cq,

vt, J = 12.8 Hz, $C(CH_3)_3$), 28.0 (CH_3, vt, J = 3.2 Hz, $C(CH_3)_3$), 27.3 (CH_3, vt, J = 3.1 Hz, $C(CH_3)_3$).

General Procedure for Determining Equilibrium Constants K_1, K_2, K_3 (Scheme 1): Samples were prepared as described below in benzene. Molarities of species were determined by carefully measuring the final volume of solution. Both ^1H and ^{31}P spectra were used to determine ratios of species. ^{31}P spectra were taken with a delay time of 15 seconds to ensure the integrals were accurate based on the 5 x T1 of **14f**.

Reaction of (POCOP)Ir(H)(C_6H_5) (12) and *p*-$CH_3OC_6H_4NH_2$ (11a): To a vial in the glovebox under argon, **9** (0.088 mmol, 55.35 mg), NaO*t*Bu (0.8 equiv., 0.07 mmol, 6.0 mg), **11a** (0.041 mmol, 5.1 mg, 0.010 M), and benzene (4 mL) were added. The reaction mixture was allowed to stir for 1.5 hours. An aliquot was removed and analyzed by ^{31}P NMR. The equilibrium constants were calculated based on the concentrations of all the species in solution, (K_1 = 1014, K_2 = n/a). A second aliquot was removed after another hour to ensure reaction was at equilibrium. The reaction was repeated with an increase in the concentration of **11a** to 0.05 M (K_1 = 1189, K_2 = n/a). No **14a** could be detected.

Reaction of (POCOP)Ir(H)(C_6H_5) (12) and *p*-$CH_3C_6H_4NH_2$ (11b): The general procedure for **11a** was followed using **9** (0.069 mmol, 43.45 mg), NaO*t*Bu (0.9 equiv., 0.062 mmol, 6.0 mg), **11b** (0.20 mmol, 21.43 mg, 0.050 M), and benzene (4 mL). (K_1 = 462, K_2 =

0.04). The reaction was repeated with an increase in the concentration of **11b** to 0.10 M (K_1 = 448, K_2 = 0.04).

Reaction of (POCOP)Ir(H)(C_6H_5) (12) and $C_6H_5NH_2$ (11c): The general procedure for **11a** was followed using **9** (0.075 mmol, 46.9 mg), NaO*t*Bu (0.9 equiv., 0.067 mmol, 6.47 mg), **11c** (0.2 mmol, 0.18 μL, 0.050 M), and benzene (4.0 mL). (K_1 = 188, K_2 = 0.07). The reaction was repeated with an increase in the concentration of **11c** to 0.10 M (K_1 = 189, K_2 = 0.08).

Reaction of (POCOP)Ir(H)(C_6H_5) (12) and *p*-$ClC_6H_4NH_2$ (11d): The general procedure for **11a** was followed using **9** (0.074 mmol, 46.15 mg), NaO*t*Bu (0.9 equiv., 0.066 mmol, 6.4 mg), **11d** (0.392 mmol, 50 mg, 0.10 M), and benzene (4 mL). (K_1 = 50, K_2 = 1). The reaction was repeated with an increase in the concentration of **11d** to 0.15 mol/L (K_1 = 60, K_2 = 1).

Reaction of (POCOP)Ir(H)(C_6H_5) (12) and *p*-$CF_3C_6H_4NH_2$ (11e): The general procedure for **11a** was followed using **9** (0.138 mmol, 86.6 mg), NaO*t*Bu (0.9 equiv., 0.124 mmol, 11.9 mg), **11e** (0.08 mmol, 12.9 mg, 0.010 M), and benzene (8 mL). (K_3 = 272). The reaction was repeated with an increase in the concentration of **11e** to 0.050 M (K_3 = 259). No **13e** could be detected.

Reaction of (POCOP)Ir(H)(C_6H_5) (12) and $C_6F_5NH_2$ (11f): The general procedure for **11a** was followed using **9** (0.038 mmol, 23.75 mg), NaO*t*Bu (0.9 equiv., 0.0343 mmol, 3.3

mg), **11f** (0.0721 mmol, 13.2 mg, 0.009 M), and benzene (8 mL) was added. (K_3 = 2010). The reaction was repeated with an increase in the concentration of **11f** to 0.012 M (K_3 = 2300). No **13f** could be detected.

Reaction with (POCOP)Ir(H)(C_6H_5) (12) and 3,5-$(CF_3)_2C_6H_3NH_2$ (11g): The general procedure for **11a** was followed using **9** (0.158 mmol, 99.05 mg), NaO*t*Bu (0.9 equiv., 0.142 mmol, 13.65 mg), **11g** (0.08 mmol, 18 mg, 0.010 M), and benzene (8 mL). (K_3 = 2700). The reaction was repeated with an increase in the concentration of **11g** to 0.050 M (K_3 = 2850). No **13g** could be detected.

Low Temperature Oxidative Addition of *p*-Chloroaniline to 10: To a screw cap NMR tube, **10** was generated by reaction of **9** (0.023mmol, 15mg) with NaO*t*Bu (0.023 mmol, 2.3 mg) in 0.4 mL of toluene-d_8 at 100°C for 1h. The reaction mixture was cooled to -78°C in a dry ice/acetone bath and a 0.1 mL of a 2.3M solution of *p*-chloroaniline (0.23 mmol) was added via syringe. The reaction warmed in the NMR probe until the solution consisted solely of **13c**, after which the oxidative addition was monitored at -12°C. A data plot is included in supporting information.

Kinetic Analysis of the Reductive Elimination Reactions of 14e-g: In a screw cap NMR tube, **10** was generated by reaction of **9** (0.023mmol, 15mg) with NaO*t*Bu (0.023 mmol, 2.3 mg) in 0.5 mL of toluene-d_8 at 100°C for 1h. Aniline **11e, f** or **g** were added to the solution of **10** and allowed to react for 45 minutes. The NMR tube was cooled to -78°C in a

dry ice/acetone bath, followed by addition of ethylene to the reaction mixture via syringe. The NMR tube was warmed to 9°C in the probe and the reductive elimination was monitored by ^{1}H NMR spectroscopy. A plot of kinetic data for **14f** is included in supporting information.

Kinetic Analysis of the Dissociation of $H_2NC_6H_4$-*p*OMe (11a) from 13a: (POCOP)Ir(H)(Cl) **9** (10 mg, 0.016 mmol), NaO*t*Bu (1.7 mg, 0.018 mmol), and toluene-d_8 (0.4 mL) were heated for 1 hr. at 100°C in a J. Young NMR tube to generate the tolyl hydride complexes **17**. *p*-Methoxyaniline **11a** (3.5 mg, 0.024 mmol) and 1,3,5-trimethoxybenzene (0.1 mL, 0.11 M solution in toluene-d_8) was added to the NMR tube. After freeze-pump-thawing the NMR sample, ethylene (10-20 equiv., 3.6-7.2 mL at 23°C) was introduced via a gas tight syringe at liquid nitrogen temperature. The reaction was then monitored via low temperature NMR spectroscopy at -8°C. A plot of kinetic data is included in supporting information.

(POCOP)Ir(H)(NHC_6F_5)(CO) (20f): To a Schlenk flask, **9** (101 mg, 0.16 mmol), NaO*t*Bu (17mg, 0.18mmol), **11f** (33mg, 0.18 mmol), and toluene(5 mL) were added and stirred at room temperature for 1 hour. The reaction mixture was cooled to -78°C then CO was purged through the solution until the color lightened. The toluene was removed under vacuum and the product was extracted with pentane. The pentane was reduced under vacuum until the product began to precipitate. The pentane was then cooled to -78°C and the precipitate was filtered and washed with cold pentane. (60 mg, 46% yield).

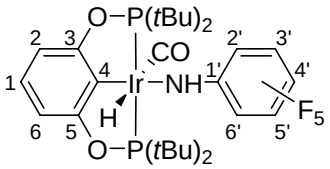

20f

^{1}H NMR (500 MHz, C_6D_6): δ 6.74 (t, $^{3}J_{H\text{-}H}$ = 8.0 Hz ,1H, 1-H), 6.59 (d, $^{3}J_{H\text{-}H}$ = 8.0 Hz, 2H, 2- and 6-H), 2.33 (s, 1H, N*H*), 1.20 (vt, $J_{P\text{-}H}$ = 7.7 Hz, 18H, P(*t*Bu)$_2$), 1.11 (vt, $J_{P\text{-}H}$ = 7.3 Hz, 18H, P(*t*Bu)$_2$), -8.56 (t, $J_{P\text{-}H}$ = 17.9 Hz, 1H, Ir*H*). ^{31}P{^{1}H} NMR (162 MHz, C_6D_6): δ 57.6. ^{19}F NMR (376.5 MHz, C_6D_6): δ -163.3 (bs), -169.0 (t), -186.7 (septet). ^{13}C{^{1}H} NMR (125.8 MHz, C_6D_6): δ 179.4 (C_q, *C*=O), 163.8 (C_q, vt, $J_{P\text{-}C}$ = 3.7 Hz, C3 and C5), 140.4-135.8 (m, C_q, Ar-F_5: C2', C6', C3', C5', and C4'), 126.8 (CH, s, C1), 106.0 (CH, t, vt, $J_{P\text{-}H}$ = 4.8 Hz, C2 and C6), 43.0 (Cq, vt, $J_{P\text{-}H}$ = 12.6 Hz, *C*(CH_3)$_3$), 40.6 (Cq, vt, $J_{P\text{-}H}$ = 11.4 Hz, *C*(CH_3)$_3$), 28.1 (CH_3, vt, $J_{P\text{-}H}$ = 2.9 Hz, C(*C*H_3)$_3$), 27.2 (CH_3, vt, $J_{P\text{-}H}$ = 2.4 Hz, C(*C*H_3)$_3$). C4 and C1' not observed due to low intensity. IR (C_6D_6): 2022 cm^{-1}. Elemental analysis calculated for $C_{29}H_{41}O_3P_2N_1F_5Ir$ (800.80): C: 43.50, H: 5.16, N: 1.75. Found: C: 43.70, H: 5.25, N: 1.71.

Reductive Elimination of *p*-trifluoromethylaniline from (POCOP)Ir(H)(CO)(NHC$_6$H$_4$-*p*CF$_3$) 20e: In a J. Young NMR tube, tolyl complexes **17** were generated by heating the reaction mixture of (POCOP)Ir(H)(Cl) **9** (15 mg, 0.024 mmol), NaO*t*Bu (2.3 mg, 0.024 mmol), and 0.5 mL of toluene-d_8 for 1 hour at 100°C. The reaction mixture was cooled to room temperature. The addition of *p*-CF_3-aniline **11e** (6.0 μL, 0.048 mmol) formed complex **14e**. After freeze-pump-thawing the reaction mixture, a gastight syringe was used to add sufficient CO at liquid N_2 temperature to generate pressures of 1, 2,

and 3 atmospheres of CO in the head space at 25°C. The reaction was monitored at 63°C by ^{1}H NMR spectroscopy.

Procedure for Monitoring Reaction of Benzamide Complex 22a with PPh_3: A stock solution of (POCOP)Ir(H)(NH(CO)Ar) was prepared in the glovebox under Ar by stirring (POCOP)Ir(H)(Cl) **9** (112.7 mg, 0.18 mmol), NaO*t*Bu (20.7 mg, 0.22 mmol), benzamide **21a** (26.2 mg, 0.22 mmol), and toluene-d_8 (3.0 mL) until the color of the solution turned pale orange, ca. 30 minutes. The excess benzamide and NaO*t*Bu were filtered out through a 0.02 micron syringe filter. The concentration of the stock solution (0.063 M) was measured via ^{1}H NMR using 2.0 μL of mesitylene as a standard. Aliquots (0.5mL) of the stock solution were added to three J. Young NMR tubes containing known amounts of PPh_3 (0.147 mmol, 0.294 mmol, 0.588 mmol). The NMR tubes were heated to 100°C for three days, after which the reaction was stopped by placing the NMR tubes in cold water. The K_{eq} was calculated by measuring the ratios of **22a** and **26** by ^{31}P NMR. $K_{eq} = 0.18$.

Procedure for Monitoring Reaction of Benzamide Complexes 22b with PPh_3: A stock solutions was prepared using **9** (92.5 mg, 0.148 mmol), NaO*t*Bu (71.0 mg, 0.74 mmol), **22b** (161.6 mg, 0.74 mmol), and toluene-d_8 (6.0 mL). Aliquots of the stock solution (0.6 mL, 0.021 M) were placed in three J. Young tubes with known amounts of PPh_3 (0.126 mmol, 0.252 mmol, 0.378 mmol). The reaction was heated to 100°C overnight, after which the reaction was stopped by placing the NMR tubes in cold water. The the K_{eq} was calculated by measuring the ratios of **22b** and **26** by ^{31}P NMR. $K_{eq} = 0.067$.

(POCOP)Ir(PPh$_3$) (24): In a Schlenk flask **9** (104 mg, 0.166 mmol), NaO*t*Bu (17.6 mg, 0.183 mmol), PPh_3 (46 mg, 0.174 mmol), and toluene (10 mL) were combined and stirred overnight. Toluene was removed under vacuum until the product precipitated. The product was filtered, washed with cold toluene, and dried under vacuum to yield an orange solid (74 mg, 52% yield).

^{1}H NMR (500 MHz, C_6D_6): δ 8.06 (t, 6H, PPh_3), 6.9-7.1 (m, 12H, aromatic protons), 1.072 (vt, $J_{P\text{-}H}$ = 6.8 Hz, 36H, P(*t*Bu)$_2$). ^{31}P{^{1}H} NMR (162 MHz, C_6D_6): δ 181.2 (d, $J_{P\text{-}P}$ = 5.2 Hz), 15.8 (t, $J_{P\text{-}P}$ = 5.5 Hz). ^{13}C{^{1}H} NMR (100.6 MHz, C_6D_6): δ 166.4 (C_q, vt, $J_{P\text{-}C}$ = 6.5 Hz, C3 and C5), 141.5, 135.7, 133.7, 129, 127.0, 125.7 (CH, s, C1), 102.7 (CH, t, vt, C2 and C6), 41.0 (Cq, vt, $J_{P\text{-}H}$ = 11.6 Hz, *C*$(CH_3)_3$), 28.7 (CH_3, s). Elemental analysis calculated for $C_{40}H_{54}O_2P_3Ir$ (851.99): C: 56.39, H: 6.39. Found: C: 56.19, H: 6.37. Crystallographic data is included in the supporting information.

Kinetic Analysis of the Reductive Elimination of Benzamide 22a: A stock solution (0.06 M) of (POCOP)Ir(H)(NH(CO)C_6H_5) **23a** was prepared under Ar by stirring (POCOP)Ir(H)(Cl) **9** (75.1 mg, 0.12 mmol), NaO*t*Bu (12.7 mg, 0.132 mmol), benzamide **22a** (16.0 mg, 0.132 mmol), and toluene-d_8 (2 mL) until the color of the solution turned pale orange. The excess benzamide and NaO*t*Bu were filtered out through a 0.02 micron syringe filter. To a screw cap NMR tube, 10 equiv. of **22a** (15 mg, 0.124 mmol), 10 equiv. of PPh_3 (32.5 mg, 0.124 mmol), the stock solution of **23a** (0.21 mL, 0.06 M), and toluene-d_8 (0.4 mL) were added. The reaction was heated to 100°C in the NMR probe and over time the disappearance of **23a** signals were monitored via ^{1}H NMR. A plot of kinetic data is included in supporting information.

(POCOP)Ir(H)(NH(CO)(Ph) (22a): (POCOP)Ir(H)(Cl) (**9**) (100 mg, 0.16 mmol), NaO*t*Bu (18.4 mg, 0.192 mmol), $H_2N(CO)C_6H_5$ (**21a**) (23.2 mg, 0.192 mmol), and 5.0 mL of benzene were added to a Schlenk flask and allowed to stir for 1.5 hours until color changed to a light orange color. The solution was filtered though a 0.2 micron syringe filter, and the benzene was sublimed at 0°C to yield a yellow/orange colored solid (71.6 mg, 63% yield).

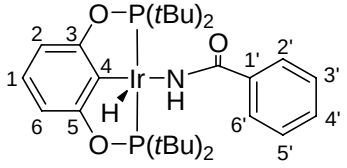

22a

^{1}H NMR (500 MHz, C_6D_6): δ 7.64-7.62 (m, 2H, 2'- and 6'-H), 7.12-7.07 (m, 3H, 3'-, 4', and 5'-H), 6.87-6.79 (m, 3H, 1-, 2-, and 3-H), 5.90 (bs, 1H, N*H*), 1.40 (vt, $J_{P\text{-}H}$ = 6.9 Hz, 18H, P(*t*Bu)$_2$), 1.28 (vt, $J_{P\text{-}H}$ = 7.0 Hz, 18H, P(*t*Bu)$_2$), -30.25 (t, $J_{P\text{-}H}$ = 13.2 Hz, 1H, Ir*H*). ^{31}P{^{1}H} NMR (162 MHz, C_6D_6): δ 164.2. ^{13}C{^{1}H} NMR (125.8 MHz, C_6D_6): δ 176.4 (C_q, t, $J_{P\text{-}C}$ = 1.3 Hz, *C*O), 166.6 (C_q, vt, $J_{P\text{-}C}$ = 6.0 Hz, C3 and C5), 138.4 (C_q, s, C1'), 130.1 (CH, s, C4'), 128.3 (CH, s, C3' and C5'), 126.3 (CH, s, C2' and C6'), 124.1 (CH, s, C1), 118.5 (C4), 104.5 (CH, t, $J_{P\text{-}C}$ = 5.4 Hz, C2 and C6), 42.5 (Cq, vt, $J_{P\text{-}H}$ = 12.0 Hz, *C*(CH$_3$)$_3$), 39.9 (Cq, vt, $J_{P\text{-}H}$ = 11.8 Hz, *C*(CH$_3$)$_3$), 28.8 (CH$_3$, vt, $J_{P\text{-}H}$ = 3.3 Hz, C(*C*H$_3$)$_3$), 27.6 (CH$_3$, bvt, $J_{P\text{-}H}$ = 2.2 Hz, C(*C*H$_3$)$_3$). Elemental analysis calculated for $C_{29}H_{46}O_3P_2N_1Ir$ (710.85): C: 49.00, H: 6.52, N: 1.97. Found: C: 49.22, H: 6.59, N: 2.00.

(POCOP)Ir(H)(NH(CO)(C_6F_5) (22b): (POCOP)Ir(H)(Cl) (**9**) (100 mg, 0.16 mmol), NaO*t*Bu (18.4 mg, 0.192 mmol), $H_2N(CO)C_6F_5$ (**21b**) (40.5 mg, 0.192 mmol), and 5.0 mL of benzene were added to a Schlenk flask and allowed to stir for 1.5 hours until the color

changed to a light orange color. The solution was filtered though a 0.2 micron syringe filter, and the benzene was sublimed at 0°C to yield a yellow/orange colored solid (101.6 mg, 79% yield).

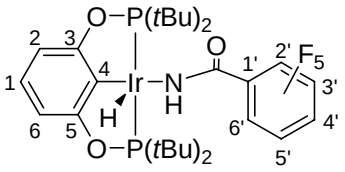

22b

^{1}H NMR (500 MHz, C_6D_6): δ 6.87-6.78 (m, 3H, 1-, 2-, 6-H), 5.49 (bs, 1H, N*H*), 1.44 (vt, $J_{P\text{-}H}$ = 7.0 Hz, 18H, P(*t*Bu)$_2$), 1.22 (vt, $J_{P\text{-}H}$ = 7.0 Hz, 18H, P(*t*Bu)$_2$), -35.72 (t, $J_{P\text{-}H}$ = 13.0 Hz, 1H, Ir*H*^{19}F NMR (376.5 MHz, C_6D_6): δ -141.76 (m), -155.25 (m), -166.61 (m). ^{13}C{^{1}H} NMR (125.8 MHz, C_6D_6): δ 167.2 (C_q, vt, $J_{P\text{-}C}$ = 5.8 Hz, C3 and C5), 163.0 (C_q, s, *C*O), 144.5 (C_q, dm, $^{1}J_{F\text{-}C}$ = 241.8 Hz, C2' and C6'), 141.1 (C_q, dm, $^{1}J_{F\text{-}C}$ = 254.3 Hz, C4'), 137.7 (C_q, dm, $^{1}J_{F\text{-}C}$ = 252.0 Hz, C3' and C5'), 125.4 (CH, s, C1), 119.9 (C_q, m, C4), 116.2 (C_q, m, C1'), 104.7 (CH, t, vt, $J_{P\text{-}H}$ = 5.3 Hz, C2 and C6), 42.8 (Cq, vt, $J_{P\text{-}H}$ = 12.1 Hz, *C*(CH$_3$)$_3$), 39.8 (Cq, vt, $J_{P\text{-}H}$ = 12.1 Hz, *C*(CH$_3$)$_3$), 28.3 (CH$_3$, vt, $J_{P\text{-}H}$ = 3.3 Hz, C(*C*H$_3$)$_3$), 27.6 (CH$_3$, vt, $J_{P\text{-}H}$ = 3.1 Hz, C(*C*H$_3$)$_3$). Elemental analysis calculated for $C_{29}H_{41}O_3P_2N_1F_5Ir$ (800.80): C: 43.50, H: 5.16, N: 1.75. Found: C: 43.70, H: 5.25, N: 1.71.

References and Notes

(1) Janowicz, A. H.; Bergman, R. G. *J. Am. Chem. Soc.* **1982**, *104*, 352.

(2) Jones, W. D.; Feher, F. *Organometallics* **1983**, *2*, 562.

(3) Hoyano, J. K.; McMaster, A. D.; Graham, W. A. G. *J. Am. Chem. Soc.* **1983**, *105*, 7190.

(4) Shilov, A. E.; Shul'pin, G. B. *Chem. Rev.* **1997**, *97*, 2879.

(5) Arndtsen, B. A.; Bergman, R. G.; Mobley, T. A.; Peterson, T. H. *Acc. Chem. Res.* **1995**, *28*, 154.

(6) Crabtree, R. H. *J. Chem. Soc., Dalton Trans.* **2001**, 2951.

(7) Crabtree, R. H. *Dalton Transactions* **2003**, 3985.

(8) Lersch, M.; Tilset, M. *Chem. Rev.* **2005**, *105*, 2471.

(9) Jun, C.-H.; Lee, J. H. *Pure Appl. Chem.* **2004**, *76*, 577.

(10) Ishiyama, T. *Kagaku to Kogyo (Tokyo)* **2003**, *56*, 1237.

(11) Kakiuchi, F.; Chatani, N. *Adv. Synth. Catal.* **2003**, *345*, 1077.

(12) Labinger, J. A.; Bercaw, J. E. *Nature (London)* **2002**, *417*, 507.

(13) Hartwig, J. F.; Andersen, R. A.; Bergman, R. G. *Organometallics* **1991**, *10*, 1875.

(14) Glueck, D. S.; Winslow, L. J. N.; Bergman, R. G. *Organometallics* **1991**, *10*, 1462.

(15) Bryndza, H. E.; Tam, W. *Chem. Rev.* **1988**, *88*, 1163.

(16) Fulton, J. R.; Holland, A. W.; Fox, D. J.; Bergman, R. G. *Acc. Chem. Res.* **2002**, *35*, 44.

(17) Utsunomiya, M.; Hartwig, J. F. *J. Am. Chem. Soc.* **2004**, *126*, 2702.

(18) Hartwig, J. F. *Pure Appl. Chem.* **2004**, *76*, 507.

(19) Beller, M.; Breindl, C.; Eichberger, M.; Hartung, C. G.; Seayad, J.; Thiel, O. R.; Tillack, A.; Trauthwein, H. *Synlett* **2002**, 1579.

(20) Utsunomiya, M.; Kuwano, R.; Kawatsura, M.; Hartwig, J. F. *J. Am. Chem. Soc.* **2003**, *125*, 5608.

(21) Uchimaru, Y. *Chem. Comm.* **1999**, 1133.

(22) Casalnuovo, A. L.; Calabrese, J. C.; Milstein, D. *J. Am. Chem. Soc.* **1988**, *110*, 6738.

(23) Ladipo, F. T.; Merola, J. S. *Inorg. Chem.* **1990**, *29*, 4172.

(24) Liu, F.; Pak, E. B.; Singh, B.; Jensen, C. M.; Goldman, A. S. *J. Am. Chem. Soc.* **1999**, *121*, 4086.

(25) Kanzelberger, M.; Singh, B.; Czerw, M.; Krogh-Jespersen, K.; Goldman, A. S. *J. Am. Chem. Soc.* **2000**, *122*, 11017.

(26) Zhang, X.; Fried, A.; Knapp, S.; Goldman, A. S. *Chem. Comm.* **2003**, 2060.

(27) Kanzelberger, M.; Zhang, X.; Emge, T. J.; Goldman, A. S.; Zhao, J.; Incarvito, C.; Hartwig, J. F. *J. Am. Chem. Soc.* **2003**, *125*, 13644.

(28) Zhao, J.; Goldman, A. S.; Hartwig, J. F. *Science (Washington, DC, United States)* **2005**, *307*, 1080.

(29) Goettker-Schnetmann, I.; Brookhart, M. *J. Am. Chem. Soc.* **2004**, *126*, 9330.

(30) Goettker-Schnetmann, I.; White, P.; Brookhart, M. *J. Am. Chem. Soc.* **2004**, *126*, 1804.

(31) Goettker-Schnetmann, I.; White, P. S.; Brookhart, M. *Organometallics* **2004**, *23*, 1766.

(32) Peris, E.; Lee, J. C., Fr.; Rambo, J. R.; Eisenstein, O.; Crabtree, R. H. *J. Am. Chem. Soc.* **1995**, *117*, 3485.

(33) Crabtree, R. H. *Science (Washington, D. C.)* **1998**, *282*, 2000.

(34) Krogh-Jespersen, K.; Czerw, M.; Zhu, K.; Singh, B.; Kanzelberger, M.; Darji, N.; Achord, P. D.; Renkema, K. B.; Goldman, A. S. *J. Am. Chem. Soc.* **2002**, *124*, 10797.

(35) Crabtree, R. H. *The Organometallic Chemistry of the Transition Metals*; Third ed.; John Wiley and Sons, Inc: New York, NY, 2001.

(36) Caulton, K. G. *New J. Chem.* **1994**, *18*, 25.

(37) Holland, P. L.; Andersen, R. A.; Bergman, R. G. *Comments Inorg. Chem.* **1999**, *21*, 115.

(38) Holland, P. L.; Andersen, R. A.; Bergman, R. G.; Huang, J.; Nolan, S. P. *J. Am. Chem. Soc.* **1997**, *119*, 12800.

(39) Formed by reaction of *in situ* generated **14f** followed by addition of PMe_3 at -40°C. Key NMR resonances include ^{1}H NMR (400 MHz, C_7D_8): δ -11.9 (dt, Ir-*H*, $J_{P\text{-}H}$ = 149.1 Hz (trans), $J_{P\text{-}H}$ = 23.4 Hz (cis), and ^{31}P(162 MHz, C_7D_8): δ 169.6 (m, 2P), -57.1 (m, 1P).

(40) The stability of the aryl hydride complex can be dramatically altered by incorporation of fluorine substituents in the aromatic ring. In preliminary experiments we have shown that reaction of (POCOP)Ir, **10**, with 2,3,5,6-tetrafluoroaniline yields *solely* the C-H activation product (POCOP)Ir(H)($C_6F_4NH_2$). Strengthening of the Re-aryl bond through fluorination of the aryl ring has been well-documented in earlier studies by Perutz et. al. (*Chem. Commun*., **2003**, 490)

(41) Crumpton-Bregel, D. M.; Goldberg, K. I. *J. Am. Chem. Soc.* **2003**, *125*, 9442.

(42) Crumpton, D., M.; Goldberg, K. I. *J. Am. Chem. Soc.* **2000**, *122*, 962.

(43) Jensen, M. P.; Wick, D. D.; Reinartz, S.; White, P. S.; Templeton, J. L.; Goldberg, K. I. *J. Am. Chem. Soc.* **2003**, *125*, 8614.

(44) Chin, C. S.; Chong, D.; Lee, S.; Park, Y. J. *Organometallics* **2000**, *19*, 4043.

(45) Cooper, A. C.; Huffman, J. C.; Caulton, K. G. *Inorg. Chim. Acta* **1998**, *270*, 261.

(46) Tellers, D. M.; Ritter, J. C. M.; Bergman, R. G. *Inorg. Chem.* **1999**, *38*, 4810.

(47) Baghurst, D. R.; Mingos, D. M. P.; Watson, M. J. *J. Organomet. Chem.* **1989**, *368*, C43.

CHAPTER THREE

Reactions of electron-deficient cationic iridium hydride pincer complexes with hydrogen and olefins

Introduction

Hydrocarbons, including alkenes, provide a large feedstock of inexpensive substrates that can be converted to more desirable compounds or materials. Therefore, new catalysts capable of converting olefins to more valuable products are highly sought-after. Two prominent areas of transition metal-catalyzed transformations of olefins include polymerization/copolymerization of olefins and functionalization of olefins through the formation of new C-X bonds. Transition metal catalyzed processes in general are desired because often they allow chemo-, regio-, or stereoselective control of the reaction. Additionally, these reactions have the potential of being atom economic, in which all the atoms in the starting substrates are found in the products. This provides an environmentally benign scenario as there is no waste formed at the end of the reaction.

There have been numerous reports of addition of a H-Nuc species across carbon-carbon triple and carbon-carbon double bonds with control of regioselectivity and stereoselectivity, depending on the catalyst, substrate and reaction conditions.[1] A few examples include hydroformylation,[2] hydroamination,[3-6] hydrothiolation,[7-10] and hydrocyanation.[11]

Although these reactions are all very different, they are initiated generally by one of two pathways. The first pathway involves nucleophilic attack of the reactant on a metal-olefin complex to form an alkyl species. The olefin, through binding with the metal, is activated for attack by the nucleophile. The second pathway involves insertion of the olefin into an M-H bond forming a metal alkyl species which provides an empty coordination site for the nucleophile to coordinate to the metal. Reductive elimination results in formation of the desired product. These processes are particularly facile when the olefin contains an electron-withdrawing functional group or is sterically strained in order to promote the reaction. Transformations involving common unactivated olefins such as ethylene or propylene are generally less facile and remain an important goal. A basic understanding of the behavior of new metal-olefin complexes should aid in developing new catalysts for these types of reactions.

As mentioned above, many of these transformations occur through a mechanism that involves an olefin insertion reaction. Previously in our laboratory it has been shown that (POCOP)IrH_2 (POCOP = 2,6-(OP*t*Bu_2)$_2C_6H_3$) is capable of hydrogenation chemistry through insertion of an olefin into the Ir-H bond, followed by reductive elimination of the alkyl hydride fragment (Scheme 3.1).[12,13]

Scheme 3.1. Hydrogenation of cyclooctene by (POCOP)IrH_2[12,13]

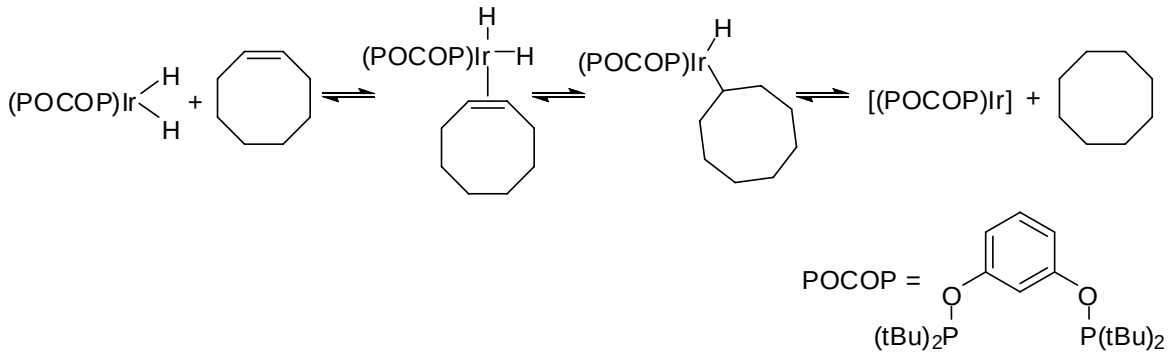

It has also been shown that the 14-electron fragment [(POCOP)Ir] is able to oxidatively add anilines, preferentially electron-withdrawing anilines, to form (POCOP)Ir(H)(NHAr) (Scheme 3.2).[14] However, when both ethylene and aniline were present, coordination of the ethylene occurred to form the stable ethylene complex. No C-N coupling occurred as might have been expected as shown in Scheme 3.3. Even when a more strained olefin, norbornene, was reacted with [(POCOP)Ir] and $H_2N(3,5\text{-bis}(CF_3)C_6H_3)$ at 23-150°C, once again only the olefin complex was observed and no C-N bonds were formed.

Scheme 3.2. Activation of electron-withdrawing anilines by [(POCOP)Ir].

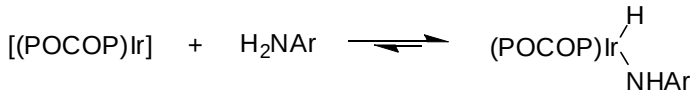

Ar = -C_6H_4-*p*CF_3, -C_6F_5, -3,5$(CF_3)C_6H_3$

Scheme 3.3. Possible routes to hydroamination of olefins

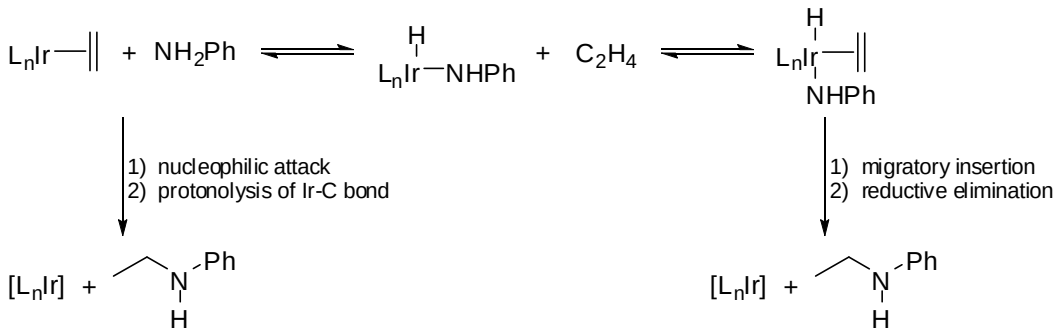

We were interested in investigating how changing the POCOP pincer complexes from neutral to cationic would affect their reactivity. A cationic complex would render the iridium center even more electron-poor which might cause the olefin to bind less strongly since there would be less π-backdonation from the iridium to the π* orbital of the olefin. This could activate the olefin to nucleophilic attack to form a new C-X bond or increase its ability to insert into a M-H or M-C bond. Therefore, the cationic complexes were developed with the goal to enhance the potential for these types of iridium systems to be involved in catalytic formation of C-X bonds. A possible reaction mechanism for this type of transformation is shown below in the Scheme 3.4.

Scheme 3.4. Possible mechanism for functionalization of an olefin by nucleophilic attack on the M-olefin

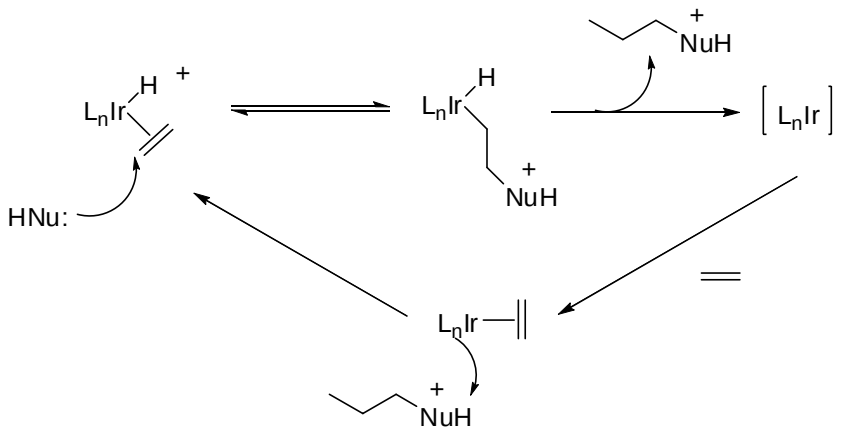

Results and Discussion

I) Synthesis of (POCOP)Ir(H)(OTf) (2) and cationic [(POCOP)Ir(H)(L)][X] (X = SbF_6 (3), BAr_F (4))

In order to synthesize cationic POCOP iridium complexes, various silver and sodium salts (AgOTf, $AgSbF_6$, and $NaBAr_F$) (Tf = triflate, BAr_F = tetrakis(3,5-bistrifluoromethylphenyl)borate) were used to abstract chloride from (POCOP)Ir(H)(Cl), **1,** in methylene chloride (Scheme 3.5). When silver triflate was used as the chloride abstractor, it was found that the triflate anion coordinated to the iridium generating a neutral species.

Scheme 3.5. Synthesis of (POCOP)Ir(H)(OTf) and cationic [(POCOP)Ir(H)(L)][X] [X = SbF_6, BAr_F]

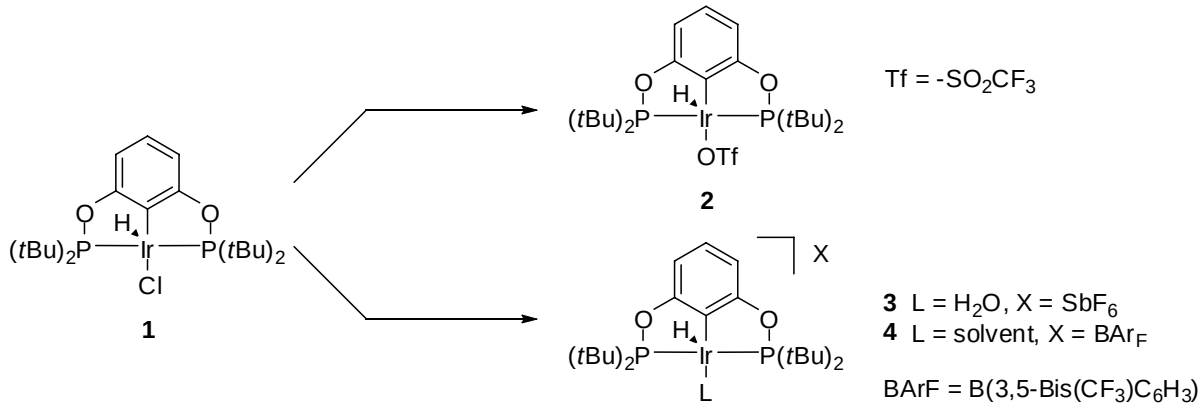

An X-ray quality crystal of **2** was obtained through slow crystallization from methylene chloride at -35°C under an argon atmosphere. An ORTEP diagram of the structure of **2** is shown in Figure 3.1. The triflate is bound in the coordination site *trans* to the *ipso* carbon of the ligand backbone. The hydride was not located, although one can assume it is in an axial position due to the ^{1}H chemical shift of -43.1 ppm which is indicative of an apical hydride with an empty coordination site *trans* to the hydride.[14,15] The C_{ipso}-Ir-O angle is unable to be measured because there is some disorder in the position of the triflate.

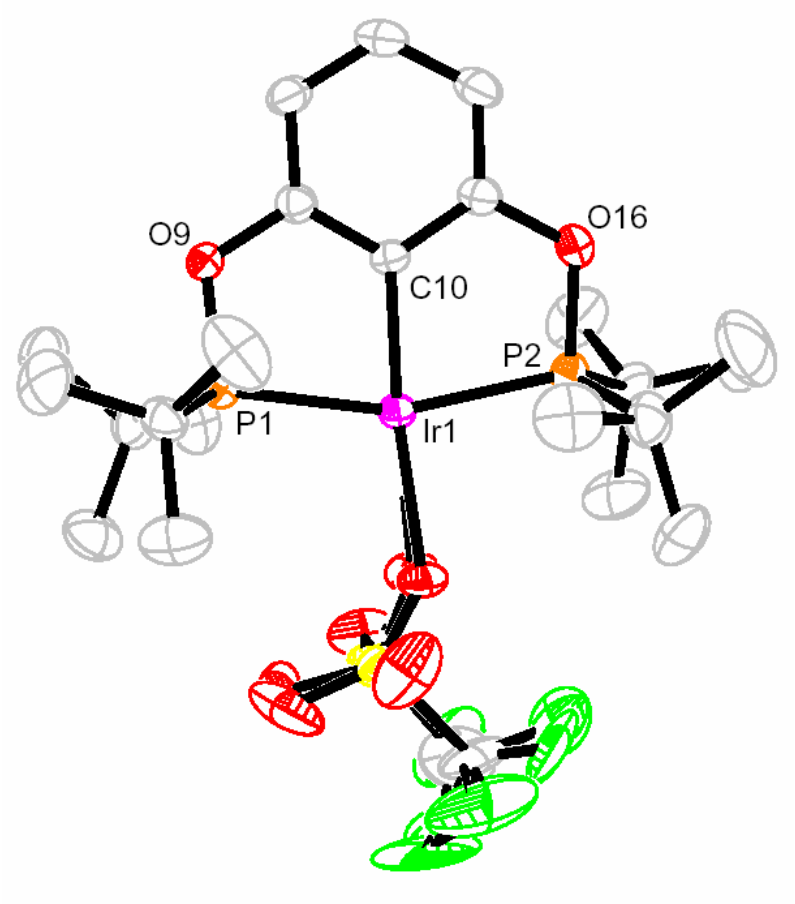

Figure 3.1. ORTEP diagram[16] of (POCOP)Ir(H)(OTf), **2**. The hydrogens have been excluded for clarity. Key bond distances (Å) and bond angles (degrees): Ir(1)–C(10) 1.993 Å, Ir(1)–P(1) 2.318 Å, Ir(1)–P(2) 2.296 Å, P(2)–Ir(1)–C(10) 80.41°, P(1)–Ir(1)–C(10) 80.08°

In order to test the lability of the bound triflate anion, a solution of **2** in methylene chloride-d_2 was exposed to one atmosphere of carbon monoxide. Initially, two products were formed (^{31}P NMR = 174.2 and 164.9 ppm). Both products bear a hydride with resonances downfield of the starting material at -10.5 and -7.3 ppm, respectively, which suggests a six-coordinate complex. When the solution is placed under a reduced pressure, the intensity of the resonance at 164.9 ppm (^{31}P NMR) decreases until the solution is comprised of only the complex represented by ^{31}P = 174.2 ppm. These two complexes are proposed to be the mono- and di- carbon monoxide adducts, **5** and **6** (Scheme 3.6). The IR spectrum of complex

5 shows a stretching frequency of 2062 cm^{-1}. Such a high frequency for a carbonyl stretch is not unexpected since the iridium center is electron poor, providing little backbonding into the π^* orbitals of the CO.

Scheme 3.6. Reaction of (POCOP)Ir(H)(OTf), **2,** with carbon monoxide

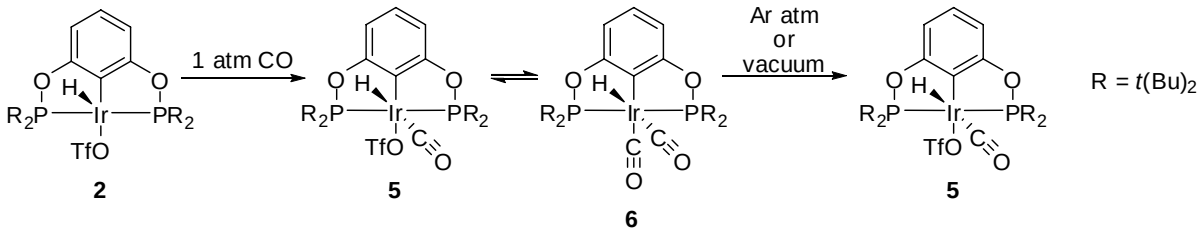

Pentafluoroaniline was also added to solution of **2** in methylene chloride-d_2. At room temperature, there was no reaction and only **2** and free pentafluoroanilne was observed in solution. After heating at 50°C overnight, the ^{31}P and ^{1}H NMR spectra taken at room temperature showed 4% of a decomposition product that contained no aniline bound to iridium. Therefore, the triflate anion has a higher binding affinity for the $[(POCOP)IrH]^+$ cation than aniline. Unfortunately, the results of both the above experiments indicate that the triflate ligand is coordinated more strongly than desired, and probably is not the optimum choice as counter-anion.

Reaction of **1** with $AgSbF_6$ in CH_2Cl_2 formed the H_2O complex **3** despite attempts to exclude water from the reaction mixture. (It was expected that methylene chloride might bind to the 14-electron $[(POCOP)IrH]^+$ cation.) The ^{1}H NMR spectrum shows the hydride resonance at -43.05 ppm, indicating a 5-coordinate species, as well as a very broad peak at ca. 4.05, spanning 1.5 ppm, for the coordinated water. An X-ray quality crystal was obtained through slow crystallization from methylene chloride at -35°C under an argon atmosphere.

The ORTEP diagram of the structure is shown in Figure 3.2. Water is bound *trans* to the *ipso* carbon with a C_{ipso}-Ir-O angle of 178.2°. Similar to **2**, the hydrogen was unable to be located but can be assumed to be in an axial position with an ^1H chemical shift of -43.0 ppm.

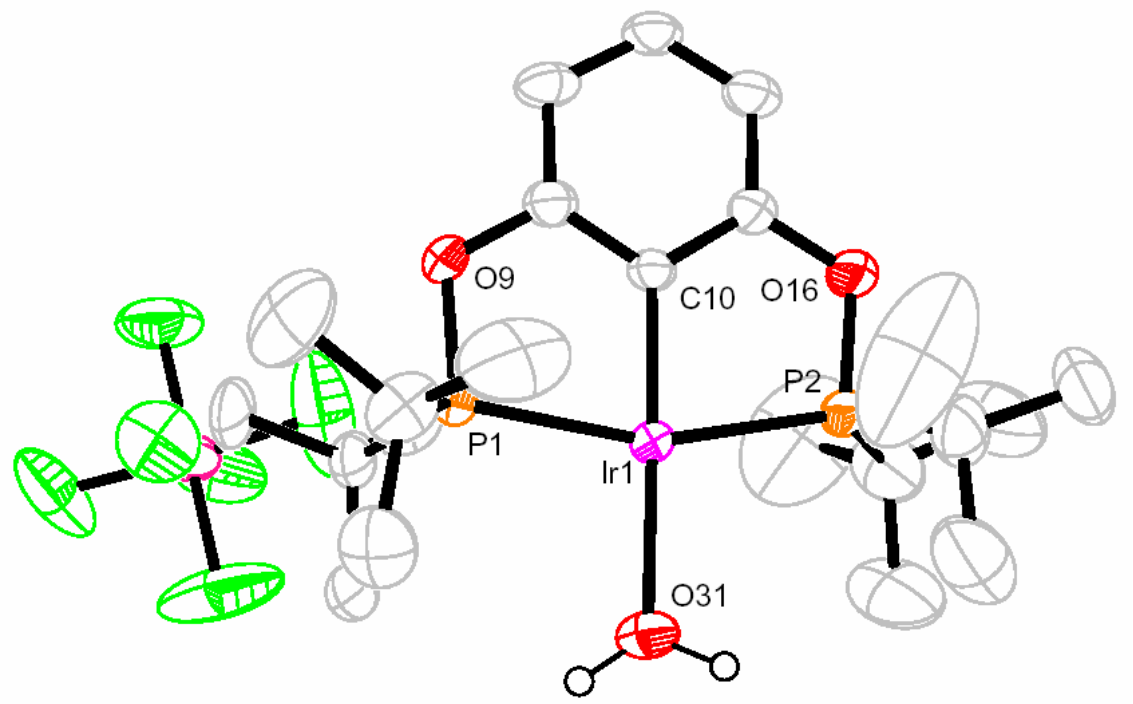

Figure 3.2. ORTEP diagram[16] of [(POCOP)Ir(H)(H_2O)][BAr_F], **3**. The hydrogens have been excluded for clarity. Key bond distances (Å) and bond angles (degrees): Ir(1)–C(10) 1.991 Å, Ir(1)–O(31) 2.210 Å, Ir(1)–P(1) 2.301 Å, Ir(1)–P(2) 2.302 Å, P(1)–Ir(1)–C(10) 80.37°, P(2)–Ir(1)–C(10) 80.12°, C(10)–Ir(1)–O(31) 178.22°

The reaction of **1** with $NaBAr_F$ was slower than the reactions with silver salts metioned above. This is due the low solubility of $NaBAr_F$ in methylene chloride, and therefore the reaction had to be stirred overnight. The ^1H iridium hydride chemical shift of the species formed is -41.92 ppm which indicates that there is no ligand *trans* to the hydride. It seems likely that methylene chloride is coordinated *trans* to the *ipso* carbon in this species, but no clean NMR evidence nor crystal structure was obtained to support this. One can assume,

however, that the structure of **4** is analogous to **3**. By adding a ligand that can strongly coordinate to the metal (such as an olefin), the cationic complex can be stabilized and the species of the type [(POCOP)Ir(H)(L)][BAr_F] can be fully characterized.

II. Synthesis and Dynamics of [(POCOP)Ir(H)(L)][BAr_F] (L = H_2 (9), Ethylene (10), Propylene (11), Norbornene (12), and Methyl Acrylate (MA) (13))

a) Synthesis, Characterization and Dynamics of [(POCOP)Ir(H)(H_2)][BAr_F] (9)

Formation of transition-metal dihydrogen complexes and their structures have been of interest since the first report of a stable M-(η^2-H_2) complex, (iPr$_3$P)$_2$(CO)$_3$W(η^2-H_2), by Kubas.[17] More recently, Crabtree,[18-20] Heinekey,[21-23] Parkin,[24] and others have presented extensive work on elucidating the structures of various "trihydride" complexes. There are two possible structures that have been proposed in the literature, a classical trihydride complex and a non-classical dihydrogen/hydride complex. Two features have been employed to distinguish these two structures, T_1(min) values and H/D coupling constants. Generally, small T_1 values (4-100 ms) indicate the existence of a bound dihydrogen with a short H-H distance and therefore a dihydrogen/hydride structure. Examination of the H-D coupling constants in a partially deuterated substrate provides a way to differentiate the structures as well. The $^1J_{H\text{-}D}$ coupling constant for free HD is 43.2 Hz. However, when dihydrogen coordinates to a metal, the $^1J_{H\text{-}D}$ coupling constant lowers to around 30 Hz, for example 33.5 Hz in Kubas' complex.[17,25] The $^2J_{H\text{-}D}$ coupling constant between two terminal hydrides is much lower and tends to be less than 2 Hz.

Crabtree and coworkers synthesized a cationic iridium dihydrogen hydride complex [IrH_3(bq)(PPh_3)$_2$][SbF_6] (bq = benzoquinoline) (Scheme 3.7) by displacement of an aquo

ligand by H_2. The complex is thermally stable under an atmosphere of hydrogen gas, but if purged with nitrogen in the presence of water, the H_2 is displaced by the aquo ligand. A crystal of this complex could not be obtained to verify the structure because the H_2 was labile in the solid state. However, an H/D coupling constant of 29.5 Hz was measured, indicating that the structure was the dihydrogen/hydride, not the classical trihydride.

Scheme 3.7. Equilibrium between $[IrH(H_2O)(bq)(PPh_3)_2][SbF_6]$ and $[IrH_3(bq)(PPh_3)_2][SbF_6]$ by Crabtree et. al.

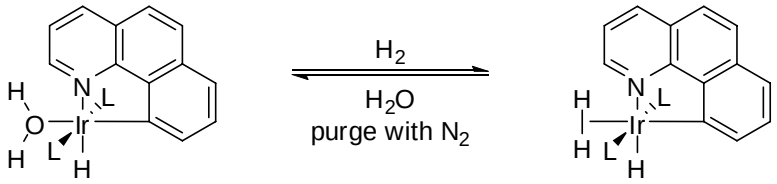

7 **8**

^{1}H NMR studies on complex **8** performed by Crabtree et al. showed at room temperature a single resonance representing the weighted average of the three hydrogens bound to iridium. However at temperatures below 260 K, the exchange rate of the dihydrogen and hydride decreases and the two signals separate. The dihydrogen resonance appears at -2.9 ppm, integrating for 2 protons, while the hydride resonates at -15.3 ppm. Through line-broadening studies, the exchange rate between the hydrogens was estimated to be 350-500 s^{-1} at 260 K. This corresponds to a $\Delta G^{\ddagger}$ of ca. 12.0 kcal/mol. Possible mechanisms for exchange are presented later in this section.

Previously, Göttker-Schnetmann in our group prepared an anionic trihydride complex, $[(POCOP)IrH_3][Na]$.[26] The $^1H\{^{31}P\}$ NMR resonances for the hydrides appear as a triplet at -

13.33 and as a doublet at -13.55. The $^2J_{H\text{-}H}$ coupling constant between the protons is 4.8 Hz ($J_{H\text{-}D} = J_{H\text{-}H}/7$), indicating that the structure is the classical trihydride and can be viewed as an 18-electron Ir(III) complex. Were this an η^2-H_2 complex $[(POCOP)Ir(H_2)H]^-$ this would be a 16-electron anionic Ir(I) complex. It is not surprising that such an electron-rich, unsaturated system would prefer to undergo oxidative addition of hydrogen to form the classical tryhydride.

For comparison we were interested in generating a cationic iridium "trihydride" complex such as $[(POCOP)Ir(H_3)][BArF]$, **9**, and determining if the structure is a classical or nonclassical trihydride (Figure 3.3). Since this complex would be electron-deficient, it would be more likely to exist in the non-classical dihydrogen/hydride form.

9a **9b**

Figure 3.3. The non-classical dihydrogen/hydride vs. the classical trihydride for $[(POCOP)IrH_3][BAr_F]$, **9**

Complex **9** was synthesized by two different routes. The first method involves the additon of $HBAr_F$ to a solution of $(POCOP)IrH_2$ in methylene chloride. However, $HBAr_F$ exists as a diethyl ether complex, $[H(OEt_2)_2][BArF]$, where Et_2O is a potential ligand. To avoid the addition of ether to the reaction mixture, **9** can be produced by hydrogenation of the propylene complex $[(POCOP)Ir(H)(C_3H_6)][BAr_F]$, **11,** (for preparation see below) in methylene chloride (Scheme 3.8). The H_3 complex, **9**, is cleanly generated and the only side product is one equivalent of propane which does not interfere with the NMR characterization.

While complex **9** can be quantitatively generated *in situ*, because the coordinated hydrogen is quite labile attempts to isolate this complex have been unsuccessful.

Scheme 3.8. Generation of [(POCOP)Ir(H)(H_2)][BAr_F], **9,** by hydrogenation of [(POCOP)Ir(H)(C_3H_6)][BAr_F], **11**

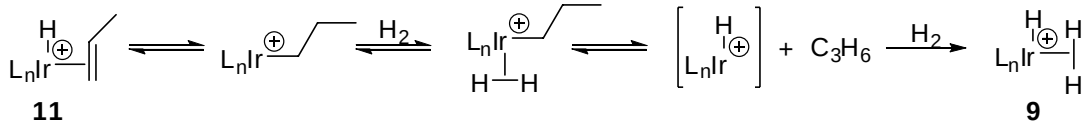

At room temperature the proton NMR spectrum of **9** shows a broad iridium hydride band between -13 and -15 ppm integrating for three protons. However at temperatures below ca. 200 K, this resonance separates into two broad signals, 0.033 ppm and -41.9 ppm, in a two to one ratio, respectively.[27] Both of these peaks were too broad to determine ^{31}P coupling. The large difference in chemical shift of the two protons immediately suggests that this complex is a dihydrogen/hydride, as compared to a trihydride in analogy to the Crabtree complex, **8**. Also, based on the resonance frequency of similar POCOP iridium pincer complexes, the very high upfield shift of -41.9 ppm is indicative of a hydride with an empty *trans* coordination site. However, more definitive proof of this structure was desired.

It order to obtain more detailed structural information, complex **9** was partially deuterated by purging both D_2 and H_2 through the solution. This generated a sample that contained a mixture of H_3, H_2D, HD_2, and D_3 complexes. The ^1H NMR signal at δ 0.03 was too broad and complex to determine a J_{HD} coupling constant. In the normal ^2H NMR spectrum at 173 K, the peaks representing H-D and D-D coordinated to the iridium could be seen in approximately a 1:1 ratio. Although the H-D coupling could be observed (Figure

3.4), it was difficult to obtain an accurate measurement of the H-D coupling constant. To circumvent this problem and accurately determine the coupling constant, a one-dimensional HMQC NMR experiment was performed in which the observed nucleus is deuterium. This experiment allowed only signals that contain H-D coupling to be visible, suppressing all signals that do not have coupling to ^{1}H (i.e. the D_2 signal). This HMQC experiment is depicted in Figure 3.4 where the bottom spectrum shows the normal ^{2}H-NMR spectrum, while the top spectrum shows the result of the one-dimensional ^{2}H-HMQC experiment where the doublet resonance for the partially deuterated complex is clearly observable. The measured J_{HD} coupling constant was 33.0 Hz, consistent with the $J_{H\text{-}D}$ of an η^2-HD ligand and supporting the assignment of **9** as an iridium(hydride)(dihydrogen).

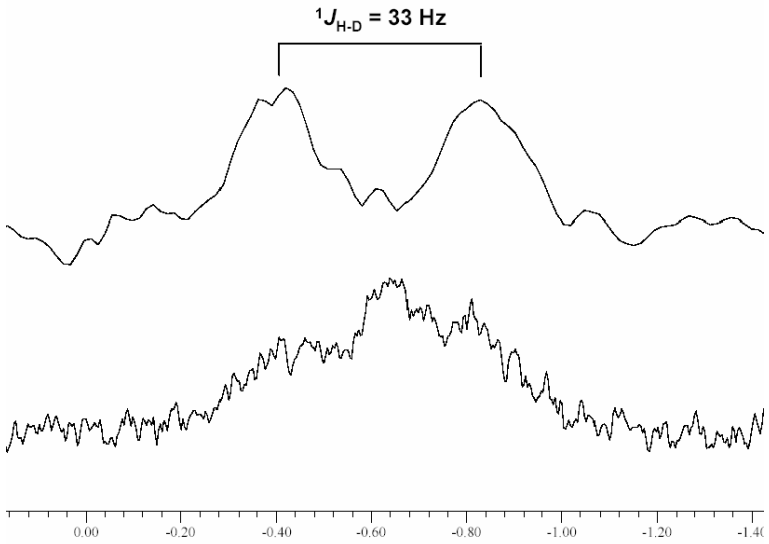

Figure 3.4. Overlay of the ^{2}H NMR spectrum of the dihydrogen region of a partially deuterated sample of [(POCOP)Ir(H)(H_2)][BAr_F], **9,** in CH_2Cl_2. The top spectrum is a deuterium observed 1D-HMQC. The bottom spectrum is a ^{2}H NMR. These spectra are not referenced but correlate to the σ-bound dihydrogen peak.

Similar to the Crabtree system, the three hydrogens on iridium interchange. Three possible mechanisms for the hydrogen exchange for [(POCOP)Ir(H)(H_2)][BAr_F] **9** are shown in Scheme 3.9. In the first mechanism, A, the dihydrogen oxidativly adds to the iridium center forming the classical trihydride intermediate. From this intermediate, reductive coupling of H_2 can lead to the starting complex, where no site exchange has occurred, or the complex in which H_a, originally the terminal hydride, has been incorporated into the η^2-H_2 site. Mechanism B involves a proton transfer from the dihydrogen to the hydride through a transition state in which there is partial and symmetrical bonding of the migrating hydrogen to both remaining hydrogens. No trihydride intermediate is required. In the last mechanism, C, the exchange of the hydrogens occurs through a triangular H_3^+ intermediate in which all hydrogens become equivalent.

Scheme 3.9. Modes of hydrogen exchange for [(POCOP)Ir(H)(H_2)][BAr_F], **9**

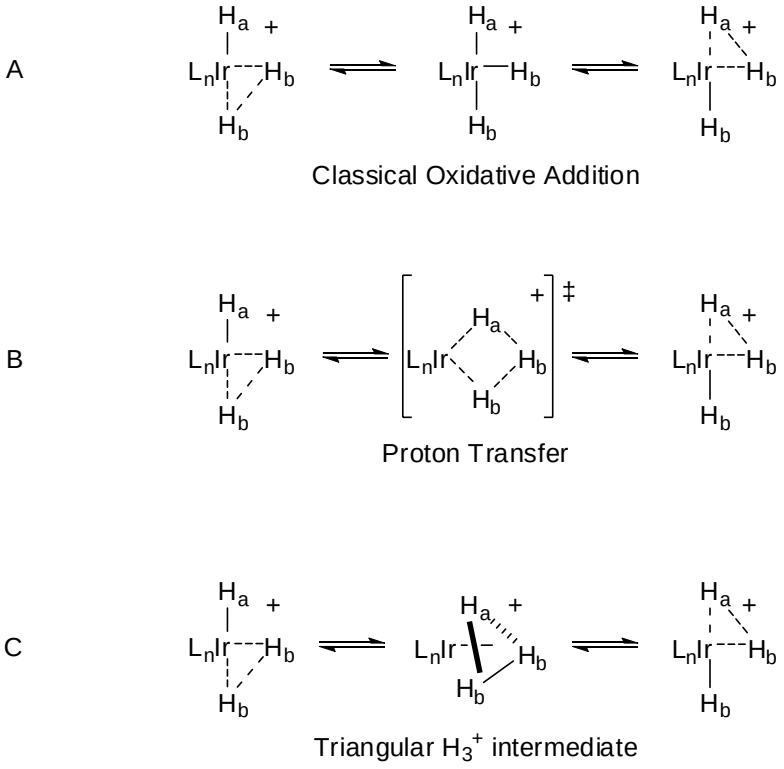

The exchange rate for the dihydrogen/hydride complex was measured for both the trideutero $\mathbf{9_D}$ and triproteo $\mathbf{9_H}$ complexes by line-broadening techniques. For $\mathbf{9_D}$, the line-width of the η^2-D_2 resonance was measured in the temperature range of 183.9-207.5 K. On the other hand, the rate for $\mathbf{9_H}$ was calculated by measuring the line-broadening of the hydride signal from 175.3 K to 196.8 K. The rate of exchange in the triproteo complex corresponded to $\Delta G^{\ddagger}$ = 9.1 kcal/mol (measured at 188 K, Appendix II, Scheme II.2 and Table II.2), while the rate in the trideuterated complex corresponded to $\Delta G^{\ddagger}$ = 9.8 kcal/mol (measured at 205 K, Appendix II, Scheme II.1 and Table II.1) for the exchange of the hydride with the proton on the σ-bound dihydrogen. Based on the energy barriers, the rate at 200 K was calculated for both $\mathbf{9_D}$ and $\mathbf{9_H}$. From these rates, an isotope effect of k_H/k_D ca. 6 was calculated (Appendix II, Table II.3). The existence of an isotope effect in which the energy barrier for the deuterated complex is higher was expected since the breaking of the H-H (or D-D) bond in the η^2-H_2 (η^2-D_2) would have to be involved in the transition state and the zero point energy in η^2-D-D is lower than that in η^2-H-H. There is no way, however, to distinguish between the three different mechanisms under these reaction conditions.

b) Synthesis and Characterization of [(POCOP)Ir(H)(L)][BAr_F] L = C_2H_4 (10), C_3H_6 (11), norbornene (12), methyl acrylate (13)

Similar to the cationic dihydrogen/hydride complexes, the cationic olefin hydride complexes can be synthesized by two methods (Scheme 3.10). The preferred method involves treatment of (POCOP)Ir(H)(Cl) **1** with $NaBAr_F$ in the presence of olefin in methylene chloride. Alternatively, addition of $HBAr_F$ to the isolated (POCOP)Ir(olefin) complexes produces the olefin hydride complexes.

Scheme 3.10. Synthesis of [(POCOP)Ir(H)(olefin)][BAr_F]

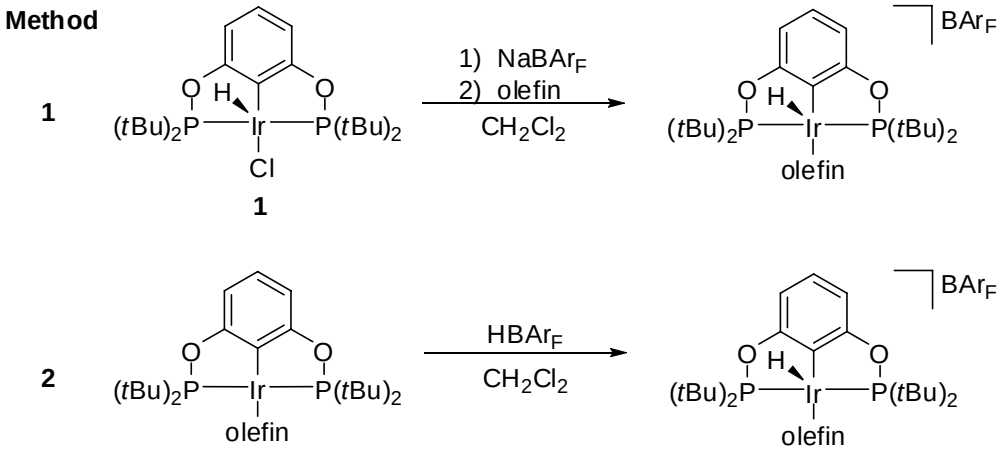

Both the ethylene complex **10** and propylene complex **11** can be generated quickly and cleanly by purging a mixture of (POCOP)Ir(H)(Cl), **1**, and $NaBAr_F$ with either ethylene or propylene gas. Since the solution is saturated with olefin, and therefore, the olefin concentration is high, this reaction is complete within fifteen minutes as indicated by a color change from light red to pale orange. Removal of the salt by syringe filtration under argon and evaporation of the solvent yields the pure product as a pale orange powder (Scheme 3.11).

Scheme 3.11. Formation of [(POCOP)Ir(H)(L)][BAr_F] L = C_2H_4 (**10**), C_3H_6 (**11**)

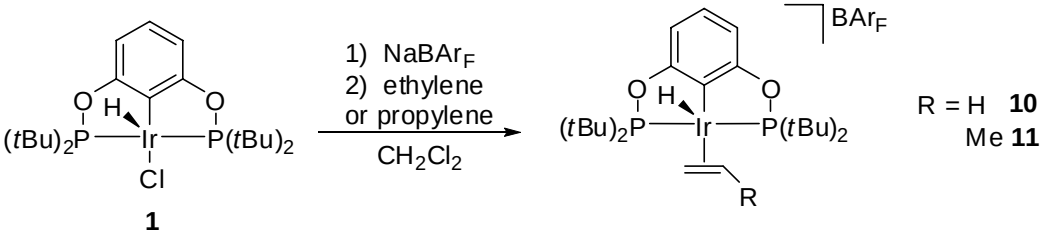

At room temperature the bound ethylene of **10** is rapidly rotating on an NMR timescale as evident by a single ethylene resonance in the ^{1}H NMR spectrum at 4.15 ppm. The upfield shift of the hydride in the ^{1}H NMR spectrum of -42.83 ppm, is consistent with a 5-coordinate complex where the hydride is situated in the apical position *trans* to an empty coordination site. This geometry requires the *t*-butyl groups *cis* to the iridium hydride be distinct from those *trans* to the hydride. In fact, two *t*-butyl signals, seen as virtual triplets due to strong phosphorus-phosphorus coupling, suggest the existence of a vertical mirror plans bisecting the ligand backbone. This is supported by a single ^{31}P resonance at 182.0 ppm for the two equivalent phosphorus atoms.

The propylene complex **11** displays some characteristics similar to the ethylene complex **10** such as an ^{1}H NMR hydride signal at -42.90 ppm. However, there are some very noticeable differences. Typically, in the ^{1}H spectra of POCOP-pincer complexs, the aryl backbone of the ligand has two resonances associated with it, a triplet for the central hydrogen (*para* to the iridium-bound carbon) and a doublet for the two equivalent hydrogens adjacent to the central one. In the propylene complex **11**, the two adjacent hydrogens are now inequivalent and are seen as two doublets in the ^{1}H NMR spectrum at 6.90 and 6.86 ppm. There are also now four resonances for the *t*-butyl groups, indicating none of the *t*-butyl groups are related by symmetry. The ^{31}P NMR also supports this as there are two doublet signals (182.7 ppm, 175.0 ppm, J_{PP} = 260.1 Hz) for the two inequivalent phosphorus nuclei that are strongly coupled with each other. It is likely that the propylene, similar to the ethylene, is also rotating rapidly at room temperature; however since none of the conformations possess a mirror plane bisecting the ligand backbone, rapid rotation does not result in averaging the ^{31}P signals or the *t*-butyl pairs.

The structure of [(POCOP)Ir(H)(C_3H_6)][BAr_F], **11**, was confirmed by X-ray analysis. A crystal was grown by slow diffusion of pentane into a solution of **11** in methylene chloride at room temperature under an argon atmosphere. An ORTEP diagram of **11** is shown in Figure 3.5 and supports the structure determined by NMR spectroscopy. The propylene is rotated slightly from alignment of the C-C double bond with the plane with the ligand backbone. This rotation likely occurs to decrease the steric interactions between the methyl groups of the propylene and the *t*-butyl groups.

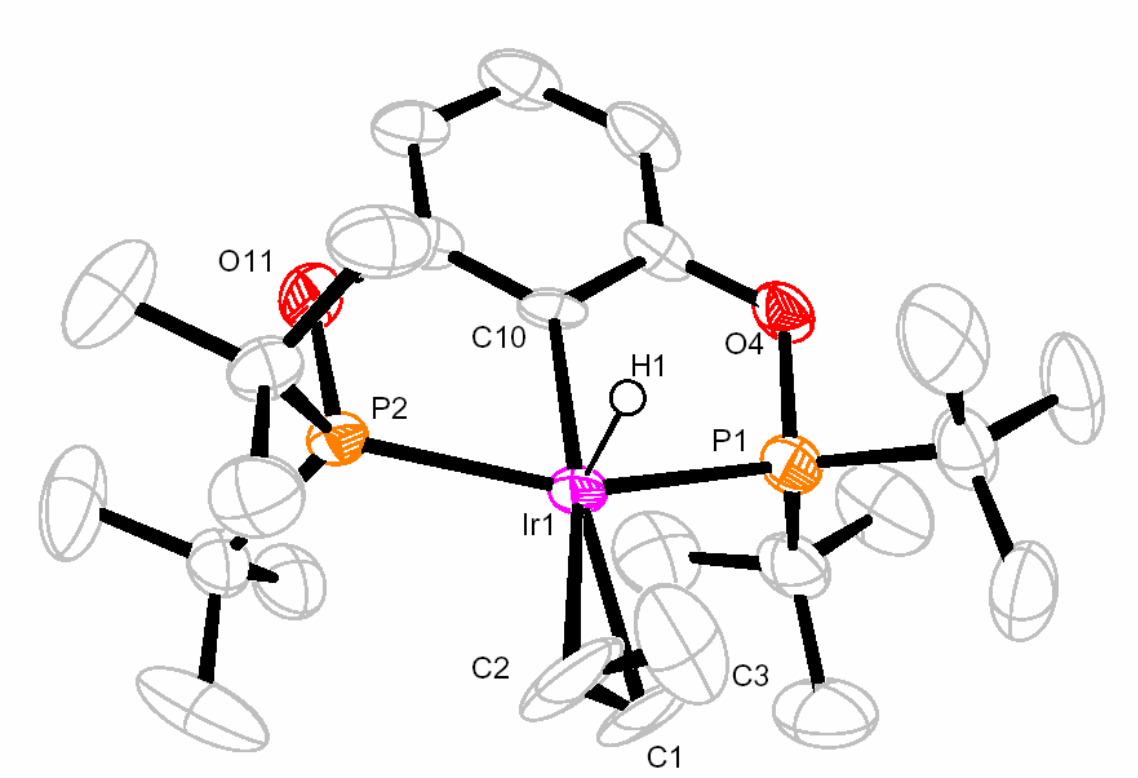

Figure 3.5. ORTEP diagram[16] of [(POCOP)Ir(H)(C_3H_6)][BAr_F]. The hydrogens and counterion have been excluded for clarity. Key bond distances (Å) and bond angles (degrees): Ir(1)–C(10) 2.046 Å, Ir(1)–P(1) 2.338 Å, Ir(1)–P(2) 2.338 Å, Ir(1)–C(1) 2.255 Å, Ir(1)-C(2) 2.276 Å, C(1)-C(2) 1.141 Å, P(1)–Ir(1)–C(10) 78.57°, P(2)–Ir(1)–C(10) 78.72°, C(2)–C(1)–Ir(1)-P(2) -39.78°

The norbornene complex **12** is synthesized in a similar manner as the ethylene and propylene complexes (Scheme 3.12). In order for this reaction to go to completion in a respectable time, excess norbornene must be added to the reaction mixture. After filtration and removal of the solvent, the crude product must be washed with pentane to remove the excess norbornene. A plane of symmetry passing through the plane of the POCOP ligand backbone is evident by both ^{31}P NMR and ^{1}H NMR spectroscopy. A single resonance is observed at 176.0 ppm in the ^{31}P NMR spectrum and only two triplet ^{1}H signals are seen for the *t*-butyl signals, one for the pair *cis* to the iridium hydride and one for the pair *trans*. The hydride resonance is located at -45.9 ppm as in the other olefin complexes, indicating a 5-coordinate complex with an empty coordination site *trans* to the hydride. The ^{1}H olefinic signals and the methine protons are observed at 4.71 and 3.44 ppm, respectively, in the ^{1}H NMR spectrum. The resonances for the two diastereotopic protons on the C_7 methylene carbon are very distinct doublets at 0.90 and 0.22 ppm. The endo and exo protons are further downfield at 1.90 and 1.33 ppm.

Scheme 3.12. Synthesis of [(POCOP)Ir(H)(norbornene)][BAr_F], **12**

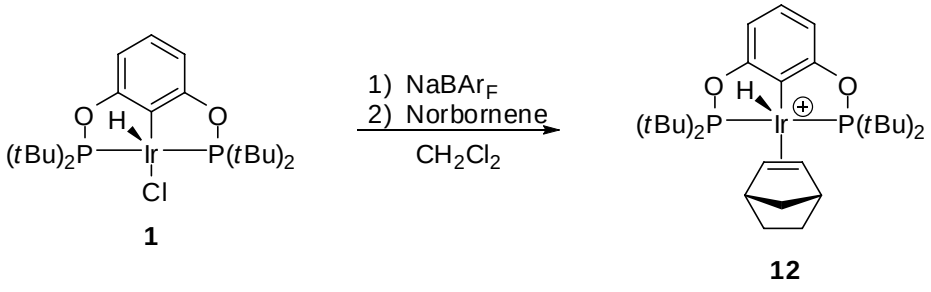

The structure of [(POCOP)Ir(H)(norbornene)][BAr_F], **12**, is confirmed by X-ray diffraction. The ORTEP diagram with key bond length and angles is shown in Figure 3.6.

The crystal was grown by slow diffusion of pentane in to a solution of **12** in methylene chloride under an argon atmosphere at room temperature. The carbon-carbon double bond is almost perfectly parallel with the plane of the ligand; however, it is slightly shifted above the plane. The hydride was not able to be located.

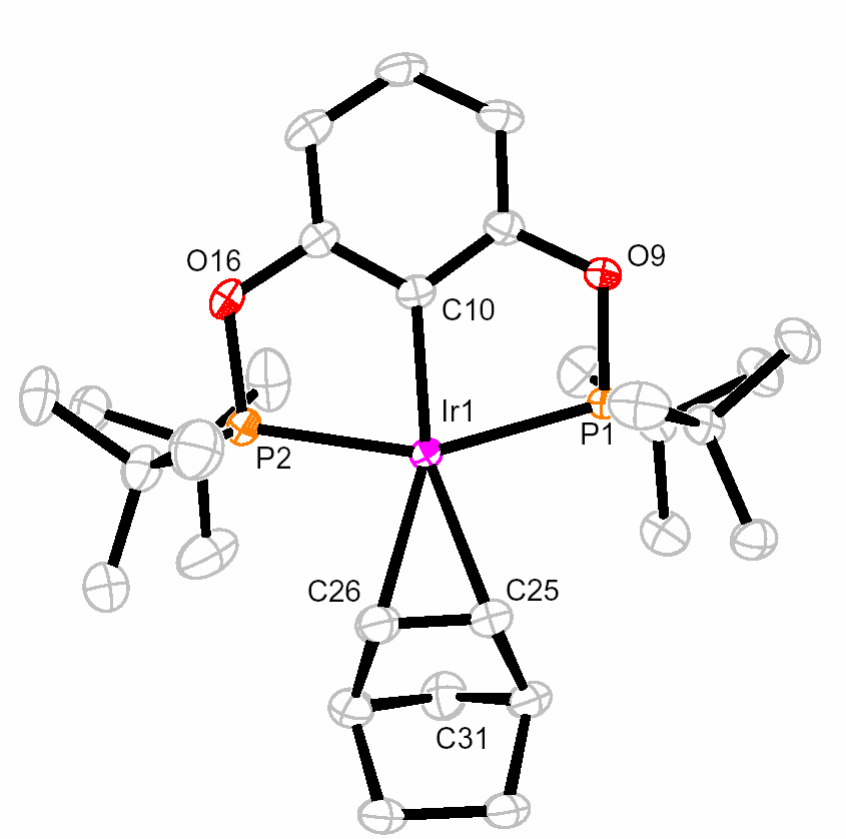

Figure 3.6. ORTEP diagram[16] of [(POCOP)Ir(H)(norbornene)][BAr_F], **12**. The hydrogen and BAr_F counterion have been omitted for clarity. Key bond distances (Å) and bond angles (degrees): Ir(1)–C(10) 2.051 Å, Ir(1)–P(1) 2.353 Å, Ir(1)–P(2) 2.348 Å, Ir(1)–C(25) 2.289 Å, Ir(1)-C(26) 2.287 Å, C(25)-C(26) 1.397 Å, P(1)–Ir(1)–C(10) 77.67°, P(2)–Ir(1)–C(10) 77.80°, C(25)-Ir(1)-C(10) 157.20°, C(26)-Ir(1)-C(10) 156.45°

Isolation of [(POCOP)Ir(H)(MA)][BAr_F], **13**, proved difficult. When $NaBAr_F$ and excess methyl acrylate were added to a solution of (POCOP)Ir(H)(Cl), **1**, the final product was a sticky solid that was very difficult to purify. Therefore, **13** was generated *in situ* by addition of $HBAr_F$ to (POCOP)Ir(MA) **14** (Scheme 3.13). (POCOP)Ir(MA) was cleanly prepared by

reaction of **1** with NaO*t*Bu and methyl acrylate in benzene. Removal of solvent under vacuum yielded **14** as a brick red solid.

Scheme 3.13. Synthesis of [(POCOP)Ir(H)(MA)][BAr_F], **13**

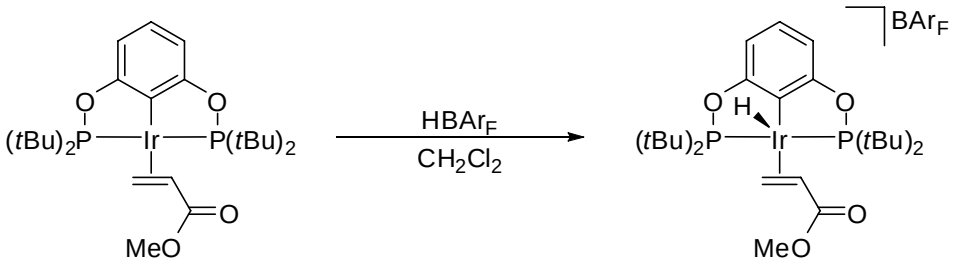

14 **13**

Upon mixing $HBAr_F$ and (POCOP)Ir(MA), **14**, in methylene chloride, the ^1H NMR spectrum of the the product **13** showed some distinctive peaks. At room temperature three broad resonances representing the methyl acrylate olefinic protons of the two rotamers, **13a** and **13b**, in fast exchange were observed at 3.33, 5.35 and 5.15 ppm. The $^{31}P\{^1H\}$ spectrum exhibited two broad phosphorus doublets at 179.8 and 175.8 (J_{PP} = 228.0 Hz). A third complex is also observed in the reaction mixture that has one multiplet at 2.92 ppm and a triple resonance at 2.22 ppm in the ^1H NMR spectrum. These two signals represent the methylene protons of the insertion product **15**. It is believe that the insertion product is in slow equilibrium with the olefin hydride complexes, with an equilibrium constant of roughly 0.13, favoring the olefin hydide. The ^{31}P chemical shift of the insertion product is 153.4 ppm which is significantly further upfield from the olefin hydride complexes. This upfield shift is likely indicative of an interaction of the carbonyl oxygen with the iridium as shown in Scheme 3.14. A similar upfield shift have been seen in the neutral POCOP system, (POCOP)Ir(H)(NH(CO)(C_6H_5)), reported in Chapter 2 which was also attributed to an

interaction of the carbonyl oxygen with Ir. Attempts to grow X-ray quality crystals of this complex were unsuccessful possible due to multiple complexes present in solution.

Scheme 3.14. Rotation and insertion of methyl acrylate in [(POCOP)Ir(H)(MA)][BAr_F], **13**

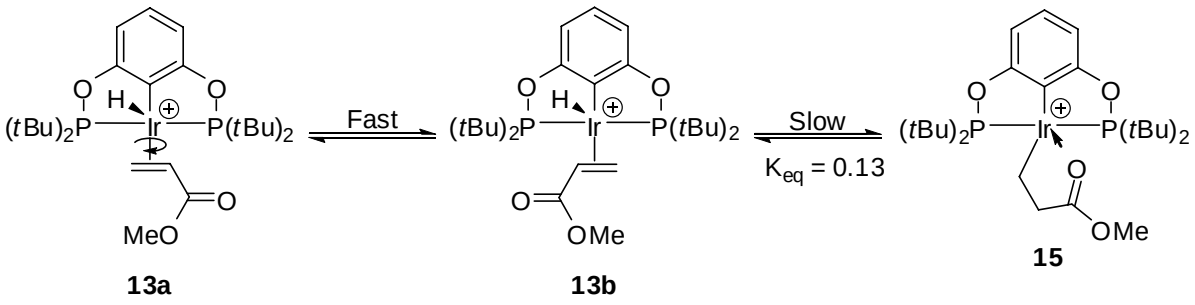

c. Dynamics of [(POCOP)Ir(H)(L)][BAr_F] L = C_2H_4 (10), C_3H_6 (11), norbornene (12), methyl acrylate (13)

In order to gain further understanding about the behavior of these cationic olefin hydride complexes **10-13**, variable temperature NMR experiments were performed to observe any dynamic behavior. The dynamics were studied using both line-broadening and spin-saturation studies. Initially, it was believed that both rotation of the olefin and insertion of the olefin into the Ir-H bond were occurring. However, the NMR experiments are complicated and deserve an in-depth discussion.

Low temperature studies to observe olefin rotation

[(POCOP)Ir(H)(C_3H_6)][BArF] **11** was dissolved in methylene chloride-d_2 and cooled to 175.3 K in the NMR probe. Upon cooling, analysis of the ^{1}H NMR spectra show that the olefin and hydride signals broaden and shift slightly (resonances marked 1a-4a, Figure 3.7).

At temperatures below 205 K the resonances begin to sharpen and a second set of minor signals appear below ca. 184 K (resonances marked 1b-4b, Figure 3.7). The chemical shifts above at 205 K represent a weighted average between the two complexes in fast exchange.

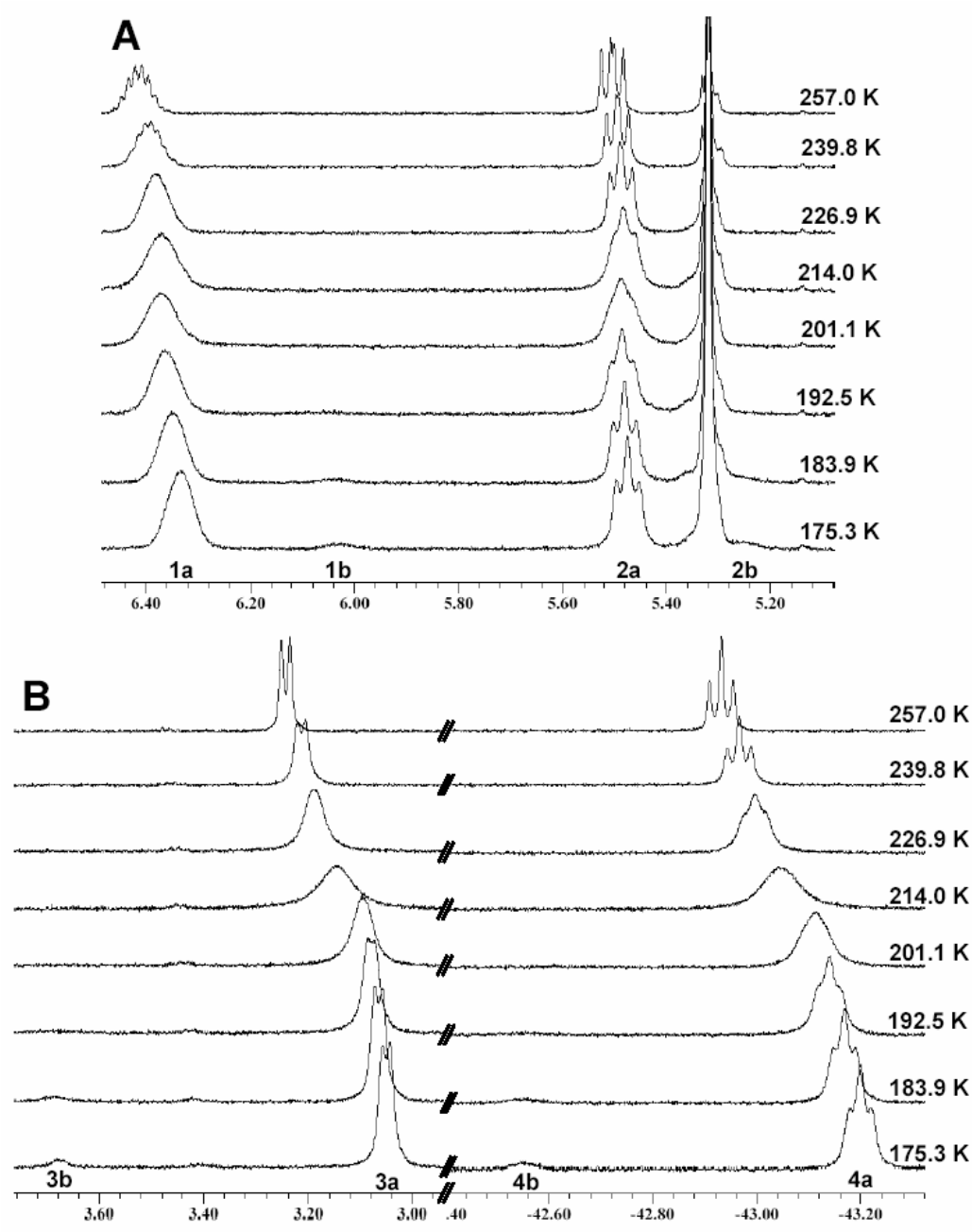

Figure 3.7. Variable temperature stacked ^{1}H NMR spectra of [(POCOP)Ir(H)(C_3H_6)][BAr_F] **11**.

There are two possible explanations for this behavior. The first is an equilibrium between two rotamers, **11a** and **11b** (Scheme 3.15), in which one rotamer is greatly favored over the other. The second possibility is an equilibrium between **11c**, a solvated form of **11** (Scheme 3.16). The hydride chemical shifts of the two complexes are -42.56 and -43.20 ppm, both of which are characteristic for five-coordinate (POCOP) iridium pincer complexes. If solvent had coordinated to the complex, a significant down field ^{1}H chemical shift for the hydride would be expected. Therefore, it seems most likely that the two complexes are rotamers.

Scheme 3.15. Propylene rotation in [(POCOP)Ir(H)(C_3H_6)][BAr_F]

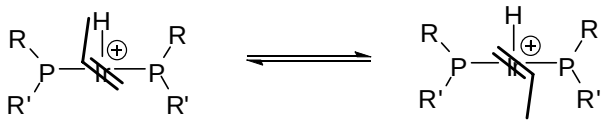

11a **11b**

Scheme 3.16. Solvation in [(POCOP)Ir(H)(C_3H_6)][BAr_F]

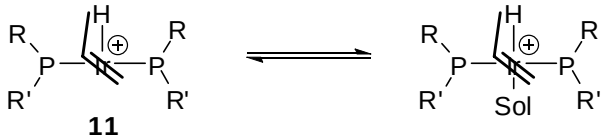

11 **11c**

As shown in the ^{1}H NMR spectra (Figure 3.7), the two rotamers **11a,b** are of unequal populations. At 175 K, the two complexes, **11a** and **11b**, are exchanging slowly on an NMR timescale and can be observed as separate resonances (Scheme 3.15). The equilibrium constant was measured by integration of the three pairs of signals (1a vs. 1b, 2a vs. 2b, and 4a vs. 4b). The measured K_{eq} values were 0.066, 0.063, and 0.069, with an average of 0.066

at 175.3 K. It is not clear which rotamer is favored. Using linebroadening techniques along with the K_{eq} shown above, energy barriers for the rotation from the major rotamer to the minor rotamer and vice versa have been calculated as 10.2 and 9.1 kcal/mol, respectively. (Line-broadening calculations for the rotation rate of the major isomer are shown in Appendix II, Table II.7)

A similar phenomenon is observed for [(POCOP)Ir(H)(C_2H_4)][BAr_F] **10** in which the ethylene and hydride signals broaden as the methylene chloride-d_2 solution of **10** is cooled in the NMR probe. However, at 175.3 K the ethylene resonance remains broad and does not sharpen (Figure 3.8) indicating that the coalescence between the two inequivalent ethylene protons occurs below 175.3 K. This is not unexpected as ethylene should have a lower energy barrier to rotation than propylene, and therefore, lower temperatures are needed to observe slow rotation. By assuming that the difference in frequency between the chemical shifts of the olefin protons is 25 Hz or greater, the ethylene rotation can be estimated as being less than 8.7 kcal/mol. (Calculations for this estimation are shown in Appendix II, Table II.4)

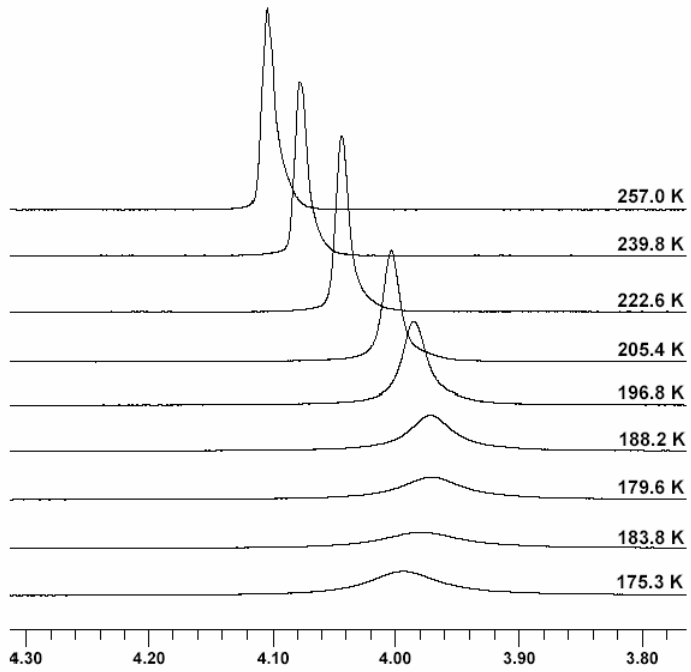

Figure 3.8. ^{1}H NMR spectra of the ethylene resonance in [(POCOP)Ir(H)(C_2H_4)][BAr_F] **10** at variable temperatures

However, there are a couple of unusual characteristics observed in the [(POCOP)Ir(H)(C_2H_4)][BAr_F] spectra. First, if only simple rotation of the olefin was occuring, the hydride resonance should not broaden since both rotamers of ethylene are equivalent. Secondly, it is abnormal for the direction of the chemical shift drift to change, however this is seen for both the ethylene and hydride resonances (Figure 3.8 and Figure 3.9). One possible explanation that would explain both of the described characteristics is that there is both a temperature dependence of the chemical shifts of the ethylene and hydride resonances, as well as the existence of an equilibrium between **10** and a solvated complex as described above. If **10** were in equilibrium with the solvated complex, an upfield shift of the hydride would be expected as the two resonances decoalesce. This is what is observed at 175.3 K in Figure 3.9. There is, however, no resonance observed at 175.3 K for the hydride

of the solvated complex. This might be expected if the resonance is very broad and the solvated species is at low concentration. As the temperature is raised above 205 K, both the ethylene and hydride chemical shifts move in the opposite direction, the hydride drifts upfield while the ethylene resonance drifts downfield. This phenomenon might be explaned by a temperature dependence of the chemical shifts or the fact that a rapid equilibrium between a solvated and unsolvated complex shifts in favor of the unsolvated complex as would be expected upon warming. This change in equilibrium would drive the shift average upfield as observed since the hydride signal of the solvated species should be downfield of that for the unsolvated species. (Scheme 3.17)

Scheme 3.17. Solvation in [(POCOP)Ir(H)(C_2H_4)][BArF]

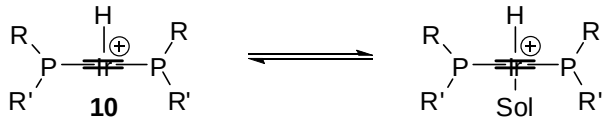

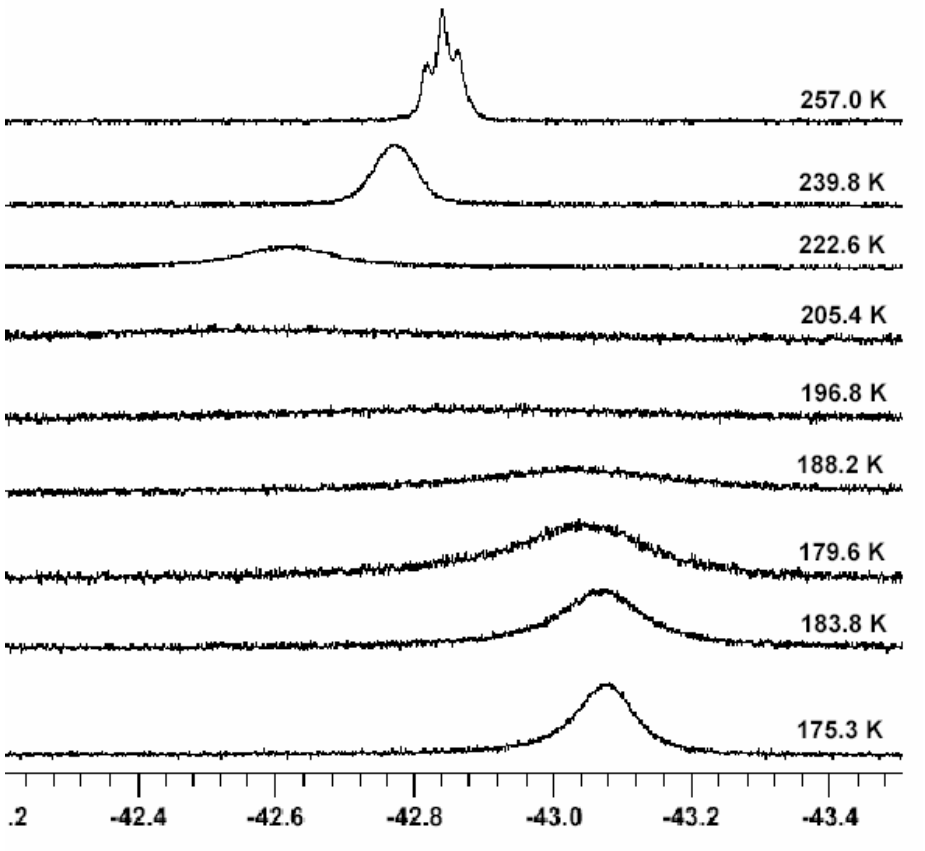

Figure 3.9. ^{1}H NMR spectra of the hydride resonance in [(POCOP)Ir(H)(C_2H_4)][BAr_F] **10** at variable temperatures

As [(POCOP)Ir(H)(norbornene)][BAr_F], **12**, is cooled in the NMR probe the rotation of the norbornene, unlike the ethylene and propylene complexes, is clearly frozen out (Figure 3.10). The two rotamers exist in about a 50:50 ratio at 174 K (Scheme 3.19). This is expected since the steric interaction between the *t*-butyl groups and the coordinated norbornene are virtually the same for either rotamer. The room temperature ^{31}P NMR spectrum shows a single resonance for the weighted average of the two rotamers at 177.8 ppm which decoalesces at about 200 K. Two equal intensity resonances are observed at 179.0 and 177.2 ppm (Appendix II, Figure II.2). The olefin, methine, hydride and the C_7 methylene protons all show decoalescence at low temperature in the ^{1}H NMR spectrum

(Figure 3.10). This data is consistent with the crystal structure shown in Figure 3.6 and the existence of two rotamers in which the olefin is parallel with the ligand backbone. If the two rotamers had a structure in which the olefin was bound perpendicular to the ligand plane, the C_7 methylene protons would not broaden or show decoalescence since the rotamers would be mirror images of each other. Using line-broadening techniques in the ^{1}H NMR spectra the rate of interconversion of the rotamers was calculated to be 167 s^{-1} at 190.8 K, corresponding to a $\Delta G^{\ddagger}$ is 9.1 kcal/mol. The calculations are shown in Appendix II, Table II.10.

Scheme 3.18. Rotation of [(POCOP)Ir(H)(norbornene)][BAr_F], **12**

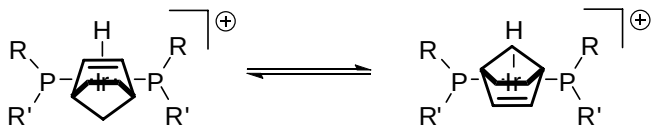

12a **12b**

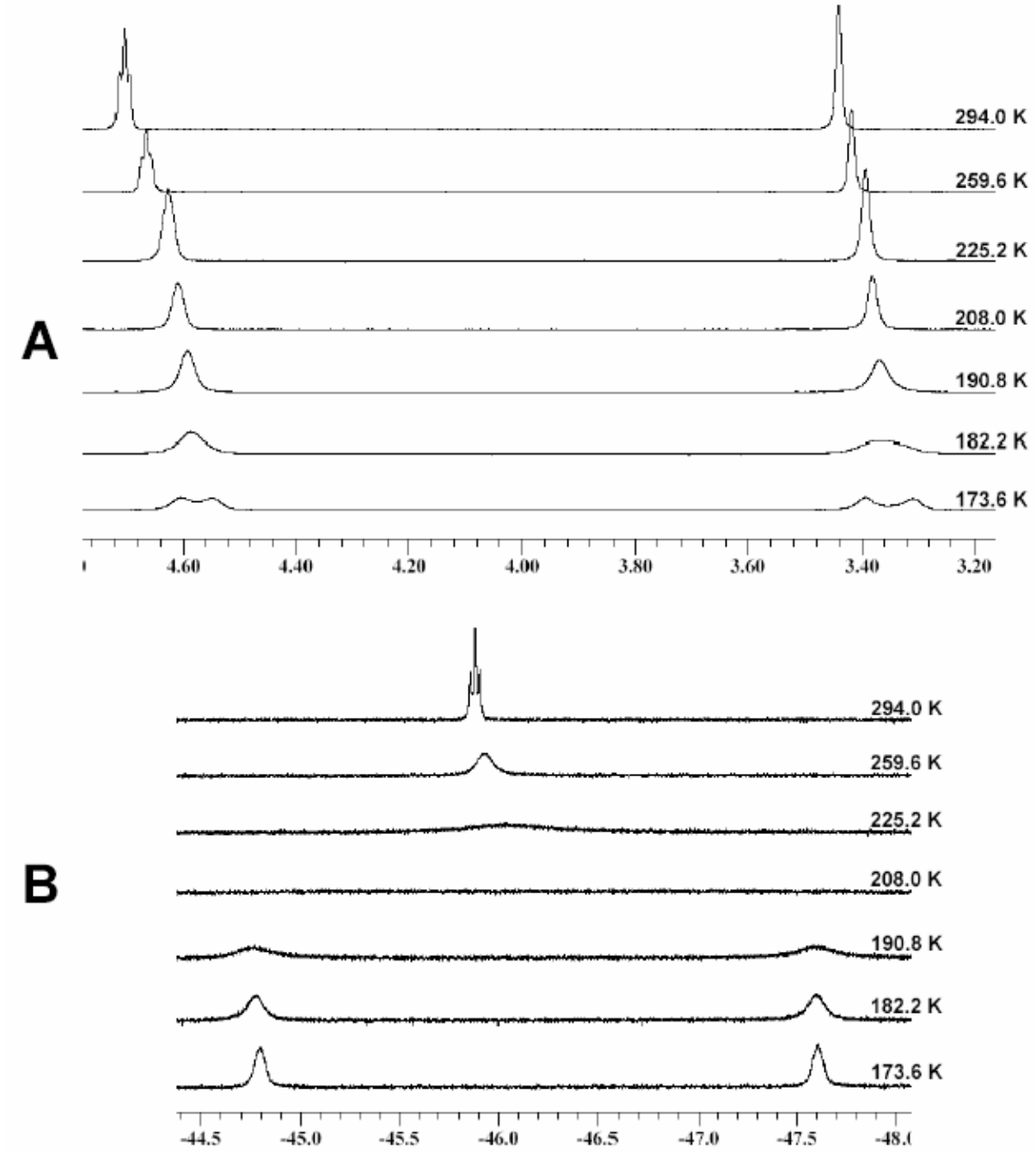

Figure 3.10. Stacked ^{1}H NMR plots of low temperature studies of [(POCOP)Ir(H)(norbornene)][BAr_F], **12**

Low temperature NMR studies were also performed on [(POCOP)Ir(H)(methyl acrylate)][BAr_F] **13** in order to measure the rate of rotation of the methyl acrylate. As the sample is cooled in the NMR probe the broad olefin signals broaden, decoalesce, and then re-

sharpen at 196.8 K (Figure 3.11). Similar to the propylene complex **11**, it is likely that the two complexes are the two rotamers in equilibrium. At 196.8 K, the equilibrium constant is 0.26 based on the ^{1}H integration. It unclear which rotamer is the more favored isomer. The hydride signals for the two rotamers are at -30.0 ppm for the major isomer and -36.2 ppm for the minor one. This suggests that in both of these isomers there may be some interaction of the carbonyl oxygen with the coordination site *trans* to the hydride. Since chemical shift for the weight averaged hydride at room temperature is at -38.5 ppm, there must be a temperature dependence off the shifts causing the weighted average to drift downfield as the temperature lowers. Based on the relative intensities of the olefinic resonances in the ^{1}H NMR spectrum for the corrdinated methyl acrylate at 197 K, an equilibrium constant, K_{eq} = 0.3, was calculated. Line broadening techniques and the equilibrium constant allow for calculation of the rate of conversion from the major to the minor rotamer and the minor to the major rotamer. These rates correspond to free energy barriers of 11.0 kcal/mol and 10.5 kcal/mol, respectively. (Calculation are shown in Appendix II, Table II.11)

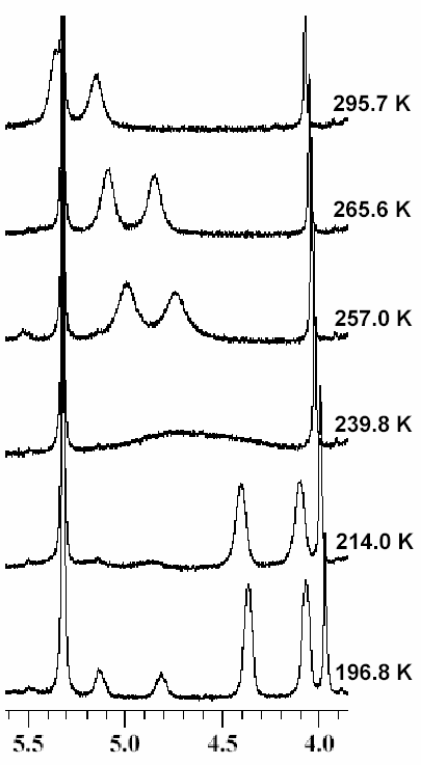

Figure 3.11. Stacked ^{1}H NMR spectra of [(POCOP)Ir(H)(MA)][BAr_F], **13**, at low temperatures.

Kinetics of Migratory Insertion Processes

For [(POCOP)Ir(H)(C_2H_4)][BArF], **10**, the rate of insertion of ethylene into the Ir-H bond to form [(POCOP)Ir(CH_2CH_3)][BAr_F] was measured by examining the exchange rate between the hydride and ethylene resonances using line-broadening techniques. As the temperature is raised to 320 K, both the ethylene and hydride resonances broaden (Figure 3.12 and 3.13). To verify that the observed broadening was due to insertion, a spin-saturation transfer experiment was performed. At 276.5 K, when the hydride signal was irradiated, the ethylene signal decreased 49%. Therefore, migration of the hydride to the ethylene followed by proton scrambling is occurring and can be attributed to the broadening of both the ethylene and the hydride signal at elevated temperatures. Interestingly, the two

resonances for the *t*-butyl signals do not average (Appendix II, Figure II.1). In other words, once the insertion occurs the alkyl chain resides on only one face of the complex and does not freely rotate to the opposite face.

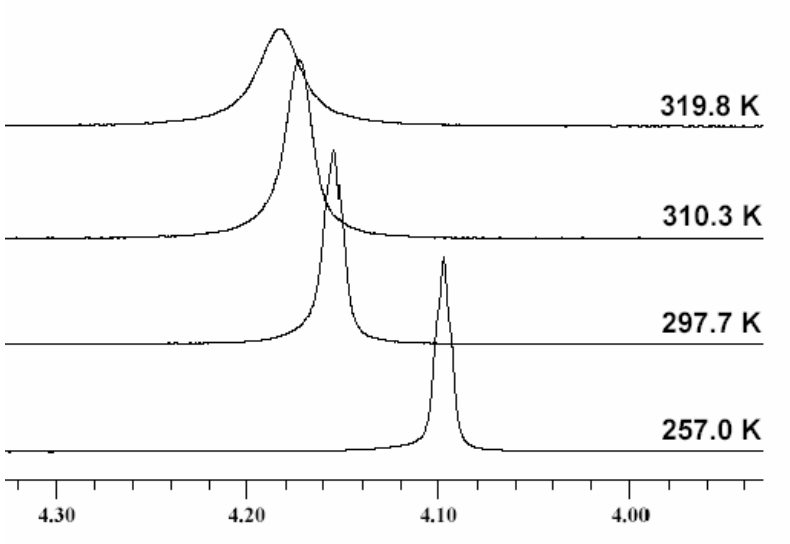

Figure 3.12. High temperature ^{1}H NMR stacked plots of the ethylene resonance of [(POCOP)Ir(H)(C_2H_4)][BAr_F], **10**

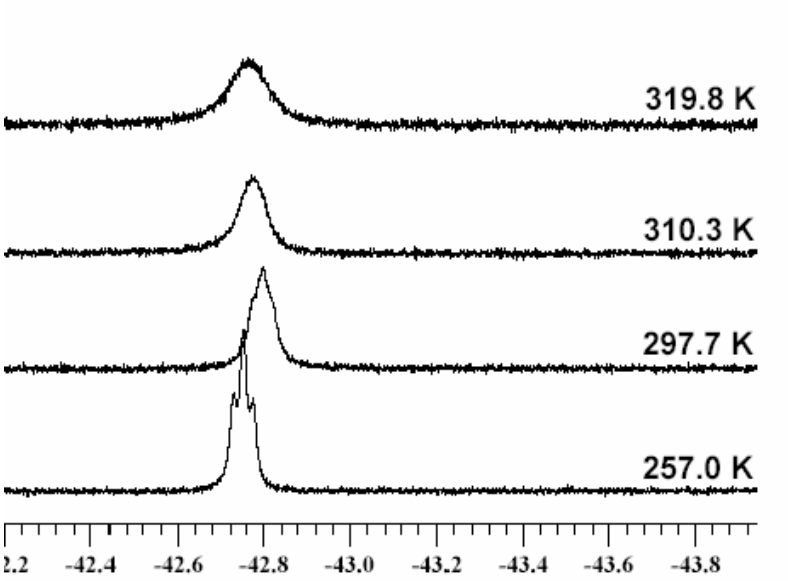

Figure 3.13. High temperature ^{1}H NMR stacked plots of the hydride resonance of [(POCOP)Ir(H)(C_2H_4)][BAr_F], **10**

Two possible pathways for exchange of the protons in the cationic ethylene complex are shown in Scheme 3.19; both account for restricted rotation after insertion. Pathway A is the direct insertion of the ethylene into the Ir-H′ bond to form a normal ethyl group (I → II). The three hydrogens can now exchange through rotation of the methyl moiety which should be very fast. However, rotation around the Ir-C_1 bond must be slower than return to Ir, otherwise the two sets of *t*-butyl signals would broaden and average. A second possibility involves the H′ migration to the bound ethylene to form the agostic complex III. In this case, "in-place" rotation of the agostic methyl group would achieve scrambling of the three hydrogens without averaging the two sets of *t*-butyl resonances. The transition state for scrambling would be the transition state for methyl rotation. Such an "in-place" rotation of an agostic methyl group to account for similar scrambling has been previously proposed.[28] The free energy diagrams for these two processes are shown in Figure 3.14. The data do not allow distinction between the two mechanisms.

Scheme 3.19. Possible mechanism for the exchange of hydrogen in [(POCOP)Ir(H)(C_2H_4)][BAr_F], **10**, (R = *t*-butyl)

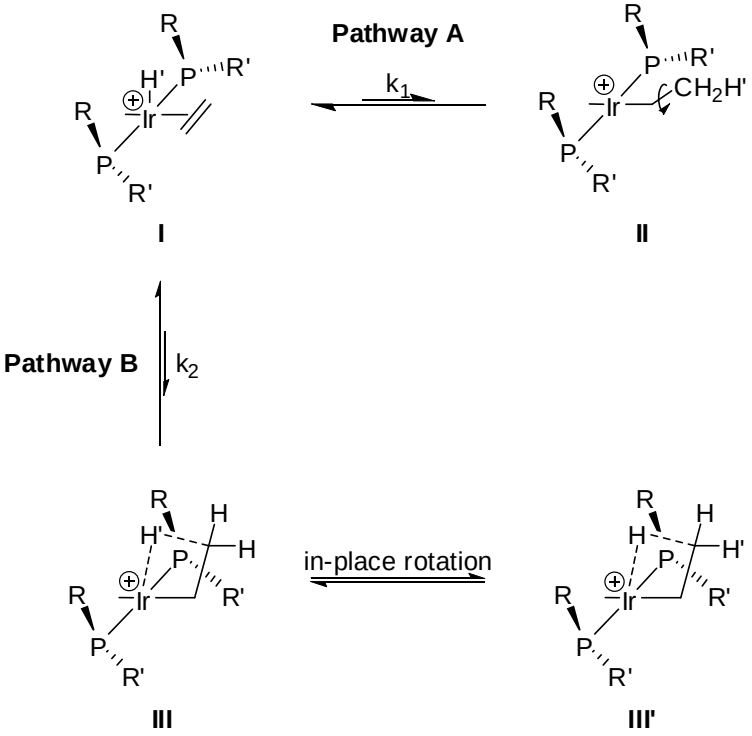

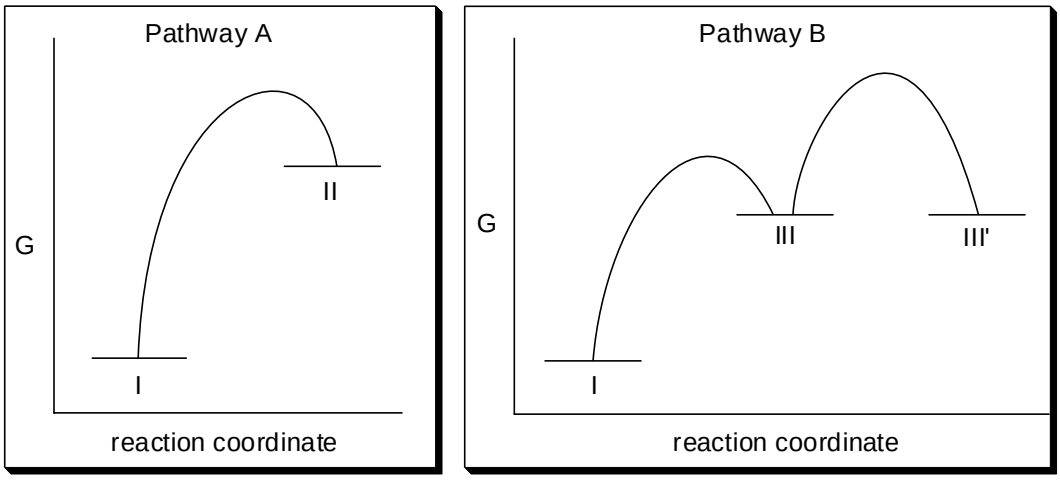

Figure 3.14. Free energy diagrams for Pathway A and B for the insertion of ethylene into the Ir-H of [(POCOP)Ir(H)(C_2H_4)][BAr_F], **10**

In mechanism A, there are three methyl protons that can β-hydride eliminate to reform the ethylene complex, however only 2/3 of the time will the exchange be observed since 1/3 of the time the same hydrogen that migrated will return to Ir. Therefore, the observed rate constant (k_{obs}) is 2/3 the actual rate constant (k). The rate, calculated as an average of the rate for both the line-broadening of the hydride and ethylene, is found to be 155 s^{-1} at 320K corresponds to $\Delta G^{\ddagger}$ = 15.6 kcal/mol. (See Table II.5 and II.6 for calculations).

For the propylene complex **11**, insertion of the propylene into the Ir-H bond could lead to two possible intermediates, the linear and the branched Ir-alkyls (Scheme 3.20). Spin-saturation transfer NMR experiments showed that proton exchange was occurring (Figure 3.15). Saturation of individual signals and observing a decrease in intensity of a companion signal indicates site exchange of these pairs. In line A of Figure 3.15, when the resonance at 3.3 ppm (H_c) was irradiated, only the signal at 5.5 ppm (H_b) showed a decrease in integration. Therefore, the only proton that H_b exchanges with is H_c. Complementary results are seen if the signal at 5.5 ppm is irradiated as shown in line B. When H_a is saturated, only

the hydride H_d is observed to decrease in intensity. And similarly, if H_d is irradiated H_a decreases. Therefore, H_d only exchanges with H_a and vice versa. These results support the insertion of the propylene into the Ir-H bond forming only the linear product, as no exchange indicating formation of the branched product is observed.

Scheme 3.20. Insertion of the primary or secondary carbon of propylene into the Ir-H bond of [(POCOP)Ir(H)(C_3H_6)][BAr_F], **11**.

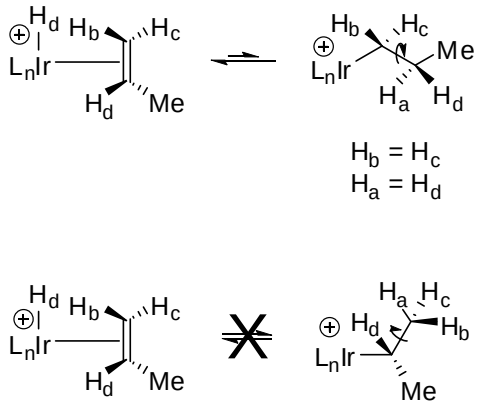

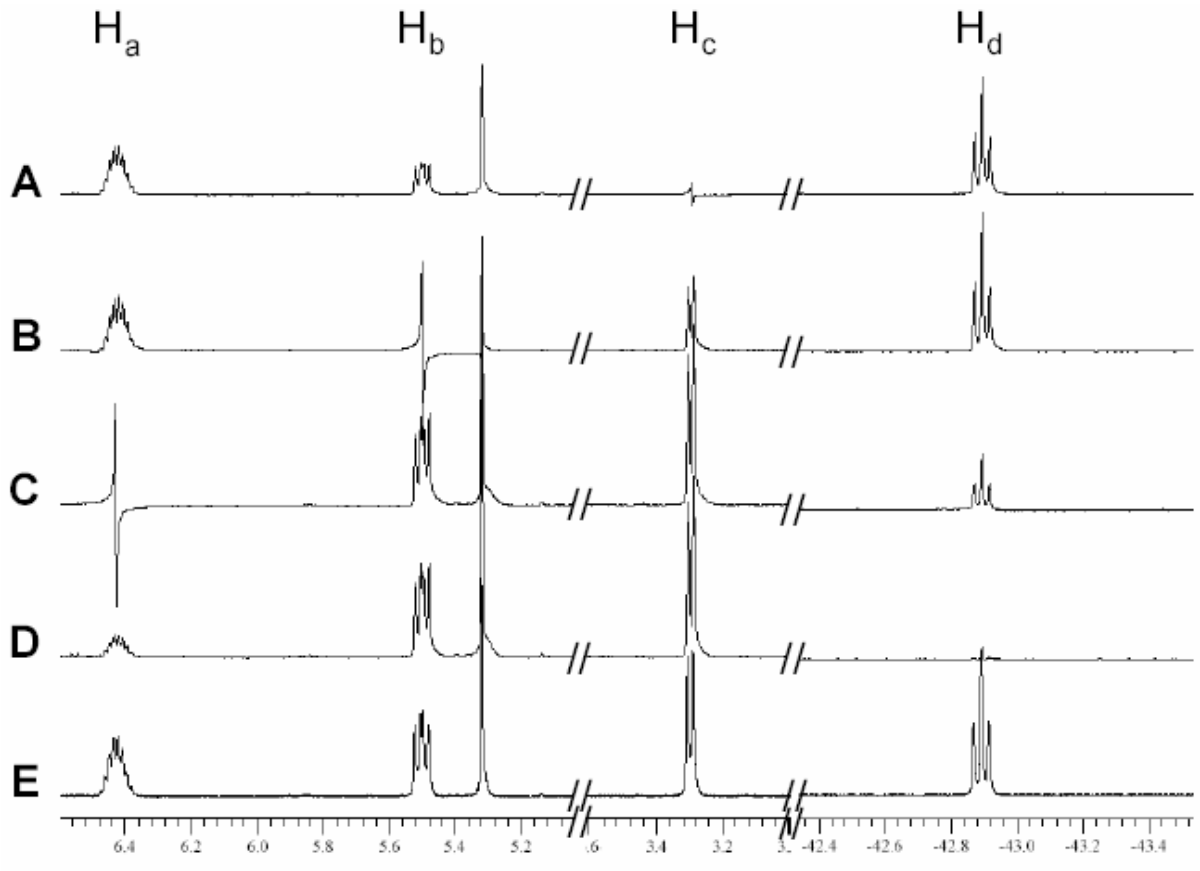

Figure 3.15. Spin-saturation transfer experiment for [(POCOP)Ir(H)(C_3H_6)][BAr_F], **11**.

As mentioned earlier, the propylene complex has both "top/bottom" and "side-to-side" inequivalence. However, insertion of the propylene into the Ir-H results in formation of a species with a mirror plane bisecting and perpendicular to the ligand plane. This can be observed in the ^{1}H NMR spectra at 320 K; the *meta* hydrogens of the ligand backbone merges to one doublet from two, and the two pairs of *t*-butyl resonances broaden and merge into two triplets. Even at these elevated temperatures, the "top" and "bottom" do not equilibrate, as seen for [(POCOP)Ir(H)(C_2H_4)][BAr_F], **10**. This hindered rotation can be attributed to steric restrictions between the propyl group and the *t*-butyl groups, or to an

agostic interaction as described for the ethylene complex. These two mechanisms are indistinguishable by these studies.

As in the ethylene case, the proton exchange rates are used to measure the rate of insertion of propylene into the Ir-H bond. In this case however, the exchange rate was measured using spin saturation transfer NMR techniques. For this technique, one ^{1}H frequency is irradiated causing the intensity of any proton that exchanges with the irradiated proton to decrease. The rate of exchange of these pairs of protons is estimated as 2.8 s^{-1} with a free energy barrier of 16.8 kcal/mol (calculations are shown in Appendix II, Tables II.8 and II.9)

In the case of [(POCOP)Ir(H)(norbornene)][BAr_F], **12**, it is impossible to see evidence of insertion by NMR spectroscopy because the bicyclic structure of norbornene prohibits the exchange of the hydrogens. The hydrogen that migrates forming the σ-norbornyl species must be the same hydrogen that returns to Ir. In order to observe the behavior of **12** at higher temperatures, a NMR tube containing a solution of **12** in chlorobenzene-d^5 was prepared. At room temperature, however, free norbornene was observed in solution. An equilibrium, which favors dissociation of norbornene at higher temperature, was formed between [(POCOP)Ir(H)(norbornene)][BAr_F], **12** and [(POCOP)Ir(H)(L)][BAr_F] (L = solvent) **4**. At 343 K the K_{eq} (**4**/**12**) = 8.3 x 10^{-4}.

The insertion product [(POCOP)Ir(CH_2CH_2(CO)OMe)][BAr_F], **15** was described in Section II.b as in slow equilibrium with [(POCOP)Ir(H)(MA)][BAr_F], **13** with a K_{eq} of 0.13 favoring the olefin complex when the reaction was carried out in methylene chloride. Similar results were observed initially when chlorobenzene-d_5 is used for a solvent. Chlorobenzene allows examination of this system at elevated temperatures. Initially, at room temperature similar results were observed as in methylene chloride, however after 2 days at

room temperature a new ^{31}P NMR signal at 160.5 ppm appears. Further heating at 70°C for 5 hours, shows formation of additional complexes with ^{31}P NMR signals at similar shifts to the cationic methyl acrylate complex **13,** as well as an increase of the peak at 160.5 ppm. If the temperature is raised to 100°C overnight, all the signals for the starting complexes are gone and more unidentified complexes are observed. The major species now is found at δ 199.7 ppm which is consistent with the ^{31}P chemical shift for (POCOP)Ir(CO). Although not conclusive, this suggests that decarbonylation of the methyl acrylate occurs.

III. Addition of Nucleophiles to [(POCOP)Ir(H)(norbornene)][BAr_F], 12

The ultimate goal of this chemistry is to use these cationic iridium olefin complexes in the formation of new C-X bonds. A few reactions were run to test the reactivity of these complexes towards nucleophiles. It is necessary to pick a nucleophile that has the appropriate balance of basicity and nucleophilicity. If the compound is either too basic or too nucleophilic, it might bind to the electron-deficient iridium center and prove unreactive to C-X formation. On the other hand, if the compound is not sufficiently nucleophilic, it will not react with the olefin. Two different nucleohphiles were tested, aniline and 4-methylthiol. The norbornene complex was chosen since typically norbornene is more reactive due to its strained bicyclic structure. A negative feature is that it is also a more labile olefin.

When **12** was treated with aniline and norbornene (1:50:74 ratio, respectively) in chlorobenzene-d_5, aniline displaced the norbornene forming a new cationic aniline complexes, [(POCOP)Ir(H)(NH_2Ph)], **16**. The ^1H NMR of this complex shows a broad singlet at 5.7 ppm for the NH_2 protons of the coordinated aniline and a hydride resonance at

-42.6 ppm. This complex displays a 172.3 ppm ^{31}P chemical shift and is stable at elevated temperatures and no change in the ^{1}H spectrum is observed after 24 hours at 60°C. After two days at 100°C, new signals appear around δ 1.4, between δ 2.2 and 2.7, and δ 3.3 in the ^{1}H NMR spectra. The only iridium complex present is **16**; no new peaks are observed in the ^{31}P NMR spectrum. It is unclear if the new ^{1}H resonances are due to formation of a C-N bond. The intensity of the new peaks is very low however, and therefore even if they do correspond to coupling products the turnover rate is extremely slow.

4-Methylthiophenol, which is less basic than aniline, was also shown to displace norbornene at room temperature. When **12** was treated with excess 4-methylthiophenol and norbornene (1 : 50 : 74, Ir : 4-methylthiophenyl: norbornene), an equilibrium was established between the norbornene complex and the 4-methylthiol complex (Scheme 3.21) with an equilibrium constant of 3.6 favoring the coordination of 4-methylthiol.

Scheme 3.21. Equilibrium between [(POCOP)Ir(H)(norbornene)][BAr_F] **12** and [(POCOP)Ir(H)(HSAr)][BAr_F] **17**

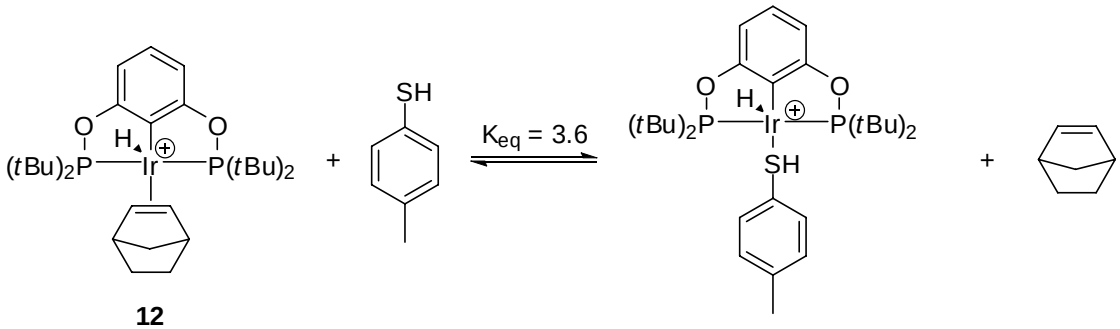

12 **17**

When this reaction mixture is heated to 60°C for 24 hours, peaks that correlate with the desired coupling product can be discerned. However, a control reaction consisting of only norbornene and 4-methylthiophenol in chlorobenzene showed similar results. It fact, in 1954

Cristol and Brindell showed that 4-methylthiophenyl adds to norbornene selectively to form the exo-norbornyl *p*-tolyl thioether by a radical process in chlorobenzene.[29] Therefore, it is uncertain whether the above reaction was metal-catalyzed or radically induced.

Summary

Cationic POCOP iridium pincer complexes have been synthesized and characterized with the goal of gaining information that might lead to a new catalyst for the funtionalization of alkenes. Investigations have included studies of the structure as well as the dyamic behavior of these complexes.

[(POCOP)Ir(H)(H_2)][BAr_F], **9,** has been synthesized and shown to be a dihydrogen/hydride complex as compared to a classical trihydride. At room termperature, the hydrogens are in fast exchange and are seen as a broad singlet at ca. -14 ppm by ^{1}H NMR. However, at 173 K, the exchange rate of the hydrogens are slow on the NMR time scale and are seen at 0.033 and -41.9 ppm in a 2:1 ratio in the ^{1}H NMR spectrum. Using a one dimensional HMQC experiment at 173 K of a partially deuterated complex for the H-D ligand was observed which indicates that H-D is bound in an η^2 fashion and the H-D coupling constant, 33 Hz. Typical η^2-dihydrogen H-D coupling constants are ca. 30 Hz, while dihydride H-D coupling constants are less than 1 Hz.

The exchange rate between the hydride and dihydrogen ligand in **9** was calculated ^{1}H NMR using line-broadening techniques and found to be 304.6 s^{-1} (197 K) with $\Delta G^{\ddagger}$ = 9.1 kcal/mol. The rate was also calculated for the deuterated complex using ^{1}H NMR spectroscopy which had to a slightly higher $\Delta G^{\ddagger}$ of 9.8 kcal/mol. This result was expected since the energy barrier for breaking a D-D bond is higher than that for a H-H bond.

Various cationic olefin hydride complexes of the type [(POCOP)Ir(H)(L)][Bar_F] (L = C_2H_4 **10**, C_3H_6 **11**, norbornene **12**, and methyl acrylate **13**) have been synthesized and characterized. All the complexes show dynamic behavior by NMR spectroscopy. Low temperature experiments were preformed on all the complexes to examine their behavior more closely. At low temperatures, the cationic ethylene complex **10** is in equilibrium with the solvated complex. However, even at the 173K, the equilibrium is rapid and only broad signals for the averaged complexes are observed. As the temperature is raised the unsolvated complex is favored, seen as a upfield chemical shift of the average hydride resonance. The rotation of ethylene is too fast to be measured by ^{1}H NMR spectroscopy.

The rotation of the olefin in the cationic propylene **11**, norbornene **12**, and methyl acrylate **13** complexes can all be observed by ^{1}H NMR spectroscopy. The ^{1}H spectrum for **11** shows a slow equilibrium (K_{eq} = 0.066) at 173 K in which one rotamer is present in significantly higher concentrations than the other. The methyl acrylate complex **13** also exhibits an equilibrium between the two rotamers of K_{eq} = 0.26 at 197 K. The two rotamers of the norbornene complex **12** are observed in a 1:1 ratio at 174 K. From the line broadening of the ^{1}H NMR resonances of the two rotamers, the free energy barrier for rotation of the norbornene is calculated to be $\Delta G^{\ddagger}$ = 9.1 kcal/mol.

The rates of migratory insertion of the cationic ethylene **10** and propylene **11** complexes were calculated using line-broadening and spin-saturation transfer NMR techniques. As expected the energy barrier for insertion is higher ($\Delta G^{\ddagger}$ = 16.8 kcal/mol) for **11** than for **10** (**(**$\Delta G^{\ddagger}$ = 15.6 kcal/mol). It is not clear whether this barrier corresponds to the true migratory insertion rate of the olefin into the Ir-H bond or if it corresponds to the breaking of an agostic bond in an "in-place" rotation mechanism. Interestingly, the migratory insertion in propylene

complex **11** shows preference for the linear propyl intermediate. No rotation of the alkyl species is observed for either complex since "top/bottom" inequivalence is maintained at elevated temperatures.

Preliminary results on the reaction of [(POCOP)Ir(H)(norbornene)][BAr_F], **12**, with the nucleophiles aniline and 4-methylthiophenyl was obtained. No attack of the nucleophiles on the coordinanted norbornene was observed and instead the norbornene was displaced by the nucleophile.

Experimental Section

General Considerations: All manipulations were carried out using standard Schlenk, high-vacuum, and glove box techniques. Argon was purified by passage through columns of BASF R3-11 (chemalog) and 4Å molecular sieves. Pentane and methylene chloride were passed through columns of activated alumina and deoxygenated by purging with N_2. Benzene was dried over 4Å molecular sieves and degassed to remove both oxygen and nitrogen. NMR spectra were recorded on Bruker DRX 400, AMX 300 and 500 MHz instruments and are referenced to residual protio solvent peaks. ^{31}P chemical shifts are referenced to an external H_3PO_4 standard. Since there is a strong ^{31}P-^{31}P coupling in the pincer complexes, many of the ^{1}H and ^{13}C signals exhibit virtual coupling and appear as triplets. These are specified as vt with the *apparent* coupling simply noted as *J*. IR spectra were recorded on an ASI ReactIR 1000 spectrometer. Elemental analyses were carried out by Atlantic Microlab, Inc. of Norcross, GA. All reagents, unless otherwise noted, were purchased from Sigma-Aldrich and used without further purification. Hydrogen and

propylene was used as received from National Specialty Gases of Durham, NC. Deuterium was purchased from Sigma-Aldrich. Ethylene was purchased from Matheson. The synthesis of the phosphinite ligand, (POCOP)Ir(H)(Cl), **1**, and (POCOP)IrH_2 have been previously described in the literature.[15] The abbreviation of BAr_F is used to represent the counterion tetrakis(3,5-trifluoromethylphenyl)borate. The ^1H and ^{13}C spectral data for BAr_F in CD_2Cl_2 is the same for all complexes listed as is therefore not reported in the characterizations below. **BAr_F:** ^1H NMR (CD_2Cl_2): δ 7.72 (s, 8H, H_o), 7.56 (s, 4H, H_p). $^{13}C\{^1H\}$ NMR (CD_2Cl_2): δ 162.2 (q, $J_{C\text{-}B}$ = 37.4 Hz, C_{ispo}), 135.2 (C_o), 129.3 (q, $J_{C\text{-}F}$ = 31.3 Hz, C_m), 125.0 (q, $J_{C\text{-}F}$ = 272.5, CF_3), 117.9 (C_p).

Synthesis of (POCOP)Ir(H)(OTf) (2): (POCOP)Ir(H)(Cl) (0.16 mmol, 100 mg), AgOTf (0.163 mmol, 41.9 mg) and 10 mL of methylene chloride were added to a Schlenk flask and allowed to stir for 2.5 hrs. The silver salts were removed by filtration through a 0.2 micron syringe filter under an argon atmosphere in the glove box. An orange powder was recovered after removal of the solvent under vacuum. (96 mg, 81 % yield)

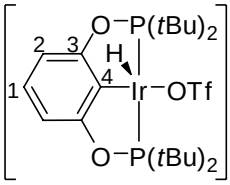

2

^1H NMR (400 MHz, CD_2Cl_2): δ 6.78 (t, $^3J_{H\text{-}H}$ = 8.2 Hz, 1H, 1-H), 6.52 (d, $^3J_{H\text{-}H}$ = 8.2 Hz, 2H, 2-H), 1.33 (m, 36H, P(tBu)$_2$), -43.12 (t, $J_{P\text{-}H}$ = 12.8 Hz, 1H, Ir*H*). $^{31}P\{^1H\}$ NMR (162 MHz, CD_2Cl_2): δ 177.3.

Reaction of 2 with carbon monoxide (5 and 6): A NMR tube fitted with a septum was charged with a solution of **2** (15mg, 0.02 mmol) in CD_2Cl_2 (0.5 mL). Carbon monoxide was purged through the solution for 5 minutes until the color changed from yellow to nearly colorless. The ^{31}P and ^{1}H NMR showed two complexes in a 1:1 ratio, the mono- and di-carbonyl complexes (**5** and **6**). Under slight vacuum the solution turns yellow, and only one complex is observed, the monocarbonyl complex, **5**.

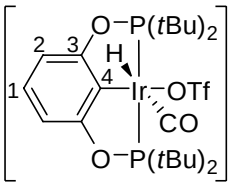

5

5: ^{1}H NMR (500 MHz, CD_2Cl_2): δ 7.14 (t, $^{3}J_{H\text{-}H}$ = 8.2 Hz, 1H, 1-H), 6.79 (d, $^{3}J_{H\text{-}H}$ = 8.3 Hz, 2H, 2-H), 1.57 (vt, J = 8.8 Hz, 18H, P(tBu)$_2$), 1.36 (vt, J = 8.2 Hz, 18H, P(tBu)$_2$), -10.463 (t, $J_{P\text{-}H}$ = 14.78 Hz, 1H, Ir*H*). $^{31}P\{^{1}H\}$ NMR (121 MHz, CD_2Cl_2): δ 174.2.

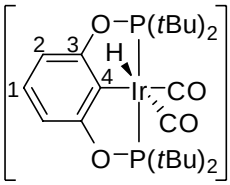

6

6: ^{1}H NMR (300 MHz, CD_2Cl_2): δ 6.83 (t, $^{3}J_{H\text{-}H}$ = 8.0 Hz, 1H, 1-H), 6.46 (d, $^{3}J_{H\text{-}H}$ = 8.0 Hz, 2H, 2-H), 1.58 (vt, overlapped with **5**, 18H, P(tBu)$_2$), 1.37 (vt, overlapped with **5**, 18H, P(tBu)$_2$), -7.29 (t, $J_{P\text{-}H}$ = 16.1 Hz, 1H, Ir*H*). $^{31}P\{^{1}H\}$ NMR (162 MHz, C_6D_6): δ 164.9.

Synthesis of [(POCOP)Ir(H)(H_2O)][SbF_6] (3): (POCOP)Ir(H)(Cl) (0.16 mmol, 100 mg), $AgSbF_6$ (0.163 mmol, 56 mg) and 10 mL of methylene chloride were added to a Schlenk flask and allowed to stir for 2.5 hrs. The silver salts were removed by filtration

through a 0.2 micron syringe filter under an argon atmosphere in the glove box. An orange powder was recovered after removal of the solvent under vacuum. (90 mg, 68 % yield)

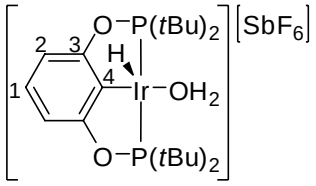

3

^{1}H NMR (400 MHz, CD_2Cl_2): δ 6.84 (t, $^{3}J_{H\text{-}H}$ = 8.1 Hz, 1H, 1-H), 6.58 (d, $^{3}J_{H\text{-}H}$ = 8.1 Hz, 2H, 2-H), 3.2-4.6 (b, 2H, H_2O), 1.35 (vt, J = 7.6 Hz, 36H, P(tBu)$_2$), -43.05 (t, $J_{P\text{-}H}$ = 12.6 Hz, 1H, IrH). ^{31}P{^{1}H} NMR (162 MHz, CD_2Cl_2): δ 175.8.

Synthesis of [(POCOP)Ir(H)(solvent)][BAr$_F$] (4): (POCOP)Ir(H)(Cl) (0.32 mmol, 200 mg), NaBAr$_F$ (0.35 mmol, 311.4 mg) and 20 mL of methylene chloride were added to a Schlenk flask and allowed to stir for overnight. The sodium salts were removed by filtration through a 0.2 micron syringe filter under an argon atmosphere in the glove box. The solid was washed with pentane three times and dried under vacuum. An orange powder was recovered after removal of the solvent under vacuum. (373 mg, 80.2% yield)

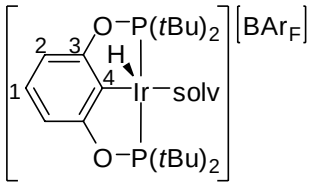

4

^{1}H NMR (400 MHz, CD_2Cl_2): δ 7.72 (s, 8H, BAr$_F$), 7.56 (s, 4H, BAr$_F$), 6.81 (t, $^{3}J_{H\text{-}H}$ = 7.6 Hz, 1H, 1-H), 6.57 (d, $^{3}J_{H\text{-}H}$ = 7.6 Hz, 2H, 2-H), 1.35 (m, 36H, P(tBu)$_2$), -41.92 (t, $J_{P\text{-}H}$ = 12.1 Hz, 1H, IrH). ^{31}P{^{1}H} NMR (162 MHz, CD_2Cl_2): δ 175.5.

In Situ Generation of:

[(POCOP)IrH(H_2)][BAr_F] (9_H): A solution of [(POCOP)Ir(H)(C_3H_6)][BAr_F] (10 mg, 0.0066 mmol) in methylene chloride-d^2 (0.5 mL) was added to a medium-walled screw cap NMR tube. H_2 was purged through solution at -78 °C, shaking the tube occasionally for two minutes.

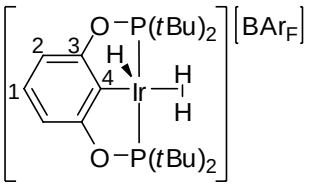

9

^{1}H NMR (500 MHz, CD_2Cl_2, 173 K): δ 7.16 (bs, 1H, 1-H), 6.82 (d, $^3J_{H\text{-}H}$ = 6.0 Hz, 2H, 2-H), 1.17 (m, 36H, P(*t*Bu)$_2$), 0.033 (b, 2H, *H_2*), -41.88 (t, $J_{P\text{-}H}$ = 12.1 Hz, 1H, Ir*H*). At 295 K, the hydride resonance is a broad singlet at -14 ppm. $^{31}P\{^1H\}$ NMR (202 MHz, CD_2Cl_2, 173 K): δ 194.7.

[(POCOP)Ir(D)(D_2)][BAr_F] 9_D: **[**POCOP)Ir(D)(D_2)][BAr_F] was generated using the same procedure as **9_H** with the addition of deuterium gas instead of hydrogen gas.

Partially deuterated sample of [(POCOP)Ir(H/D)(H_2/HD/D_2)][BAr_F]: The partially deuterated sample was generated by the same procedure mentioned above, however H_2 was purged through the solution for one minute, followed by D_2 for one minute.

General Procedure for the Synthesis of [(POCOP)Ir(H)(olefin)][BAr_F] (10-12): In a Schlenk flask under argon 1 equiv. of (POCOP)Ir(H)(Cl) **1**, 1.1 equiv. of $NaBAr_F$, and excess olefin were stirred in methylene chloride for 15 min. The reaction mixture was then filtered

with a 0.2 micron syringe filter under an inert atmosphere in the glove box. The product was isolated after removal of the methylene chloride solvent under reduced pressure.

[(POCOP)Ir(H)(C_2H_4)][BAr_F] (10): The general procedure was employed using **1** (0.08 mmol, 50 mg) and $NaBAr_F$ (0.089 mmol, 77.9 mg) in CH_2Cl_2 (10mL) and purging ethylene through the reaction mixture. The color changed from pale red to orange within 5 minutes indicating the completion of the reaction. Following filteration and solvent removal, the product was isolated as a pale orange solid (104 mg, 87.7% yield).

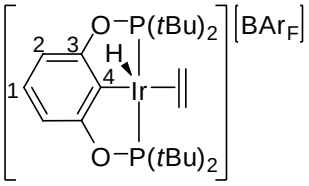

10

^{1}H NMR (500 MHz, CD_2Cl_2): δ 7.22 (t, $^3J_{H\text{-}H}$ = 8.0 Hz, 1H, 1-H), 6.92 (d, $^3J_{H\text{-}H}$ = 8.0 Hz, 2H, 2-H), 4.15 (s, 4H, C_2H_4), 1.34 (vt, J = 7.5 Hz, 18H, P(tBu)$_2$), 1.27 (vt, J = 8.0 Hz, 18H, P(tBu)$_2$), -42.83 (b, 1H, IrH). ^{31}P{^{1}H} NMR (162 MHz, CD_2Cl_2): δ 182.0. ^{13}C{^{1}H} NMR (125.8 MHz, CD_2Cl_2): δ 167.0 (C_q, vt, J = 5.6 Hz, 2C, 3-C), 133.8 (C_q, m, 1C, 4-C), 132.3 (CH, s, 1C, 1-C), 107.1 (CH, t, $J_{P\text{-}C}$ = 6.0 Hz, 2C, 2-C), 55.1 (CH_2, s, 2C, C_2H_4), 45.7 (C_q, vt, J = 12.1 Hz, $C(CH_3)_3$), 42.8 (C_q, vt, J = 13.5 Hz, $C(CH_3)_3$), 28.9 (CH_3, vt, J = 2.1 Hz, $C(CH_3)_3$), 28.1 (CH_3, vt, J = 1.9 Hz, $C(CH_3)_3$). Elemental analysis calculated for $C_{56}H_{56}BF_{24}IrO_2P_2$ (1481.98): C: 45.39, H: 3.81. Found: C: 45.18, H: 3.69.

[(POCOP)Ir(H)(C_3H_6)][BAr_F] (11): The general procedure was employed using **1** (0.08 mmol, 50 mg) and $NaBAr_F$ 0.087 mmol, 77.8 mg) in CH_2Cl_2 (10mL) and purging propylene through the reaction mixture. The color changed from pale red to orange within five minutes

indicating the completion of the reaction. Following filtration and solvent removal, the product was isolated as a pale orange solid (103 mg, 86% yield).

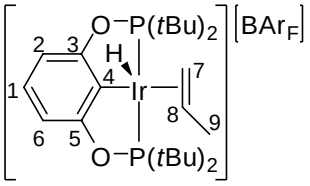

11

^{1}H NMR (500 MHz, CD_2Cl_2): δ 7.21 (t, $^{3}J_{H\text{-}H}$ = 8.1 Hz, 1H, 1-H), 6.90 (d, $^{3}J_{H\text{-}H}$ = 7.9 Hz, 1H, 2-H), 6.86 (d, $^{3}J_{H\text{-}H}$ = 8.2 Hz, 1H, 6-H), 6.43 (m, 1H, 8-H), 5.5 (dd, $^{3}J_{H\text{-}H}$ = 12.0 Hz, $J_{P\text{-}H}$ = 8.5 Hz 1H, 7-H_{trans}), 3.3 (d, $^{3}J_{H\text{-}H}$ = 8.0 Hz, 1H, 7-H_{cis}), 1.9 (d, $^{3}J_{H\text{-}H}$ = 5.5 Hz, 3H, 9-H), 1.46 (d, $J_{P\text{-}H}$ = 15.3 Hz, 9H, P(*t*Bu)$_2$), 1.35 (d, $J_{P\text{-}H}$ = 14.6 Hz, 9H, P(*t*Bu)$_2$), 1.34 (d, $J_{P\text{-}H}$ = 15.3 Hz, 9H, P(*t*Bu)$_2$), 1.17 (d, $J_{P\text{-}H}$ = 14.6 Hz, 9H, P(*t*Bu)$_2$), -42.9 (t, $J_{P\text{-}H}$ = 11.6 Hz, 1H, Ir*H*). ^{31}P{^{1}H} NMR (162 MHz, CD_2Cl_2): δ 182.7 (dd, J_{PP} = 260.1 Hz), 175.0 (dd, $J_{P\text{-}P}$ = 260.1 Hz). ^{13}C{^{1}H} NMR (125.8 MHz, CD_2Cl_2): δ 167.2 (C_q, m, 2C, 3-C and 5-C), 132.4 (CH, s, 1C, 1-C), 131.3 (C_q, m, 1C, 4-C), 106.9 (CH, m, 2C, 2-C and 6-C), 77.8 (CH, s, 1C, 7-C), 66.2 (CH_2, s, 1C, 8-C), 45.6 (C_q, d, $J_{P\text{-}H}$ = 22.3 Hz, 2C, *C*$(CH_3)_3$), 42.5 (C_q, d, $J_{P\text{-}H}$ = 20.5 Hz, 1C, *C*$(CH_3)_3$), 41.9 (C_q, d, $J_{P\text{-}H}$ = 20.9 Hz, 1C, *C*$(CH_3)_3$), 29.4 (CH_3, d, $J_{P\text{-}H}$ = 3.5 Hz, C(*C*$H_3)_3$), 29.2 (CH_3, d, $J_{P\text{-}H}$ = 3.5 Hz, C(*C*$H_3)_3$), 28.4 (CH_3, d, $J_{P\text{-}H}$ = 2.9 Hz, C(*C*$H_3)_3$), 28.11 (CH_3, d, $J_{P\text{-}H}$ = 3.5 Hz, C(*C*$H_3)_3$). Elemental analysis calculated for $C_{57}H_{58}BF_{24}IrO_2P_2$ (1496.01): C: 45.76, H: 3.91. Found: C: 45.64, H: 3.84.

[(POCOP)Ir(H)(C_7H_{10})][BAr_F] (12): The general procedure was employed using **1** (0.16 mmol, 100 mg), $NaBAr_F$ 0.176 mmol, 156 mg), and norbornene (1.6 mmol, 150 mg) in CH_2Cl_2 (7 mL). Excess norbornene is necessary for the reaction to proceed at a reasonable rate. The product was a pale orange solid (194mg, 78.4% yield).

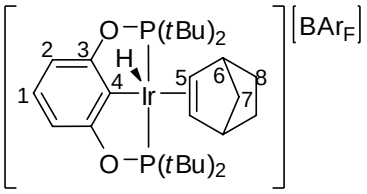

12

^{1}H NMR (500 MHz, CD_2Cl_2): δ 7.16 (t, $^{3}J_{H\text{-}H}$ = 8.0 Hz, 1H, 1-H), 6.87 (d, $^{3}J_{H\text{-}H}$ = 8.0 Hz, 2H, 2-H), 4.71 (7, $^{3}J_{H\text{-}H}$ = 4.2 Hz, 2H, 5-H), 3.44 (s, 2H, 6-H), 1.90 (d, $^{3}J_{H\text{-}H}$ = 8.2 Hz, 2H, 8-H), other pair of 8-H protons is overlapped with P(*t*Bu)$_2$, 1.41 (vt, *J* = 7.7 Hz, 18H, P(*t*Bu)$_2$), 1.33 (vt, *J* = 7.5 Hz, 18H, P(*t*Bu)$_2$), 0.90 (d, $^{3}J_{H\text{-}H}$ = 10.0 Hz, 1H, 7-H), 0.22 (d, $^{3}J_{H\text{-}H}$ = 10.1 Hz, 1H, 7-H), -45.9 (t, $J_{P\text{-}H}$ = 11.2 Hz, 1H, Ir*H*). ^{31}P{^{1}H} NMR (162 MHz, CD_2Cl_2): δ 176.0. ^{13}C{^{1}H} NMR (125.8 MHz, CD_2Cl_2): δ 166.0 (C_q, t, $J_{P\text{-}H}$ = 5.4 Hz, 2C, 3-C), 131.5 (CH, s, 1C, 1-C), 130.4 (C_q, m, 1C, 4-C), 106.7 (CH, t, $J_{P\text{-}H}$ = 5.9 Hz, 2C, 2-C), 78.0 (CH, s, 2C, 5-C), 47.1 (CH, s, 2C, 6-C), 46.4 (C_q, vt, *J* = 11.4 Hz, 2C, *C*$(CH_3)_3$), 43.7 (C_q, vt, *J* = 13.0 Hz, 2C, *C*$(CH_3)_3$), 40.6 (CH_2, s, 1C, 7-H), 29.5 (CH_3, vt, *J* = 2.1 Hz, C(*C*$H_3)_3$), 28.6 (CH_3, vt, *J* = 2.0 Hz, C(*C*$H_3)_3$), 27.9 (CH_2, s, 2C, 8-C). Elemental analysis calculated for $C_{61}H_{62}BF_{24}IrO_2P_2$ (1548.36): C: 47.33, H: 4.04. Found: C: 47.46, H: 3.93.

(POCOP)Ir(C$_2$H$_3$(CO)OCH$_3$) (14): **1** (100 mg, 0.16 mmol), NaO*t*Bu (18.4 mg, 0.19 mmol) and benzene (10 mL) were added to a Schlenk flask under argon. The reaction mixture was stirred for one hour at 75°C. The reaction mixture was cooled to room temperature and methyl acrylate (19 μL, 0.23 mmol) was syringed into the flask and stirred for 20 minutes. After filtering the mixture through a 0.2 micron syringe filter under argon, the solvent was removed under vacuum yielding a brick red solid (71 mg, 65.7% yield).

^{1}H{^{31}P} NMR (400 MHz, C_6D_6): δ 6.963 (t, $^{3}J_{H\text{-}H}$ = 8.0 Hz, 1H, 1-H), 6.85 (d, $^{3}J_{H\text{-}H}$ = 8.0 Hz, 2H, 2-H), 4.40 (dd, $^{3}J_{cis}$ = 6.8 Hz, $^{3}J_{trans}$ = 10.0 Hz, 1H), 4.17 (dd, $^{3}J_{gem}$ = 0.8 Hz, $^{3}J_{trans}$ = 10.0 Hz 1H), 3.45 (s, 3H, -O*Me*), 2.64 (dd, $^{3}J_{cis}$ = 6.8 Hz, $^{3}J_{gem}$ = 0.8 Hz, 1H), 1.43 (s, 18H,

P(*t*Bu)$_2$), 1.18 (s, 18H, P(*t*Bu)$_2$). $^{31}P\{^1H\}$ NMR (162 MHz, C_6D_6): δ 175.7. Elemental analysis calculated for $C_{26}H_{45}IrO_4P_2$ (675.80): C: 46.21, H: 6.71. Found: C: 45.99, H: 6.74.

In situ generation of [(POCOP)Ir(H)(C_2H_3(CO)OCH_3)][BAr_F] (13) and [(POCOP)Ir(C_2H_4(CO)OCH_3)][BAr_F] (15): **14** (10 mg, 0.015 mmol), [H(OEt_2)$_2$][BAr_F] (16.5 mg, 0.016 mmol), and and CD_2Cl_2 (0.5 mL) were added to a screw cap NMR tube. After mixing, a color change was observed from brick red to light orange. **13**: ^1H NMR (500 MHz, ClC_6D_5): δ 8.41 (s, 8H, BAr_F), 7.78 (s, 4H, BAr_F), *para* H on ligand backbone is underneath other peaks, 6.91 (b, 2H), 5.20 (bs, 1H, olefinic), 4.94 (bs, 1H, olefinic), 3.12 (s, 3H, -O*Me*), 2.96 (bs, 1H, olefinic), 1.16 (b, 36 H, *t*Butyls), -39.2 (bs, 1H, Ir-*H*). $^{31}P\{^1H\}$ NMR (162 MHz, ClC_6D_5): δ 179.2 (d, J = 182.4 Hz), 176.90 (d, J = 213.6 Hz). **14**: ^1H NMR (500 MHz, ClC_6D_5): δ 8.41 (s, 8H, BAr_F), 7.78 (s, 4H, BAr_F), *para* H on ligand backbone is underneath other peaks, 6.79 (d, 2H, ^3J = 8.2 Hz), 3.78 (s, 3H, -O*Me*), 2.69 (m, 2H), 1.93 (t, ^3J = 7.2 Hz, 2H), *t*butyls are overlapping with **13**. $^{31}P\{^1H\}$ NMR (162 MHz, ClC_6D_5): δ 153.4.

In situ (POCOP)Ir(H)($NH_2C_6H_5$)][BAr_F] (16): In a J. Young NMR Tube, **12** (10 mg, 0.0064 mmol), aniline (29.16 μL, 0.32 mmol), and norbornene (44.6 mg, 0.474 mmol) was dissolved in chlorobenzene-d^5 (0.5 mL). The product **16** was observed by NMR spectroscopy.

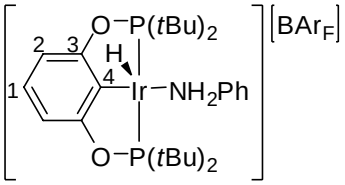

16

^{1}H NMR (400 MHz, ClC_6D_5): δ 8.41 (s, 8H, BAr_F), 7.78 (s, 4H, BAr_F), 6.11 (s, 2H, N*H*$_2$), -43.73 (s, 1H, Ir-*H*), other peaks are overlapped with free norbornene and anilines signals. ^{31}P{^{1}H} NMR (162 MHz, ClC_6D_5): 172.5 (s).

In situ [(POCOP)Ir(H)(HSC$_6$H$_4$-*p*Me)][BArF] (17): In a J. Young NMR tube, **1** (10 mg, 0.016 mmol), $NaBAr_F$ (15.6 mg, 0.018 mmol), and 4-methylthiophenyl (2.2 mg, 0.018 mmol) were dissolved in chlorobenzene-d^5 (0.5 mL). **17** was observed by NMR.

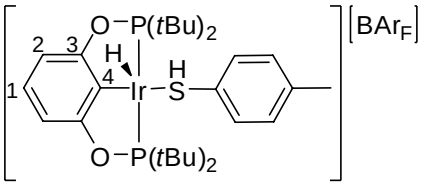

17

^{1}H NMR (400 MHz, ClC_6D_5): δ 8.41 (s, 8H, BAr_F), 7.78 (s, 4H, BAr_F), 7.38 (m, 3H, Ar), 7.15 (m, 2H, Ar), 7.10 (t, 1H, $^{3}J_{HH}$ = 8.0 Hz, 1-H), 6.83 (d, 2H, $^{3}J_{HH}$ = 8.0 Hz, 2-H), 5.19 (s, 1H, S*H*), -41.69 (t, $^{3}J_{PH}$ = 13 Hz, 1H, Ir-*H*). ^{31}P{^{1}H} NMR (162 MHz, ClC_6D_5): 176.7 (s).

References and Notes

(1) Beller, M.; Seayad, J.; Tillack; Jiao *Angew. Chem. Int. Ed.* **2004**, *43*, 3368.

(2) van Leeuwen, P. W. N. M.; Kamer, P. C. J.; Reek, J. N. H.; Dierkes, P. *Chem. Rev.* **2000**, *100*, 2741.

(3) Muller, T. E.; Beller, M. *Chem. Rev.* **1998**, *98*, 675.

(4) Walsh, P. J.; Baranger, A. M.; Bergman, R. G. *J. Am. Chem. Soc.* **1992**, *114*, 1708.

(5) Baranger, A. M.; Walsh, P. J.; Bergman, R. G. *J. Am. Chem. Soc.* **1993**, *115*, 2753.

(6) Pohlki, F.; Doye, S. *Chem. Soc. Rev.* **2003**, *32*, 104.

(7) Burling, S.; Field, L., D.; Messerle, B. A.; Vuong, K. Q.; Turner, P. *Dalton Trans.* **2003**, 4181.

(8) Ananikov, V. P.; Malyshev, D. A.; Beletskaya, I. P.; Aleksandrov, G. G.; Eremenko, I. L. *Adv. Synth. Catal.* **2005**, *347*, 1993.

(9) Cao, C.; Fraser, L. R.; Love, J. A. *J. Am. Chem. Soc.* **2005**, *127*, 17614.

(10) Weiwer, M.; Coulombel, L.; Dunach, E. *Chem. Commun.* **2006**, 332.

(11) Casalnuovo, A. L.; RajanBabu, T. V. In *Transition Metals for Organic Synthesis (2nd Edition)*; Beller, M., Bolm, C., Eds.; Wiley: Weinheim, 2004; Vol. 1, pp 149-156.

(12) Göttker-Schnetmann, I.; Brookhart, M. *J. Am. Chem. Soc.* **2004**, *126*, 9330.

(13) Göttker-Schnetmann, I.; White, P. S.; Brookhart, M. *Organometallics* **2004**, *23*, 1766.

(14) Sykes, A. C.; White, P.; Brookhart, M. *Organometallics* **2006**, *25*, 1664.

(15) Göttker-Schnetmann, I.; White, P. S.; Brookhart, M. *J. Am. Chem. Soc.* **2004**, *126*, 1804.

(16) Farrugia, L. J. *J. Appl. Cryst.* **1997**, *30*, 565.

(17) Kubas, G. J.; Ryan, R. R.; Swanson, B. I.; Vergamini, P. J.; Wasserman, H. J. *J. Am. Chem. Soc.* **1984**, *106*, 451.

(18) Crabtree, R. H.; Lavin, M.; Bonneviot, L. *J. Am. Chem. Soc.* **1986**, *108*, 4032.

(19) Crabtree, R. H. *Acc. Chem. Res.* **1990**, *23*, 96.

(20) Hamilton, D. G.; Crabtree, R. H. *J. Am. Chem. Soc.* **1988**, *110*, 4126.

(21) Heinekey, D. M.; Hinkle, A. S.; Close, J. D. *J. Am. Chem. Soc.* **1996**, *118*, 5353.

(22) Oldham, W. J.; Hinkle, A. S.; Heinekey, D. M. *J. Am. Chem. Soc.* **1997**, *119*, 11028.

(23) Pons, V.; Conway, S. L. J.; Green, M. L. H.; Green, J. C.; Herbert, B. J.; Heinekey, D. M. *Inorg. Chem.* **2004**, *43*, 3475.

(24) Janak, K. E.; Shin, J. H.; Parkin, G. *J. Am. Chem. Soc.* **2004**, *126*, 13054.

(25) Kubas, G. J. *Acc. Chem. Res.* **1988**, *21*, 120.

(26) Göttker-Schnetmann, I.; White, P. S.; Brookhart, M. *Organometallics* **2004**, *23*, 1766.

(27) A similar phenomena was observed with [(POCOP)Ir(H)(H2)(H2O)][SbF6] except initially the exchange between bound and free water occurred than the decoalesence of the dihydrogen/hydride.

(28) Tempel, D. J.; Brookhart, M. *Organometallics* **1998**, *17*, 2290.

(29) Cristol, S. J.; Brindell, G. D. *J. Am. Chem. Soc.* **1954**, *76*, 5699.

APPENDIX I

Supporting Information for Chapter Two

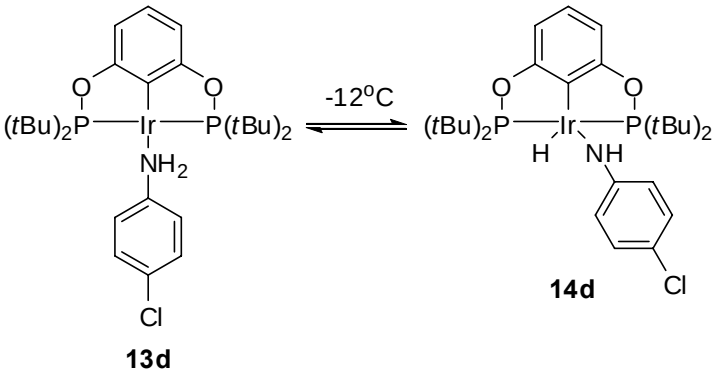

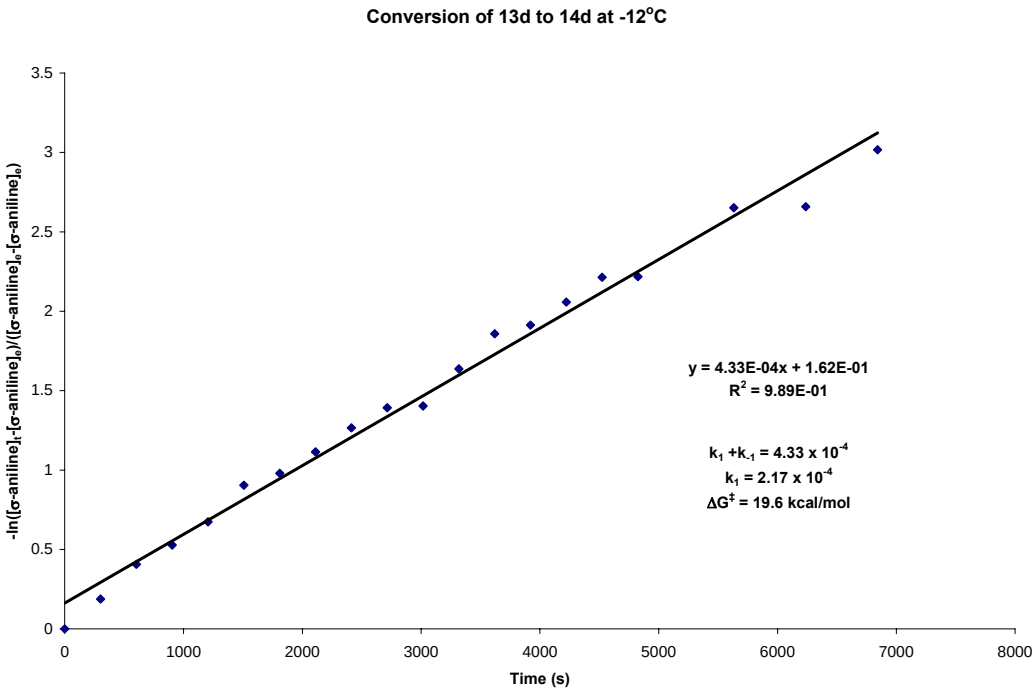

Figure I.1 First-order plot for the conversion of **13d** to **14d**

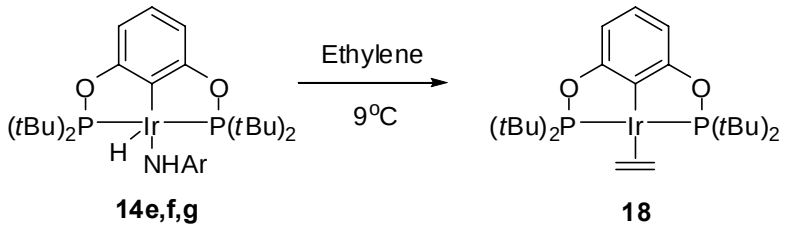

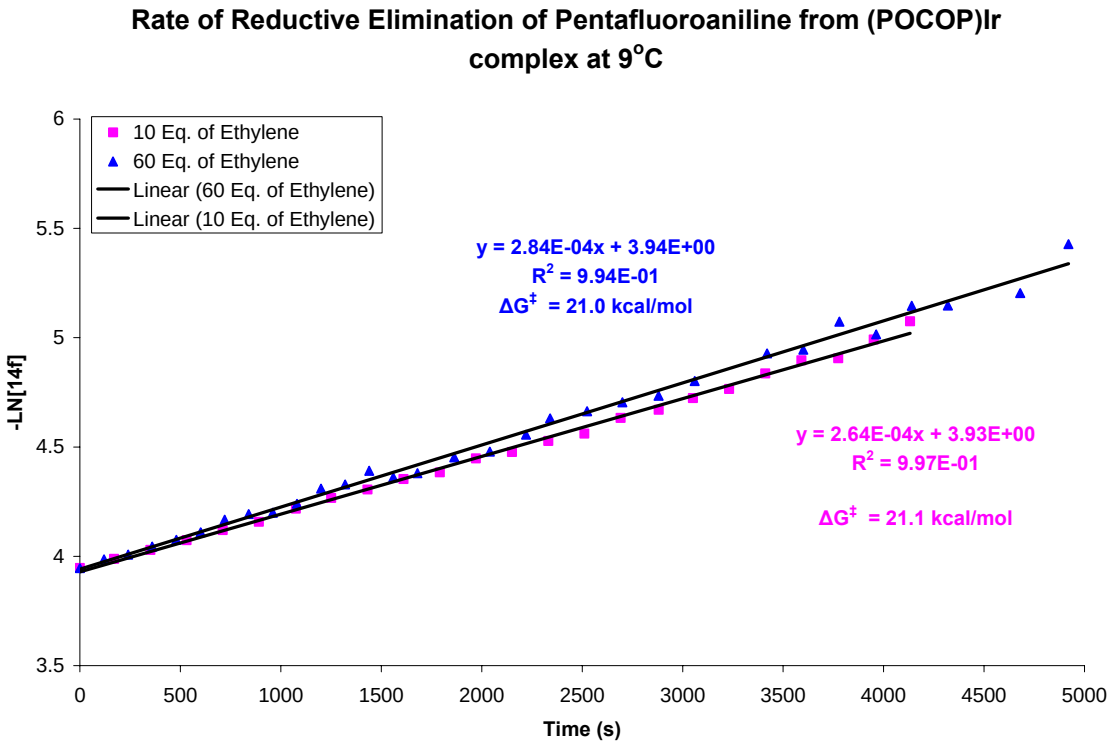

Figure I.2 First-order plot of the rate of reductive elimination of pentafluoroaniline from (POCOP)Ir(H)(NHC_6F_5)

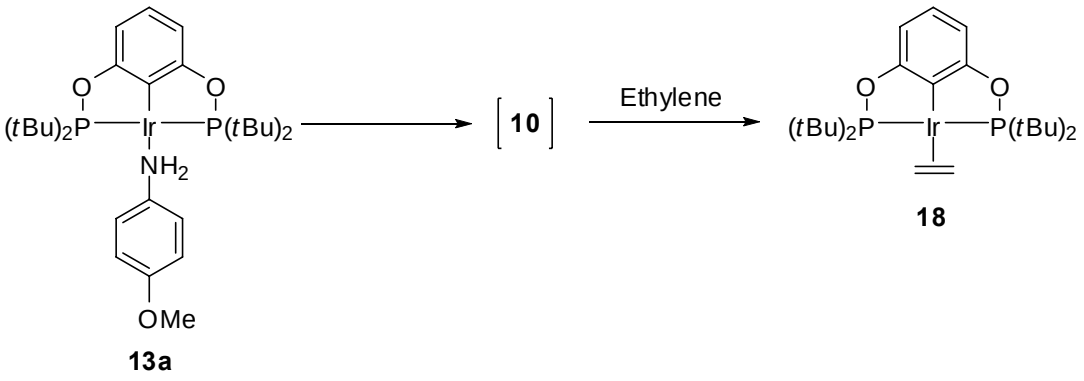

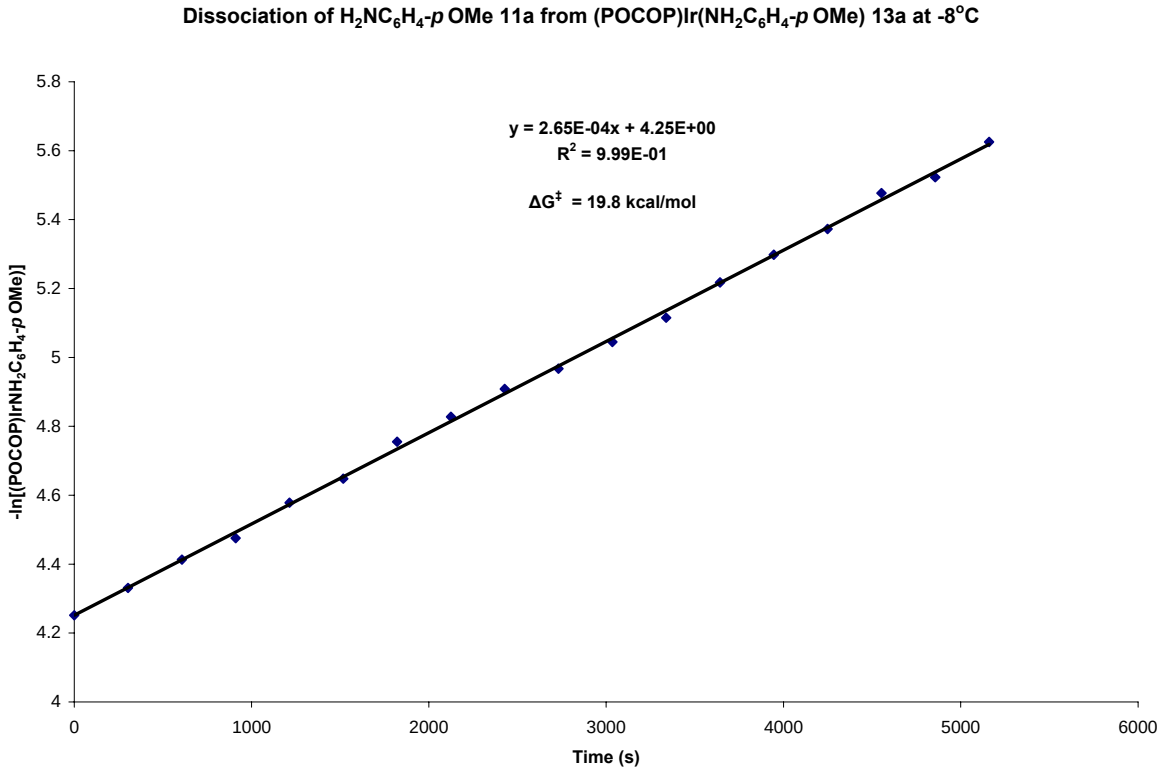

Figure I.3. First-order plot of the dissociation of $H_2NC_6H_4$-*p*OMe **11a** from (POCOP)Ir($NH_2C_6H_4$-*p*OMe) **13a**

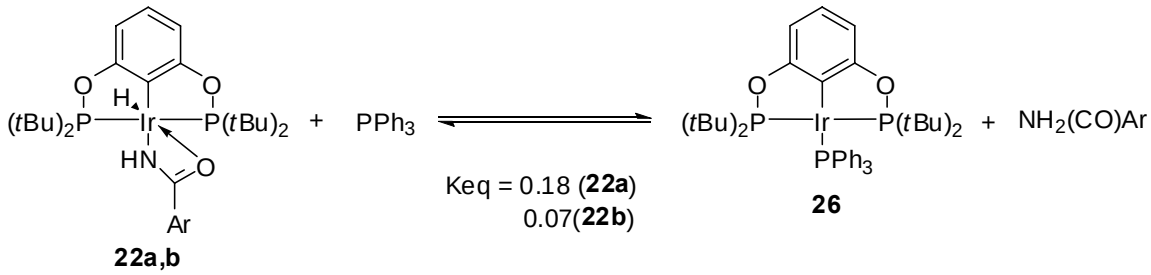

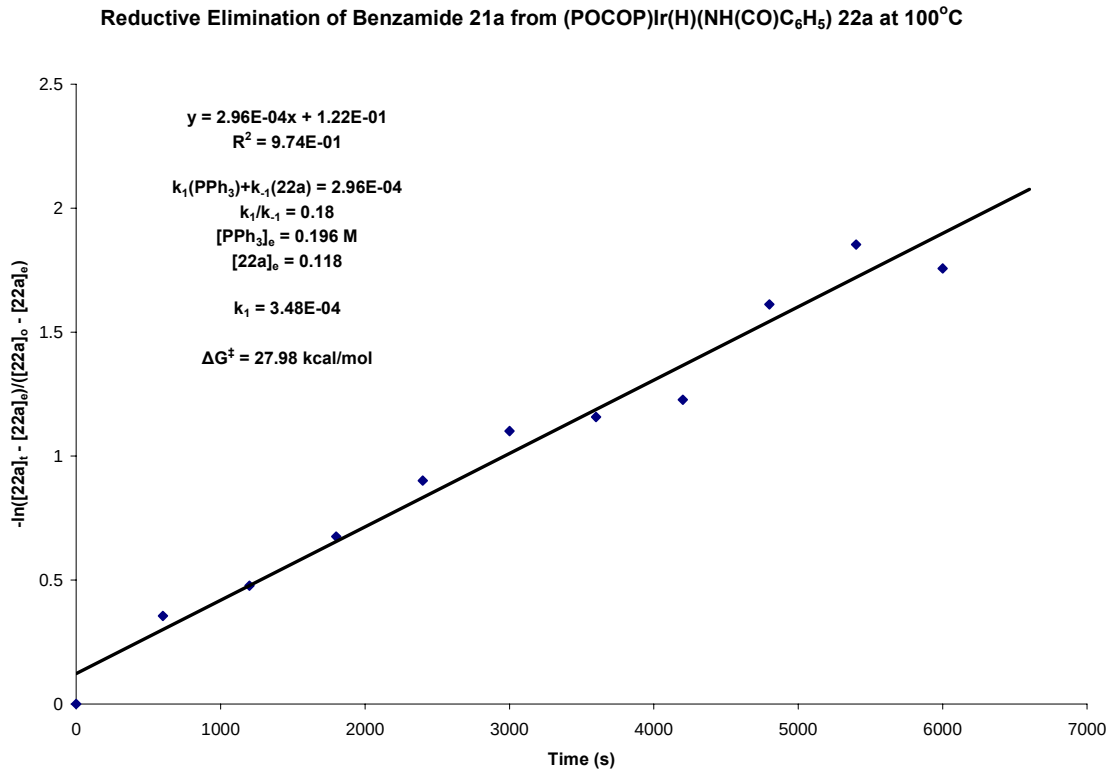

Figure I.4. First-order plot of the reductive elimination of benzamide **21a** from (POCOP)Ir(H)(NH(CO)C_6H_5) **22a**

APPENDIX II

Supporting Information for Chapter Three

Calculations and NMR spectra for dynamic process in [(POCOP)Ir(H)(L)][BAr_F] complexes **9-13**

I. [(POCOP)Ir(H)(H_2)][BAr_F] 9

Scheme II.1. Deuterium exchange with [(POCOP)Ir(D)(D_2)][BArF] $\mathbf{9_D}$

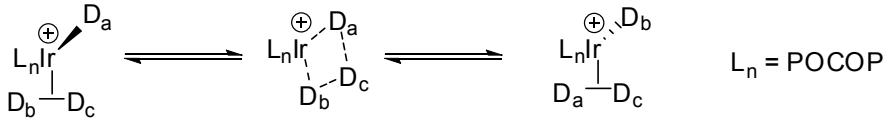

Table II.1. Line-broadening experiment based on the dideuterium resonance to measure the deuterium exchange rate in $\mathbf{9_D}$

T (K)	$W_{1/2}$ (Hz)	ΔW (Hz)	k (s^{-1}) = $2\pi*\Delta W$	$\Delta G^{\ddagger}$ (kcal/mol)
183.9	10.7			
201.1	26.8	26.8	50.6	9.8
205.4	34.0	34.0	73.2	9.8
207.5	39.0	39.0	88.9	9.9

Scheme II.2. Hydrogen exchange with [(POCOP)Ir(H)(H$_2$)][BArF] **9$_H$**

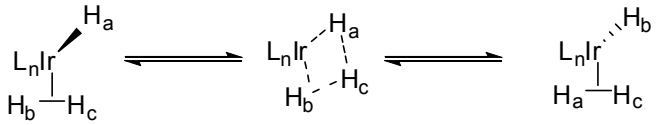

Table II.2. Line-broadening experiment based on the hydride resonance to measure the hydrogen exchange rate of **9$_H$**.

T (K)	$W_{1/2}$ (Hz)	ΔW (Hz)	k (s^{-1}) = $\pi*\Delta W$	$\Delta G^{\ddagger}$ (kcal/mol)
175.3	30.0			
188.2	59.4	29.4	92.3	9.2
192.5	83.4	53.4	167.7	9.1
196.8	127.0	97.0	304.6	9.1

Table II.3 Calculation for k_H/k_D of hydrogen exchange in [(POCOP)Ir(H)(H$_2$)][BAr$_F$] **9**

	$\Delta G^{\ddagger}$(kcal/mol)	k (s^{-1})	k_H/k_D
(H)(H$_2$)	9.1	474.1	5.8
(D)(D$_2$)	9.8	81.5	

II. [(POCOP)Ir(H)(C_2H_4)][BAr_F]

Table II.4. Estimation of the free energy barrier for the rotation of ethylene in [(POCOP)Ir(H)(C_2H_4)][BAr_F]

T (K)	Δυ (Hz)	k (s^{-1}) = π(Δυ)/(√2)	ΔG (kcal/mol)
175.3	25	55.51	8.68

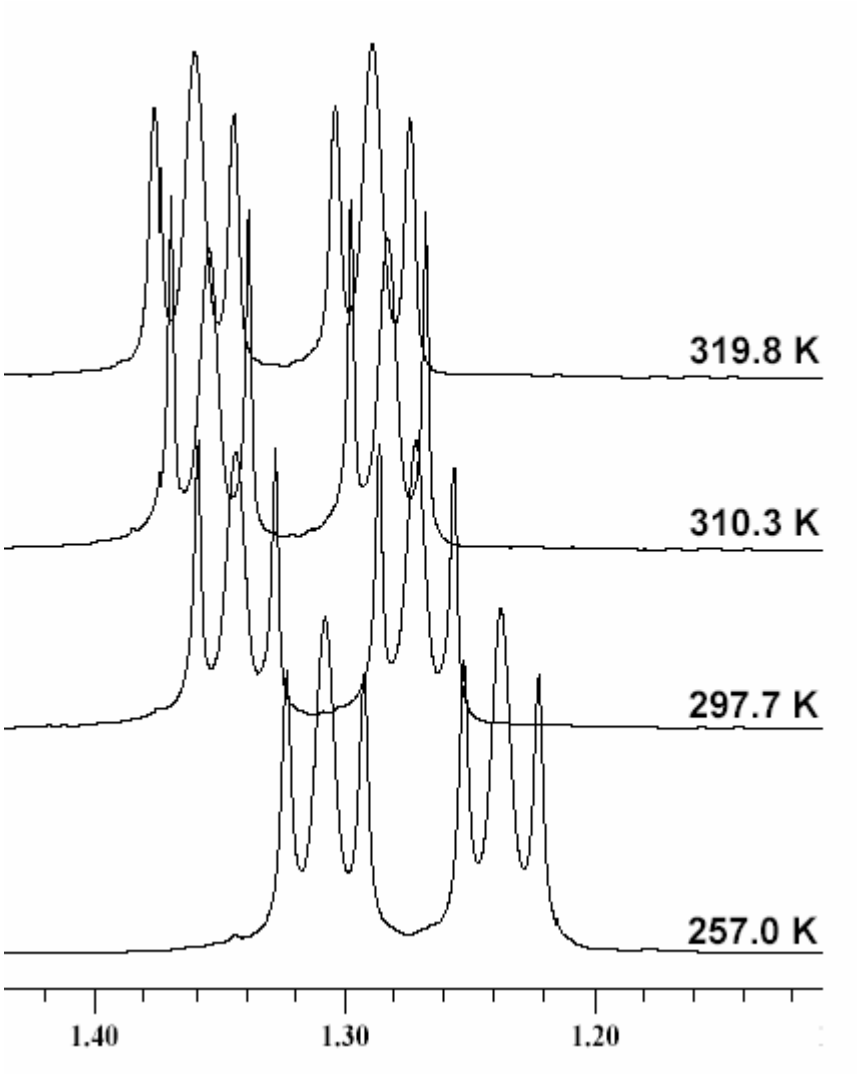

Figure II.1. ^{1}H NMR spectra of *t*-butyl resonances in [(POCOP)Ir(H)(C_2H_4)][BAr_F] at variable temperatures

Table II.5. Rate and energy barrier of the insertion of ethylene into the Ir-H bond of [(POCOP)Ir(H)(C_2H_4)][BAr_F] based on line-broadening of the ethylene resonance

T (K)	$W_{1/2}$ (Hz)	ΔW	k = 4*(3/2)πΔW (s^{-1})	$\Delta G^{\ddagger}$(kcal/mol)
257.7	4.9			
310.4	8.4	3.6	67.3	15.6
319.8	13.4	8.5	160.9	15.5

Table II.6. Rate and energy barrier of the insertion of ethylene into the Ir-H bond of [(POCOP)Ir(H)(C_2H_4)][BAr_F] based on line-broadening of the hydride resonance

T (K)	$W_{1/2}$ (Hz)	ΔW	k = (3/2)πΔW (s^{-1})	$\Delta G^{\ddagger}$(kcal/mol)
257.7	26.5			
310.4	38.8	12.4	58.3	15.7
319.8	57.9	31.4	148.0	15.6

III. [(POCOP)Ir(H)(C_3H_6)][BAr_F]

Table II.7. Rate and free energy barrier for the rotation of propylene in [(POCOP)Ir(H)(C_3H_6)][BAr_F] based on line-broadening of the major isomer in the ^{1}H NMR spectra

T (K)	W1/2 (Hz)	ΔW	k = πΔW (s-1)	$\Delta G^{\ddagger}$(kcal/mol)
175.3	15.9			
201.1	30.6	14.7	46.2	10.1
205.4	37.0	21.1	66.3	10.2

Table II.8. T_1 values for the olefinic and hydridic resonances of [(POCOP)Ir(H)(C_3H_6)][BAr_F] at 296.5 K in the ^{1}H NMR spectrum

Resonance	T1 (s)
-42	1.34
6.5	1.13
5.6	0.81
3.4	0.84

Table II.9. Rate of insertion and energy barrier for the insertion of propylene into the Ir-H bond of [(POCOP)Ir(H)(C_3H_6)][BAr_F] at 296.5K using spin-saturation transfer techniques

Irradiated	Affected	Mo	M_∞	kobs (s-1) = $(1/T_1)[(Mo/M_\infty)-1]$	k = $2k_{obs}$ (s^{-1})	$\Delta G^{\ddagger}$ (kcal/mol)
-42	6.5	1	0.31	1.96	3.91	16.55
6.5	-42	1	0.33	1.29	2.57	16.80
5.6	3.4	1	0.50	1.19	2.39	16.84
3.4	5.6	1	0.52	1.12	2.25	16.88
					average =	16.76

IV. [(POCOP)Ir(H)(norbornene)][BAr_F]

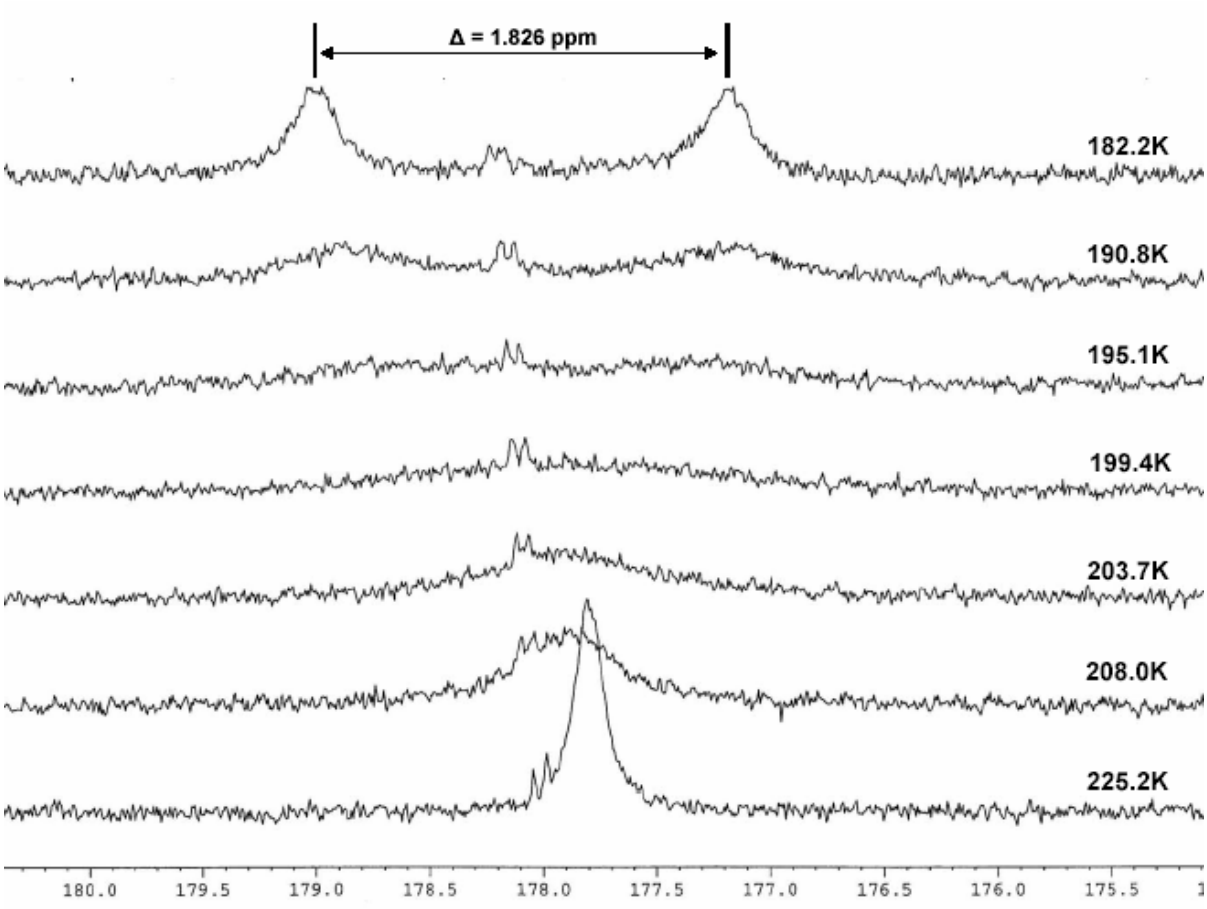

Figure II.2. Stacked ^{31}P NMR spectra of [(POCOP)Ir(H)(norbornene)][BAr_F] at variable temperatures

Table II.10. Rotation rate of norbornene in [(POCOP)Ir(H)(norbornene)][BAr_F] based on line-broadening in the ^1H NMR spectra

T (K)	$W_{1/2}$ (Hz)	ΔW	k = π*ΔW (s^{-1})	$\Delta G^{‡}$(kcal/mol)
173.6	27.8			
182.2	47.2	19.4	60.9	9.0
190.8	100.4	53.2	167.0	9.1

V. [(POCOP)Ir(H)(MA)][BAr_F]

Table II.11. Rate of rotation of methyl acrylate in [(POCOP)Ir(H)(MA)][BAr_F] based on line-broadening of the major isomer in the ^1H NMR spectra

T (K)	W1/2	ΔW1/2	k (s-1) = πΔW	ΔG‡ (kcal/mol)
196.8	25.2			
214.0	29	3.8	11.93	11.33
222.6	46.6	21.4	67.20	11.04